PARAMETRIC INFLUENCE ON ELECTROMAGNETIC FORMING PROCESSES

By

SHANTARAM K. DOND

ENGG01201404024

Bhabha Atomic Research centre, Mumbai

A thesis submitted to the

Board of Studies in Engineering Sciences

In partial fulfillment of requirements

for the Degree of

DOCTOR OF PHILOSOPHY

of

HOMI BHABHA NATIONAL INSTITUTE

July 2020

Homi Bhabha National Institute[1]

Recommendations of the Viva Voce Committee

As members of the Viva Voce Committee, we certify that we have read the dissertation prepared by Mr. Shantaram K. Dond entitled "Parametric Influence on Electromagnetic forming processes" and recommend that it may be accepted as fulfilling the thesis requirement for the award of Degree of Doctor of Philosophy.

Chairman - Dr. A. P. Tiwari	16/7/2020
Guide / Convener - Dr. Archana Sharma	Archana 16-7-2020
Co-guide - Dr. G. K. Dey	Gautam Kumar Dey 16/7/2020
Examiner - Dr. R. K. Pandey	16.07.2020
Member 1- Dr. A. K. Bhattacharjee	AKBhattacharjee 16/7/2020
Member 2- Dr. V. H. Patankar	V.H.Patankar 16/07/2020
Member 3- Dr. S. Kar	SKar

Final approval and acceptance of this thesis is contingent upon the candidate's submission of the final copies of the thesis to HBNI.

I/We hereby certify that I/we have read this thesis prepared under my/our direction and recommend that it may be accepted as fulfilling the thesis requirement.

Date: 16/07/2020

Place: BARC, Mumbai

Gautam Kumar Dey 16/7/2020
Signature
Co-guide (if any)

Signature Archana 16-7-2020
Guide

STATEMENT BY AUTHOR

This dissertation has been submitted in partial fulfillment of requirements for an advanced degree at Homi Bhabha National Institute (HBNI) and is deposited in the Library to be made available to borrowers under rules of the HBNI.

Brief quotations from this dissertation are allowable without special permission, provided that accurate acknowledgement of source is made. Requests for permission for extended quotation from or reproduction of this manuscript in whole or in part may be granted by the Competent Authority of HBNI when in his or her judgment the proposed use of the material is in the interests of scholarship. In all other instances, however, permission must be obtained from the author.

Shantaram K. Dond

DECLARATION

I, hereby declare that the investigation presented in the thesis has been carried out by me. The work is original and has not been submitted earlier as a whole or in part for a degree / diploma at this or any other Institution / University.

Shantaram K. Dond

PUBLICATIONS

Journals

- **Dond S.K.**, Hitesh Choudhary, Tanmay Kolge, Archana Sharma and G. K. Dey, "Determination of Magnetic Coupling and its Influence on the Electromagnetic Tube Forming and Discharge Circuit Parameters," Journal of Manufacturing Process, Vol. 54, June 2020, pp.19-27.

- **Dond S.K.**, Hitesh Choudhary, Tanmay Kolge, Archana Sharma, "Analysis of the Variation of the Discharge Circuit Parameters during Electromagnetic Forming Processes," International Journal of Precision Engineering and Manufacturing, 2019, Vol. 20, No. 3, pp. 375-382.

- **Dond S.K.**, Hitesh Choudhary, Tanmay Kolge, Archana Sharma and G. K. Dey, "Robust electromagnet design for pulse forming application," COMPEL - The international journal for computation and mathematics in electrical and electronic engineering, 2019, Vol. 38, No. 2, pp. 557-572.

- **Dond S.K.**, Hitesh Choudhary, Tanmay Kolge, Archana Sharma "Current Frequency Effect on Electromagnetic Tube Expansion," Proceedings of the Institution of Mechanical Engineers, Part C: Journal of Mechanical Engineering Science.,2020.

Sdond

[Shantaram K. Dond]

Conferences

- **Dond S. K.**, Tanmay Kolge, Hitesh Choudhary and Archana Sharma, "Effect of coil to tubular workpiece magnetic coupling on electromagnetic expansion process," 8th International Conference on High Speed Forming (ICHSF 2018), Ohio State University in Columbus,14-16 May 2018.

- **Dond S. K.**, Hitesh Choudhary, Tanmay Kolge, Archana Sharma and G. K. Dey, "Investigation of the Coil Failure modes in the Electromagnetic forming Process," 22nd International Conference on the Computation of Electromagnetic Fields (COMPUMAG 2019) in Paris, France, 15-19 July 2019.

- **Dond S. K.**, Hitesh Choudhary, Tanmay Kolge, Archana Sharma and G. K. Dey, "Analysis of Electromagnetic Tube Expansion With Improved Sequentially Coupled Method," Advances in Materials & Processing Technologies Conference, VIT Chennai, 11-14 December 2017

Sdond

[Shantaram K. Dond]

To

My Family

and

My Friends

Acknowledgments

Success of any work depends upon the dedication, sincerity and hard work. It also requires some ingredients such as motivation, guidance, encouragement and time.Wholehearted effort altogether makes the project useful and meaningful.

I express my foremost and deepest gratitude to many peoples who have supported and encouraged me during my Ph.D. work. I take this oppurtunity to express my sincere appreciation to all of those who made this thesis possible.

First and foremost, I would like to extend my sincere gratitude to my research guide Dr. (Mrs.) Archana Sharma for introducing me to this exciting field of science and for her dedicated help, advice, inspiration, encouragement and continuous support throughout my Ph.D. Her enthusiasm and her mission for providing high-quality work, has made a deep impression on me. My special words of thanks should also go to my research co-guide Dr. G.K. Dey for his continuous support, guidance, cooperation, encouragement and for facilitating all the requirements.

Besides my guides, I would like to acknowledge contributions of the doctoral committe Chairman Dr. A. P. Tiwari and memebrs Dr. A. K. Bhattacharjee, Dr. V. H. Patankar, Dr. S. Kar for sparing their valuble time for critical assessment of my work. Incorporation of their suggestions has helped in improving quality of this work.

I would like to thank all EMM group members for their continued support. This dissertation would not have been possible without Mr. Tanmay Kolge and Mr. Hitesh choudhary. This are the peoples who continuesly supported me and helped to grow as a person with good qualities. A special thanks to Mr. Rajesh Kakad who is always there to help me in arranging experimental set up. I also appreciate significant efforts put in by all the staff from TPD Workshop who carried out very intricate job for the experiments.

Most importantly, none of this would have been possible without the love and patience of my family. I want to thank my parents, sister and brothers for being constant source of love, concern, support and strength all these years. I owe my deepest gratitude towards my better half for her eternal support and understanding of my goals and aspirations.

Finally, I bow my head to the God almighty in deepest gratitude and seek blessings.

Date: 21/07/2020

Shantaram K. Dond

Contents

List of Tables

List of Figures

Nomenclature

List of Greek and Roman Symbols

β	Damping factor
δ	Skin depth
δ_r	Relative skin depth
σ	Electrical conductivity
μ	Permeability
μ_r	Relative permeability
ω	Coil current angular frequency
ρ	Density
ϵ^p	Effective plastic strain
$\dot{\epsilon}^p$	Strain rate
σ_s	Stress tensor
σ_y	Yield strength
A_w	Material constant for Johnson-Cook model

B_w	Material constant for Johnson-Cook model
C_w	Material constant for Johnson-Cook model
n	Material constant for Johnson-Cook model
N	Number of turns
V	Voltage
C	Capacitance
E	Electrical intensity
B	Magnetic flux density
A	Magnetic vector potenstial
F	Lorentz force
∇	Nabla operator
J	Current density
P	Pressure
K	Coupling factor
D	Tube diameter
t	Time
r	Radial axis
z	Axial axis

h	Gap between coil and tube
H	Magnetic flux intensity
f	Coil current frequency
K_H	Distribution coefficient
P_{mag}	Magnetic pressure
R_s	System resistance
L_s	System inductance
R_c	Coil resistance
L_c	coil inductance
R_w	Workpiece resistance
L_w	Workpiece inductance
R_T	Circuit total resistance
L_T	Circuit total inductance
R_{cw}	Coil-workpiece coupled circuit resistance
L_{cw}	Coil-workpiece coupled circuit inductance
i_c	Coil current
i_w	Workpiece current
I_{peak}	Peak current

l_c	Active length of coil
l_w	Workpiece length
r_1	Coil inner radius
r_2	Coil outer radius
W_i	Workpiece inner radius
W_o	Workpiece outer radius
W_t	Workpiece thickness
f_f	Filing factor
K_T	Thermal conductivity
T	Temperature

Abbreviations

EMF	Electromagnetic forming
EM	Electromagnetic
FEM	Finite element method
Al	Aluminium
2D	Two dimensional

Chapter 8

Conclusion and Future Work

8.1 Conclusions

Electromagnetic forming is a promising technology enabling numerous high speed forming applications with the use of Lorentz force. This thesis presented a study on the parametric effect on electromagnetic tube expansion.

In this thesis, The author has developed a numerical model that couples electromagnetic, structural and thermal physics involved in EM tube forming process. The developed numerical and analytical model results are in good agreement with experimental results. Design methodology of the actuator (coil) is presented in detail. Depending on the workpiece dimensions and forming requirements, selection criteria of different coil parameters are presented. It is observed that though the coil is under the mechanical and thermal stress during the forming process, the thermal effect is a leading contributor in the initiation of coil failure. The presented coil design aspects and failure analysis certainly crucial in the coil design stage of any electromagnetic forming application.

The discharge circuit parameters during EM forming process are not constant. The variation of the discharge circuit parameters estimated with the analytical model and its importance on numerical model accuracy is studied. It is observed that incorporating the dynamics of discharge circuit in the numerical analysis of EM forming certainly improves the numerical model results. For given discharge energy, there exists an optimum frequency at which we get higher forming and it is related with the relative skin depth. For the tube forming case, it is observed that at an optimum frequency, the relative skin depth is less than 1 contrast to the sheet forming case observed in the literature. Further, it is observed that the optimum frequency has a dependency on tube thickness as well as on system resistance and inductance. This study can beneficial in setting EM system parameters to get high forming and thereby good process efficiency.

Magnetic coupling between coil and workpiece is plays an important role in EM forming process still it is not much discussed before. For the tube forming case, the derived relation between coupling factor and the coil-workpiece gap is found to be exponential decay. Te discharge circuit parameters, EM process efficiency are varied exponentially with the coupling factor. Coupling factor analysed in this thesis is helpful in accurate analytical simplification of EMF discharge circuit. It is also important in the design stage of EM forming set up.

8.2 Future work

Future investigation will be on the feasibility of the electromagnetic joining by tube expansion method. In this, the electromagnetically expanding tube will be impacted on the aluminium sheet/flange to achieve the joint between tube and sheet. The developed numerical model is to be updated to analyse the behaviour of the impacting materials during the joining process. In electromagnetic welding, there are some criteria to achieve weld such as the impact velocity, stress and strain in the impacting materials. The numerical model can give important information about these parameters and will certainly reduce the experimental trials and time.

The next task is to improve coil life. In present work, diagnosis of the coil failure is performed using the numerical simulation model. It is seen that the thermal loading plays an important role in the initiation of the coil failure compared to the mechanical loading on the coil. However, experimental measurements are required to validate the numerical observations. Though the coil is functional, the accumulated deformation and degradation of the coil needs to be monitored during every experimental trial of the coil to know its health. It will help to confirm the exact reason for coil failure and also probable failure time of the coil.

Besides improving the coil life, utilisation of maximum electromagnetic energy to the workpiece deformation is also necessary to increase the EMF process efficiency and also thereby reducing stress on the coil. It is shown in this thesis that the EMF process efficiency increased exponentially with an increase in the coil-workpiece coupling factor. Considering the constraints on achieving maximum coupling factor, further study is required on estimating optimum coupling factor for given geometry and materials.

References

[1] M. Seth, V. J. Vohnout, and G. S. Daehn, “Formability of steel sheet in high velocity impact,” *Journal of Materials Processing Technology*, vol. 168, no. 3, p. 390–400, 2005.

[2] S. Fan, J. Mo, J. Fang, and J. Xie, “Electromagnetic pulse-assisted incremental drawing forming of aluminum alloy cylindrical part and its control strategy,” *The International Journal of Advanced Manufacturing Technology*, vol. 95, no. 5-8, pp. 2681–2690, 2017.

[3] A. Kapil and A. Sharma, “Magnetic pulse welding: an efficient and environmentally friendly multi-material joining technique,” *Journal of Cleaner Production*, vol. 100, p. 35–58, 2015.

[4] A. Vivek, K.-H. Kim, and G. Daehn, “Simulation and instrumentation of electromagnetic compression of steel tubes,” *Journal of Materials Processing Technology*, vol. 211, no. 5, pp. 840–850, 2011.

[5] Y. Haiping and L. Chunfeng, “Effects of current frequency on electromagnetic tube compression,” *Journal of Materials Processing Technology*, vol. 209, no. 2, pp. 1053–1059, 2009.

[6] S. Kore, P. Date, and S. Kulkarni, “Electromagnetic impact welding of aluminum to stainless steel sheets,” *Journal of Materials Processing Technology*, vol. 208, no. 1-3, p. 486–493, 2008.

[7] S. Mishra, S. K. Sharma, S. Kumar, K. Sagar, M. Meena, and A. Shyam, "40 kj magnetic pulse welding system for expansion welding of aluminium 6061 tube," *Journal of Materials Processing Technology*, vol. 240, p. 168–175, 2017.

[8] V. Psyk, D. Risch, B. Kinsey, A. Tekkaya, and M. Kleiner, "Electromagnetic forming—a review," *Journal of Materials Processing Technology*, vol. 211, no. 5, pp. 787–829, 2011.

[9] P. Kapitza, "A method of producing strong magnetic fields," *Proceedings of the Royal Society of London. Series A*, vol. 105, pp. 691–710, 1924.

[10] G. Harvey and D. Brower, "Metal forming device and method," *Google Patents*, 1962.

[11] K. Baines, J. Duncan, and W. Johnson, "Electromagnetic metal forming," in *Proceedings of the Institution of Mechanical Engineers*, 1965.

[12] G. Lal and M. Hillier, "The electrodynamics of electromagnetic forming," *International Journal of Mechanical Sciences*, vol. 10, no. 6, pp. 491–500, 1968.

[13] G. K. Lal, "Electromagnetic metal forming," *IEEE Transactions on Industry Applications*, vol. IA-8, no. 4, pp. 425–429, 1972.

[14] A. Mamalis, D. Manolakos, A. Kladas, and A. Koumoutsos, "Electromagnetic forming and powder processing: Trends and developments," *ASME Applied Mechanics Reviews*, vol. 57, no. 4, pp. 299–324, 2004.

[15] L. Qiu, X. Han, T. Peng, H. Ding, Q. Xiong, Z. Zhou, C. Jiang, Y. Lv, and L. Li, "Design and experiments of a high field electromagnetic forming system," *IEEE Transactions on Applied Superconductivity*, vol. 22, no. 3, 2012.

[16] M. Blakely, "Filler wire is for wimps (welding)," in *Fabricating and Metalworking*, ser. the Business of Metal Manufacturing, Hirotec America, 2008, pp. 31–32.

[17] H. Stadelmaier, "Magnetic properties of materials," *Materials Science and Engineering: A*, vol. 287, no. 2, p. 138–145, 2000.

[18] S. Desai, S. Kumar, P. Satyamurthy, J. Chakravartty, and D. Chakravarthy, "Analysis of the effect of collision velocity in electromagnetic welding of aluminum strips," *International Journal of Applied Electromagnetics and Mechanics*, vol. 34, no. 1-2, p. 131–139, 2010.

[19] A. K. Rajak and S. D. Kore, "Comparison of different types of coil in electromagnetic terminal - wire crimping process: Numerical and experimental analysis," *Journal of Manufacturing Processes*, vol. 34, pp. 329–338, 2018.

[20] J. Vincent, "A hybrid quasi-static/dynamic process for forming large sheet metal parts from aluminum alloys," Ph.D. dissertation, 1998.

[21] J. Bednarczyk, "Distributions of forces in the inductors used in metal processing in the pulse magnetic field," *Journal of Materials Processing Technology*, vol. 133, no. 3, p. 340–347, 2003.

[22] B. Tomas, "Magnetic pulse welding," Ph.D. dissertation, 2010.

[23] M. Kamal and G. S. Daehn, "A uniform pressure electromagnetic actuator for forming flat sheets," *Journal of Manufacturing Science and Engineering*, vol. 129, no. 2, p. 369, 2007.

[24] J. Shang, L. Wilkerson, S. Hatkevich, and G. Daehn, "Coupling of magnetic fields from power Conference on

[25] V. Vohnout, *A Hybrid Quasi-static/dynamic Process for Forming Large Sheet Metal Parts from Aluminum Alloys*.

[26] F. Song, X. Zhang, Z. Wang, and L. Yu, "A study of tube electromagnetic forming," *Journal of Materials Processing Technology*, vol. 151, no. 1-3, pp. 372–375, 2004.

[27] S. H. Lee and D. N. Lee, "Estimation of the magnetic pressure in tube expansion by electromagnetic forming," *Journal of Materials Processing Technology*, vol. 57, no. 3-4, pp. 311–315, 1996.

[28] R. Otin, R. Mendez, and O. Fruitos, "A numerical model for the search of the optimum capacitance in electromagnetic metal forming," vol. 50, no. 10, pp. 1605–1612, 2013.

[29] Q. Cao, X. Han, Z. Lai, B. Zhang, Z. Zhou, L. Qiu, and L. Li, "Effects of current frequency on electromagnetic sheet metal forming process," *IEEE Transactions on Applied Superconductivity*, vol. 24, no. 3, pp. 1–4, 2014.

[30] X. Cui, J. Li, J. Mo, J. Fang, B. Zhou, and X. Xiao, "Effect of the sheet thickness and current damping exponent on the optimum current frequency in electromagnetic forming," *The International Journal of Advanced Manufacturing Technology*, vol. 85, no. 1-4, pp. 843–851, 2015.

[31] C. Weddeling, O. K. Demir, P. Haupt, and A. E. Tekkaya, "Analytical methodology for the process design of electromagnetic crimping," *Journal of Materials Processing Technology*, vol. 222, pp. 163–180, 2015.

[32] H. Yu, J. Chen, W. Liu, H. Yin, and C. Li, "Electromagnetic forming of aluminum circular tubes into square tubes: Experiment and numerical simulation," *Journal of Manufacturing Processes*, vol. 31, pp. 613–623, 2018.

[33] A. Nassiri, C. Campbell, G. Chini, and B. Kinsey, "Analytical model and experimental validation of single turn, axi-symmetric coil for electromagnetic forming and welding," *Procedia Manufacturing*, vol. 1, pp. 814–827, 2015.

[34] K. Banik, “Factors effecting electromagnetic flat sheet forming using the uniform pressure coil,” Master’s thesis, Ohio State University, 2008.

[35] E. Thibaudeau and B. L. Kinsey, “Analytical design and experimental validation of uniform pressure actuator for electromagnetic forming and welding,” *Journal of Materials Processing Technology*, vol. 215, pp. 251–263, 2015.

[36] A. Mamalis, D. Manolakos, A. Kladas, and A. Koumoutsos, “Physical principles of electromagnetic forming process: a constitutive finite element model,” *Journal of Materials Processing Technology*, vol. 161, no. 1-2, p. 294–299, 2005.

[37] Y. Haiping, L. Chunfeng, and D. Jianghua, “Sequential coupling simulation for electromagnetic-mechanical tube compression by finite element analysis,” *Journal of Materials Processing Technology*, vol. 209, no. 2, pp. 707–713, 2009.

[38] X. Cui, J. Mo, J. Li, and X. Xiao, “Tube bulging process using multidirectional magnetic pressure,” *The International Journal of Advanced Manufacturing Technology*, vol. 90, no. 5-8, pp. 2075–2082, 2016.

[39] X. Cui, J. Mo, and F. Han, “3d multi-physics field simulation of electromagnetic tube forming,” *The International Journal of Advanced Manufacturing Technology*, vol. 59, no. 5-8, pp. 521–529, 2011.

[40] A. F. Arezoodar, H. E. Haratmeh, and M. Farzin, “Numerical and experimental investigation of inward tube electromagnetic forming- electromagnetic study,” *The International Journal of Advanced Manufacturing Technology*, vol. 88, no. 5-8, p. 1175–1185, 2017.

[41] F. Li, J. Mo, H. Zhou, and Y. Fang, “3d numerical simulation method of electromagnetic

forming for low conductive metals with a driver," *The International Journal of Advanced Manufacturing Technology*, vol. 64, no. 9-12, pp. 1575–1585, 2012.

[42] X. Cui, J. Mo, J. Li, L. Huang, Y. Zhu, Z. W. Li, and K. Zhong, "Effect of second current pulse and different algorithms on simulation accuracy for electromagnetic sheet forming," *The International Journal of Advanced Manufacturing Technology*, vol. 68, no. 5-8, pp. 1137–1146, 2013.

[43] R. Chaharmiri and A. F. Arezoodar, "The effect of sequential coupling on radial displacement accuracy in electromagnetic inside-bead forming: simulation and experimental analysis using maxwell and abaqus software," *Journal of Mechanical Science and Technology*, vol. 30, no. 5, pp. 2005–2010, 2016.

[44] D. Oliveira, M. Worswick, M. Finn, and D. Newman, "Electromagnetic forming of aluminum alloy sheet: Free-form and cavity fill experiments and model," *Journal of Materials Processing Technology*, vol. 170, no. 1-2, pp. 350–362, 2005.

[45] O. K. Demir, V. Psyk, and A. E. Tekkaya, "Simulation of tube wrinkling in electromagnetic compression," *Production Engineering*, vol. 4, no. 4, pp. 421–426, 2010.

[46] Q. Cao, L. Li, Z. Lai, Z. Zhou, Q. Xiong, X. Zhang, and X. Han, "Dynamic analysis of electromagnetic sheet metal forming process using finite element method," *The International Journal of Advanced Manufacturing Technology*, vol. 74, no. 1-4, pp. 361–368, 2014.

[47] L. Qiu, Y. Yu, Q. Xiong, C. Deng, Q. Cao, X. Han, and L. Li, "Analysis of electromagnetic force and deformation behavior in electromagnetic tube expansion with concave coil based

on finite element method," *IEEE Transactions on Applied Superconductivity*, vol. 28, no. 3, pp. 1–5, 2018.

[48] J. Correia, M. Siddiqui, S. Ahzi, S. Belouettar, and R. Davies, "A simple model to simulate electromagnetic sheet free bulging process," *International Journal of Mechanical Sciences*, vol. 50, no. 10-11, pp. 1466–1475, 2008.

[49] L. Qiu, Y. Xiao, C. Deng, Z. Li, Y. Xu, Z. Li, and P. Chang, "Electromagnetic-structural analysis and improved loose coupling method in electromagnetic forming process," *The International Journal of Advanced Manufacturing Technology*, vol. 89, no. 1-4, pp. 701–710, 2016.

[50] G. Bartels, W. Schatzing, H. Scheibe, and M. Leone, "Comparison of two different simulation algorithms for the electromagnetic tube compression," *International Journal of Material Forming*, vol. 2, no. S1, p. 693–696, 2009.

[51] E. Thibaudeau and B. L. Kinsey, "Analytical design and implementation of a uniform pressure actuator for electromagnetic forming and welding," *Volume 1: Processing*, 2013.

[52] O. Zaitov and V. A. Kolchuzhin, "Bitter coil design methodology for electromagnetic pulse metal processing techniques," *Journal of Manufacturing Processes*, vol. 16, no. 4, pp. 551–562, 2014.

[53] S. F. Golovashchenko, "Material formability and coil design in electromagnetic forming," *Journal of Materials Engineering and Performance*, vol. 16, no. 3, pp. 314–320, 2007.

[54] A. V. Mamutov, S. F. Golovashchenko, and V. S. Mamutov, "Experimental-analytical method of analyzing performance of coils for electromagnetic forming and joining operations," *Journal of Materials Processing Technology*, vol. 255, p. 86–95, 2018.

[55] Z. Lai, X. Han, Q. Cao, L. Qiu, Z. Zhou, and L. Li, "The electromagnetic flanging of a large-scale sheet workpiece," *IEEE Transactions on Applied Superconductivity*, vol. 24, no. 3, pp. 1–5, 2014.

[56] S. Gies, C. Löbbe, C. Weddeling, and A. Tekkaya, "Thermal loads of working coils in electromagnetic sheet metal forming," *Journal of Materials Processing Technology*, vol. 214, no. 11, p. 2553–2565, 2014.

[57] Q. Cao, X. Han, Z. Lai, Q. Xiong, X. Zhang, Q. Chen, H. Xiao, and L. Li, "Analysis and reduction of coil temperature rise in electromagnetic forming," *Journal of Materials Processing Technology*, vol. 225, pp. 185–194, 2015.

[58] S. Gies and A. E. Tekkaya, "Analytical prediction of joule heat losses in electromagnetic forming coils," *Journal of Materials Processing Technology*, vol. 246, pp. 102–115, 2017.

[59] S. Gies, A. Langolf, C. Weddeling, and A. Tekkaya, "Measurement of working coil temperature in electromagnetic forming processes by means of optical frequency domain reflectometry," *Case Studies in Nondestructive Testing and Evaluation*, vol. 3, pp. 15–20, 2015.

[60] A. Nassiri, S. Zhang, T. Lee, A. T, A. Vivek, B. Kinsey, and G. Daehn, "Numerical investigation of cp-ti cu110 impact welding using smoothed particle hydrodynamics and arbitrary lagrangian-eulerian methods," *Journal of Manufacturing Processes*, vol. 28, no. 3, pp. 558 – 564, 2017.

[61] X. Wang, Y. Zheng, H. Liu, Z. Shen, Y. Hu, W. Li, Y. Gao, and C. Guo, "Numerical study of the mechanism of explosive/impact welding using smoothed particle hydrodynamics method," *Materials amp; Design*, vol. 35, p. 210–219, 2012.

[62] X. Cui, J. Mo, J. Li, J. Zhao, and S. Xiao, "Produce a large aluminum alloy sheet metal using electromagnetic-incremental (em-if) forming method: Experiment and numerical simulation," in *Proceedings of the 5th International Conference on High Speed Forming*, Germany, 2012, pp. 59–70.

[63] X. Cui, J. Mo, J. Li, J. Zhao, Y. Zhu, L. Huang, Z. Li, and K. Zhong, "Electromagnetic incremental forming (emif): A novel aluminum alloy sheet and tube forming technology," *Journal of Materials Processing Technology*, vol. 214, no. 2, p. 409–427, 2014.

[64] X. Cui, J. Mo, J. Li, X. Xiao, B. Zhou, and J. Fang, "Large-scale sheet deformation process by electromagnetic incremental forming combined with stretch forming," *Journal of Materials Processing Technology*, vol. 237, p. 139–154, 2016.

[65] M. M. Plum, *Electromagnetic forming, Metals Handbook*. ASM International, 1988, vol. 14.

[66] Url. http://asm.matweb.com/search/SpecificMaterial.asp?bassnum=MA5052O.

[67] B. J. and W. L., "Experimental research on magnetic pulse welding of dissimilar metals," Master's thesis, Ghent University, 2010.

[68] H.-G. Noh, W.-J. Song, B.-S. Kang, and J. Kim, "Two-step electromagnetic forming process using spiral forming coils to deform sheet metal in a middle-block die," *The International Journal of Advanced Manufacturing Technology*, vol. 76, no. 9-12, pp. 1691–1703, 2014.

[69] J. Doley and S. Kore, "Fem study on electromagnetic formability of az31b magnesium alloy," in *Proceedings of the 6th International Conference on High Speed Forming*, Korea, 2014, pp. 273–280.

[70] N. Takatsu, M. Kato, K. Sato, and T. Tobe, "High-speed forming of metal sheets by electromagnetic force," *JSME international journal. Ser. 3, Vibration, control engineering, engineering for industry*, vol. 31, no. 1, pp. 142–148, 1988.

[71] J. R. A. Zapata and F. Bay, "Modeling and analysis of electromagnetism in magnetic forming processes," *IEEE Transactions on Magnetics*, vol. 52, no. 5, pp. 1–11, 2016.

[72] N. Derby and S. Olbert, "Cylindrical magnets and ideal solenoids," *American Journal of Physics*, vol. 78, no. 3, pp. 229–235, 2010.

[73] F. Grover, *Inductance calculations working formulas and tables*. Dover,New York, 1946.

[74] R. Kratz and P. Wider, *Principles of pulsed magnet design*. Springer, Berlin/Heidelberg, 2002.

[75] M. Kamal, "A uniform pressure electromagnetic actuator for forming flat sheets," Ph.D. dissertation, OH,USA, 2005.

[76] F. Herlach, *High magnetic fields: science and technology*. World Scientific, 2003.

[77] H. Knoepfel, *Pulsed high magnetic fields*. North-Holland Publishing Co., 1970.

[78] E. B. Rosa and F. W. Grover, *Formulas and tables for the calculation of mutual and self-induction*. Government Printing Office, 1912.

[79] S. Gies, C. Löbbe, C. Weddeling, and A. Tekkaya, "Thermal loads of working coils in electromagnetic sheet metal forming," *Journal of Materials Processing Technology*, vol. 214, no. 11, pp. 2553–2565, 2014.

[80] Al-Hassani, J. L. Duncan, and W. Johnson, "On the parameters of the magnetic forming process," *Journal of Mechanical Engineering Science*, vol. 16, no. 1, 1974.

Summary

Electromagnetic forming (EMF) is a high-velocity forming method that uses a strong electromagnetic field to deform metallic workpieces. Ability to form lightweight materials like aluminium has increased the EMF technique importance in the automobile and aerospace industries.

The first aim of this research is to propose a methodology to design a robust EM coil for EM tube expansion and second is to study the effect of process parameters on electromagnetic forming results, process efficiency and coil life.

A 40 kJ EM manufacturing machine is used for the electromagnetic expansion experiments. EMF tests are performed on different dimension aluminium 5052 tubes. A 2D numerical model is developed using COMSOL Multiphysics software. In this, electromagnetic, structural and thermal physics are coupled sequentially, and time-dependent study is performed. A 1D analytical model is also developed to estimate required magnetic field, magnetic, resultant tube velocity and displacement. The developed analytical and simulation model results are in agreement with experimental observations.

Firstly, a robust electromagnetic coil is designed and tested for aluminium tube expansion. In designed coil failure diagnosis, it has been observed that the thermal loading on the coil has a significant role in the coil failure compared to the mechanical loading.

A further study carried out with an aim to obtain the optimum frequency of discharge current

that gives maximum tube expansion at constant discharge energy. Results of tube expansion show that maximum forming is obtained at a frequency where the ratio of skin depth to tube thickness is less than 1. It is also noticed that the optimum frequency depends on the tube thickness, inductance and resistance of the system.

The importance of discharge circuit parameters dynamics during the electromagnetic forming processis studied further. Significant improvements in estimated results are observed with consideration of discharge circuit parameters dynamics in the analysis. Next study is done on the estimation of the coil-workpiece magnetic coupling coefficient K. The coupling coefficient K variation with the coil-tube gap $h$is related with curve fitting, and this K-h relation is then used to analyse the discharge circuit parameter dependency on h. The EMF process efficiency and tube displacement are found to be improved exponentially with the increase in K.

The studied aspects in this thesis will be helpful to design strong electromagnet and to improve the EMF process efficiency.

Chapter 1

Introduction

Present world desire for efficient use of energy resources due to increasing energy cost. As a part of this, recent research aimed at the alternatives for conventional methods. In the automobile industry, the fuel consumption of vehicles is a topic of constant importance. Automotive mileage can be improved by reducing the weight of automotive parts. Using the lightweight material as a replacement for heavy materials like copper, steel and cast iron is a more feasible approach to improve the fuel economy. Aluminium alloy properties such as corrosion resistance, formability and high strength to weight ratio have made it a suitable material for use in the automotive sector. Hollow aluminium alloy tubes are formed to different shapes and are widely used in the automobile and aerospace industries. The tubular parts are formed to generate circumferential and axial deformation in the material. Conventional forming methods have limitations like low forming quality, low productivity and high cost. Attempts to obtain improved formability have led interest in the high-speed forming process; among them, the process that stands out is the electromagnetic forming (EMF). EMF is a high-speed forming process that uses Lorentz force generated by the interaction between induced current density and magnetic field to deform workpiece. EMF process has advantages over quasi-static forming like improved material formability, reduced spring back and high forming precision [1] [2]. Depending on the applications, it is often required to combine aluminium alloys with different materials to improve its properties. EMF method is able to produce similar and dissimilar metal joints as strong as a weld within hundreds of microseconds. In contrast to the conventional joining techniques, this method is environmentally friendly with no fume, spatters and heat-affected zones.Though the EMF method is not commercialised yet, the area is certainly of interest in future lightweight automotive design [8].

1.1 Objectives and research significance

To date, EMF has been mainly used to form or to weld materials by compression method. In the case of electromagnetic (EM) compression, the workpiece is present inside the coil that allows freedom in selecting coil shape and size. The technology has rarely been used for high-speed EM tube expansion applications; this is mainly attributed to constraint associated with the coil size. As, in the case of EM tube expansion, the coil is placed inside the tube and hence coil size is limited by tubes inner diameter and thickness. Unpredictable life of the coil is a fundamental problem in EMF. Field strength limits, mechanical and thermal stress are critical parameters that decide the sustainability of the EM coil. Therefore, the first aim of this research is to propose a methodology to design a robust EM coil for EM tube expansion and second is to study the effect of process parameters on tubular workpiece forming and process efficiency. A numerical model is developed for the EM tube forming analysis that couples electromagnetic, structural and thermal physics. A robust helical coil is designed and used for forming of tubular workpieces. Furthermore, the influence of process parameters on tube forming results, process efficiency and coil life is analysed using the analytical, simulation and experimental study. A potential application of the present study is in the nuclear reactor industry [7] involving the joining of hollow aluminium tube to aluminium flange/end sheet by tube expansion. This study also finds its use in space frame structures that require forming of hollow aluminium tubes as well as joints by tube expansion.

1.2 Organization of thesis

In view of the above objectives, this thesis is divided into following broad topics.

- Background
- Development of analytical and numerical simulation model
- Coil design methodology for the tube forming application
- Parametric studies using experiments and numerical simulation

Chapter 2 reviews the literature works specific to the analysis performed in this thesis. A summary of previous work done in the domain such as parametric effect on electromagnetic tube expansion, coupled physics approaches of numerical simulation and coil design for EMF applications is presented.

Chapter 3 gives the details of the experimental setup and a developed numerical simulation model. Various components of the EMF machine and measuring instruments used in experimental work are explained along with their specifications. The numerical model is developed using COMSOL Multiphysics. Governing equations of used physics in the numerical model and physics coupling are explained in this chapter. Further, the numerical model results are validated by comparing them with experimental and some literature results.

In chapter 4 design methodology of a helical coil for the considered electromagnetic tube forming application is discussed. An analytical model is developed to calculate parameters like magnetic field and tube velocity based on designed coil parameters. The analytical results are compared with the experimental and numerical model results. With the help of the numerical model, the mechanical and thermal loading on the coil during forming operation is analysed to dignosis the coil failure.

With the help of experimental and numerical simulation study, the effect of the coil current frequency on electromagnetic tube expansion is analysed in chapter 5. At constant discharge energy, optimum current frequency is obtained for the used experimental setup. Here the optimum frequency refers to the frequency where maximum process efficiency occurs. The dependency of optimum frequency on the discharge circuit parameters and relative skin depth is also discussed further.

Discharge circuit parameters vary during the electromagnetic forming process. The variation of these parameters with time during the electromagnetic tube expansion is analysed in chapter 6. A developed analytical model in the previous chapter is modified by considering the nature of the dynamics of discharge circuit parameters at each time step. The estimated dynamics of discharge circuit parameters are compared with experimental measurements and its effect on discharge current as well as on numerical simulation accuracy is discussed.

Chapter 7 talks about the importance of magnetic coupling between the coil and the tube on the electromagnetic tube forming process. The coupling factor variation with the coil-tube gap is related with the curve fitting using the experimental and numerical simulation results. This relation is used to estimate the nature of process efficiency variation with the coupling factor. Further, the derived curve fitting relation is used to estimate the discharge circuit parameters at different coil-tube gap.

Chapter 8 summarises the overall work and renders future research directions.

Chapter 2

Liturature survey

The EMF concept began from the Kapitza [9] experiments, who has generated the magnetic field that is capable of deforming solid conductors. As mentioned by [8], EMF process for target oriented geometries is first used by Harvey and Brower [10] and patented the process. Many papers published during 1960-70 on electromagnetic forming are consists of the theoretical model of the phenomenon and the experimental validation [11][12][13]. With the increase in computing facilities in 1990, more work on this field is carried out on numerical simulation of the process. With the advantages of coupled 2D and 3D simulations and fast measuring devices [4], the progress in this field is increased in the past three decades. EMF can be classified based on the application such as expansion, compression, welding and crimping of the material. An extensive review of EMF is done by Psyk et al. [8] and Mamalis et al. [14]. They have covered the work carried out in the past in the EMF applications. A large quantity of research is present on numerous aspects of EMF. The emphasize of the present thesis is on the electromagnetic tube expansion, and hence, the literature review here is focused on following topics relevant to the work carried out.

- Electromagnetic expansion-parametric study

- Numerical simulation
- Tool coil used for forming

2.1 Overview of EMF process

EMF is one of the prime applications of the pulsed magnetic field. The technique uses Lorentz force for high-velocity compression and expansion of a workpiece. Figure 2.1 shows a typical schematics of the EMF applications. There are three main components present in the EMF process a capacitor bank, coil (electromagnet) and workpiece. A power supply is used to store the electrostatic energy Ec, which can be calculated from equation 2.1.

$$Ec = \frac{1}{2}CV^2 \tag{2.1}$$

Where C is the capacitance of the capacitor bank and V is the charging voltage. This stored energy Ec is discharged into the coil using a high voltage, high current switch and converted to electromagnetic energy. The overall electrical circuit is capacitive-resistive-inductive nature and hence the current through the coil is damped sinusoidal. The time-varying, pulsed magnetic field is generated by the coil and is linked with surrounding metallic workpiece. Eddy current gets induced in a workpiece with direction opposite to that of coil current direction as shown in figure 2.1.

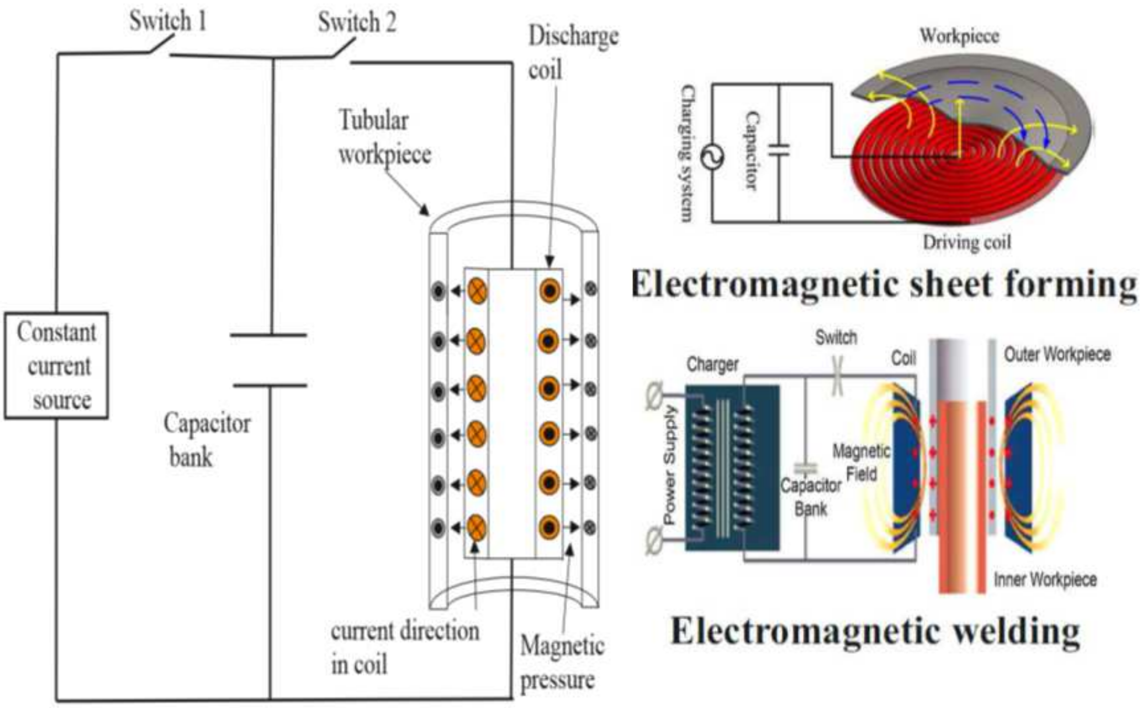

Figure 2.1: EMF applications- Tube forming, Sheet forming [15] and welding [16]

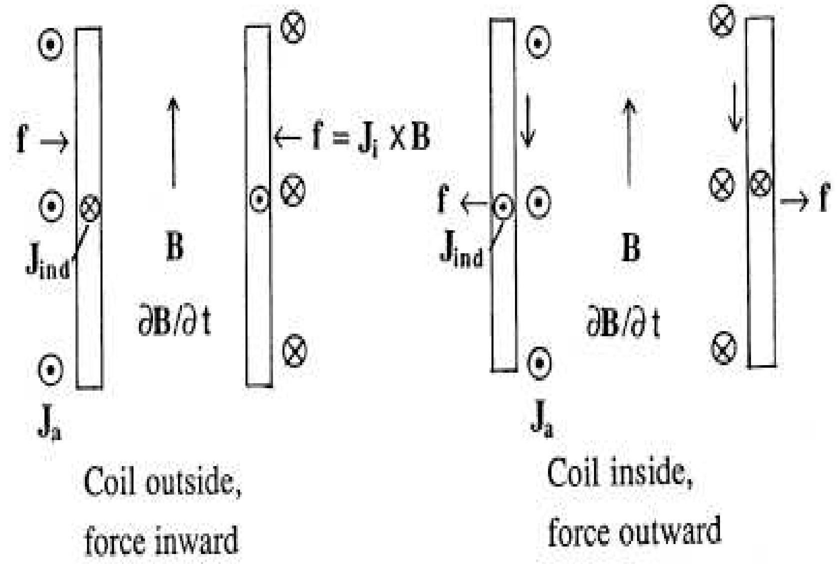

Figure 2.2: Direction of force, magnetic field and current density [17]

Lorentz force responsible for workpiece forming depends on cross products of vectors namely, workpiece induced current density and magnetic flux density as given by equation 2.2.

$$\overline{F} = \overline{J_\phi} \times \overline{B} \tag{2.2}$$

In the case of tube expansion, the current exciting coil is placed inside the tube whereas in the case of tube compression the coil is placed outside the tube. Figure 2.2 shows the Lorentz force direction relative to the position of the coil. For the sheet forming case, a flat spiral coil is used and it is placed parallel to the sheet. The shape of the sheet can be obtained by free forming process, or a die is also used for particular shapes. Electromagnetic welding [3] [6] [18] is also one of the prime applications of the electromagnetic process. In this, the workpiece on which Lorentz force is applied is impacted on the other workpiece with impact velocity in hundreds of meter per seconds. The details of EMF process analysis and involved parameters are given in chapter 4.

Industrial applications

The main industries keen in advancement for EMF applications are automobile and aerospace industries, where weight reduction is a major problem. Fabrication of aluminium parts with high-velocity EMF method helps in weight reduction and thereby improves the efficiency of automobiles. Other than these, there is significant interest in the electrical power sector [19] for lug crimping of the power cable using EMF. Figure 2.3 shows some of the EMF industry applications.

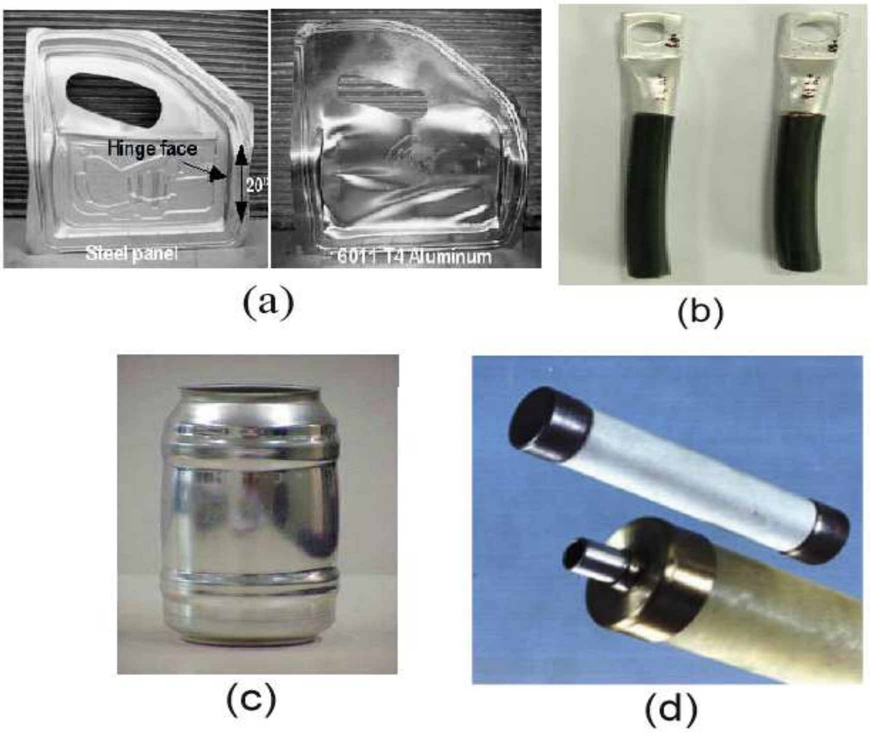

Figure 2.3: EMF applications in (a) Automobile[20] (b) Power sector [19] (c) Packaging [21](d) Nuclear industries [22]

The EMF principle is also used by [23] for manufacturing mobile phone cases [24] and for fuel cell bipolar plates manufacturing. As electrical high conductive material like aluminium frequently involved in lightweight manufacturing, EMF is a promising technology for the manufacturing industries.

EMF -Advantages and limitations

Advantages

- The process completes within hundreds of microseconds which is ideal for achieving a high production rate.
- No environmental constraints for the process. It can be performed in vacuum, inert gas or cleanroom conditions.

- High-speed forming improves the material stretching limit without rupturing as well as reduces wrinkling.[25]

- Being a not contact type process, less surface damage and better surface finishing can be achieved.

- The EMF operation completes in microseconds, and hence heat dissipation of the workpiece is very fast. This makes easy handling of the final workpiece.

Limitations

- The process is more suitable for high electrical conductivity materials.

- Only a small part of total discharge energy is used for forming process that causes poor efficiency of the process.

- A significant requirement of safety aspects due to the involvement of high current and high voltage.

- The applications of EMF are restricted still with simple geometries like tube and sheet. Significant research required for designing induction coils for complex shapes.

- Applications are limited with small thickness workpiece.

Typical process efficiency of the electromagnetic free expansion is 10-25% as reported by [8]. Figure 2.4 shows an energy transfer at different steps of the EMF process. Most of the losses are difficult to avoid.

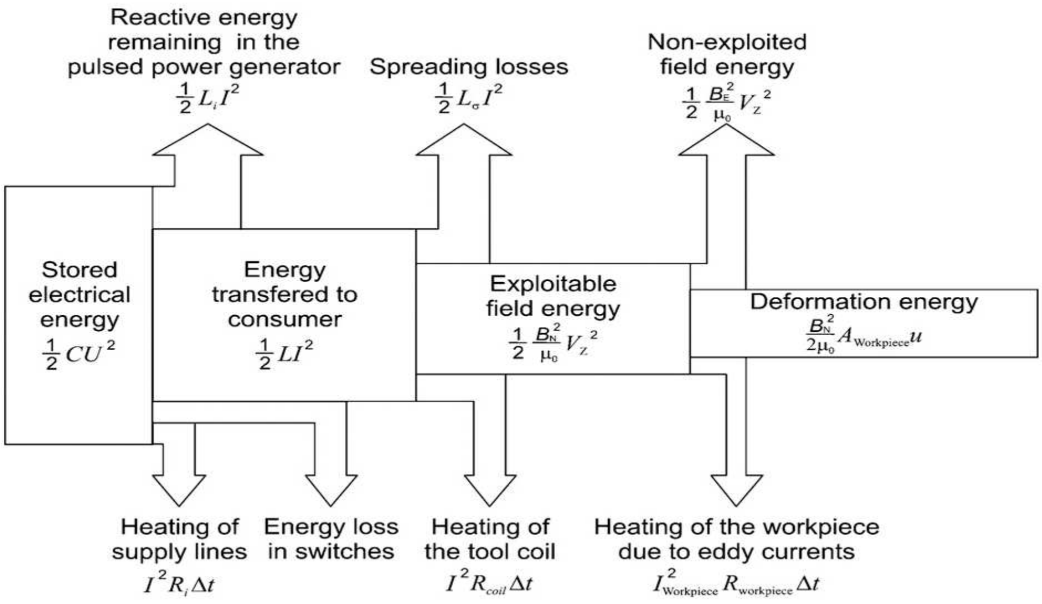

Figure 2.4: Energy transfer during electromagnetic forming [8]

However, methods like the selection of optimum parameters, good coil design can help to improve the utilisation of field energy and thereby increase the EMF process efficiency.

2.2 Electromagnetic expansion

Electromagnetic expansion applications are focused on both sheet and tubular workpiece. There are various electrical and mechanical parameters involved in the electromagnetic forming process that decides resultant forming of the workpiece. The effect of coil-tube relative position on the tube forming shapes is reported in Song et al. [26]. As sown in figure 2.5, when the tube length is smaller than the coil length, maximum force appears at the tube ends, causing the deformation of the tube ends more that the tube centre. Whereas, when the tube length is more than the coil length, maximum tube deformation occurs at the tube centre. Different tube shapes can be obtained by changing the axial position of the tube due to the effects of magnetic force distribution.

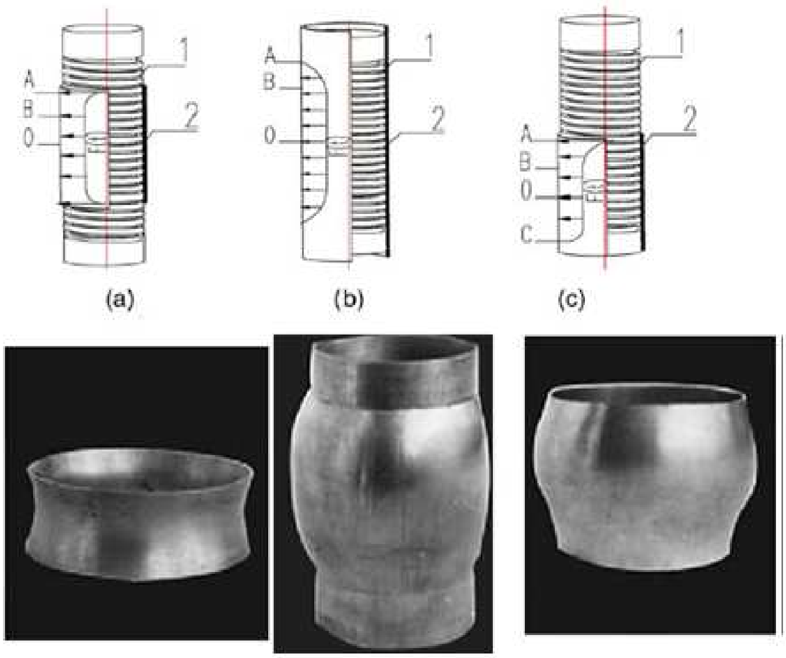

Figure 2.5: photograph of deformed workpieces [26]

The effect of tube length on the acting magnetic pressure is studied by Lee and Lee [27] using the numerical simulation method.

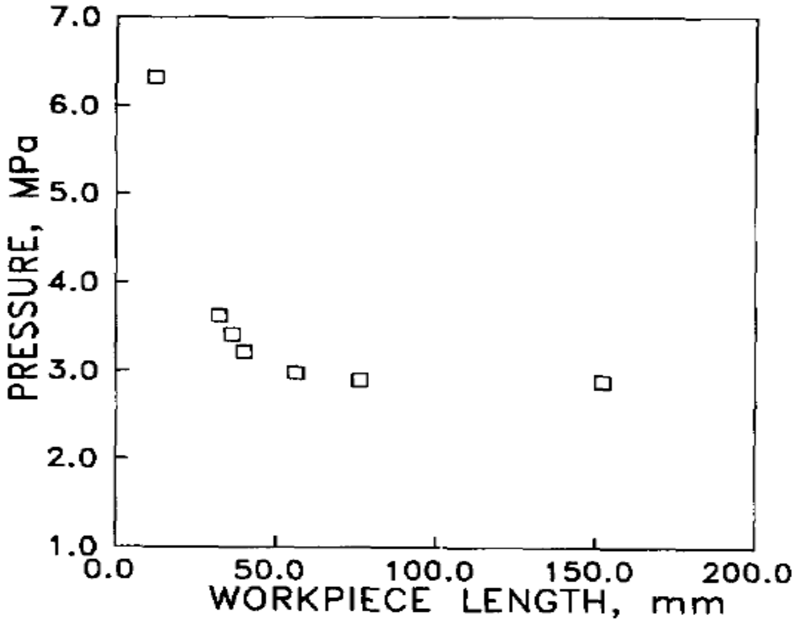

Figure 2.6: magnetic pressure change with the tube length(tube length 76 mm) [27]

Authors found that the magnetic pressure acting on the tubular workpiece is decreased with increase in the workpiece length. However, above the certain limit of tube length, the magnetic pressure remains constant. This limiting tube length is the same as the coil length as shown in figure 2.6

The electrostatic energy E_c stored in the capacitor bank is given by equation 2.3. Selection of capacitance and charging voltage play a key role in forming of the workpiece.

$$E_c = \frac{1}{2}CV^2 \tag{2.3}$$

Variation in capacitance varies the frequency of the current flowing through the electromagnetic coil. As seen earlier, the process efficiency of EMF operation is less and the selection of optimum system parameters can help to improve the process efficiency. For given discharge energy, there exists a frequency of the current in the coil that gives maximum deformation. Very few documents are available that have studied the effect of coil current frequency on the workpiece forming. The effect of frequency on tube compression is studied by Haiping and Chunfeng [5] and relates the optimum frequency for maximum deformation to high plastic strain energy (figure 2.7).

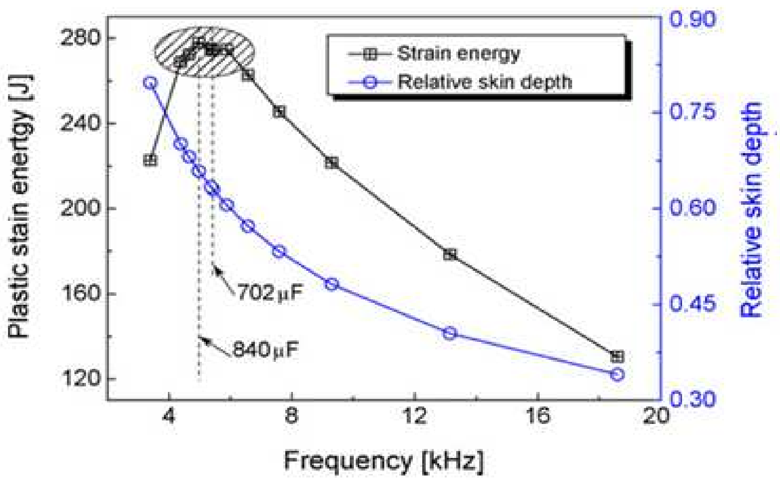

Figure 2.7: Plastic strain energy and relative skin depth [5]

Otin [28] have discussed the estimation of optimum frequency based on FEM modelling. He used Lorentz force magnitude as a base to estimate the optimum frequency. However, he considered the loose coupled approach in the numerical model where the workpiece deformation is not taken into account.

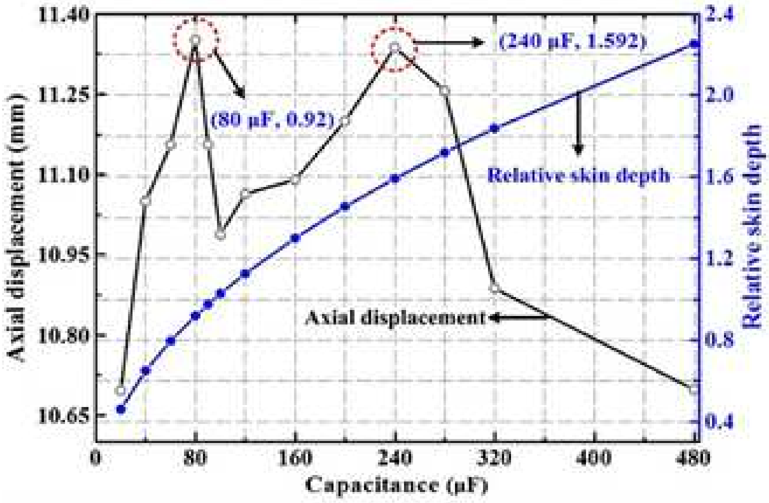

Figure 2.8: maximum axial displacement of sheet and relative skin depth [29]

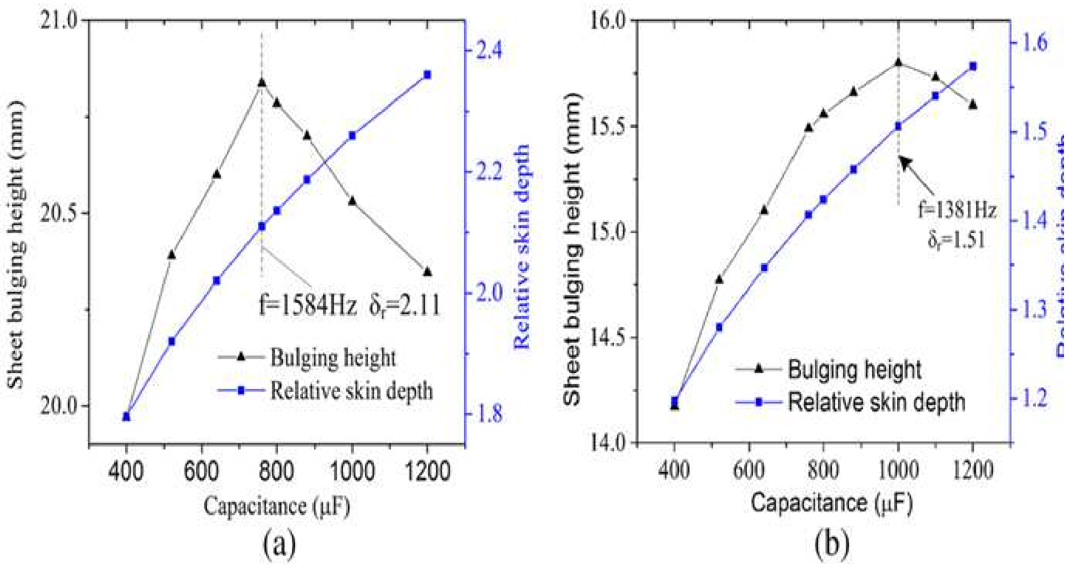

Figure 2.9: Variation of the displacement and δ_r with the capacitance for different sheet thicknesses 1mm,1.5 mm [30]

Authors, [29][30] have discussed the optimum frequency phenomenon for the sheet forming case. They have related the optimum frequency to the relative skin depth δ_r. Here δ_r is the ratio of skin depth to the thickness of the workpiece. It is observed that the optimum frequency is obtained when the δ_r is near to 1 or more than 1 (figure 2.8, 2.9). Estimation of EMF coil current is necessary to determine the generated force and workpiece velocity analytically [31]. Whereas, the coil current is also used as input to some of the numerical models [32] [19]. The discharge circuit parameters determine the coil current, and thus, the accuracy of analytical as well as numerical simulation model depends on the precise estimation of discharge circuit parameters. In EMF, the coil and workpiece are mutually coupled, and the coupling coefficient K is the fraction of magnetic flux produced by the current in the coil that links with the workpiece. While simplifying the electrical equivalent circuit of EMF as an RLC series circuit, K estimation is required. Due to the complexity in the analytical estimation of the K, many authors have made assumptions about K value in their studies. The range of K is from 0 to 1 where K=1 means coil-workpiece are tightly coupled and K=0 when coil-workpiece are magnetically isolated. Nassiri et al. [33] have assumed K as 1 in determining the discharge current and tube velocity analytically. The authors considered K value assumption as one of the factors for the error between analytical and experimental results. In the electromagnetic sheet forming case, Banik [34] assumed K as 0.7 in his study. The K is experimentally measured by Kamal et al. [23] and Thibaudeau et al. [35] for aluminium sheet forming case and observed it as 0.7 and 0.45 respectively.

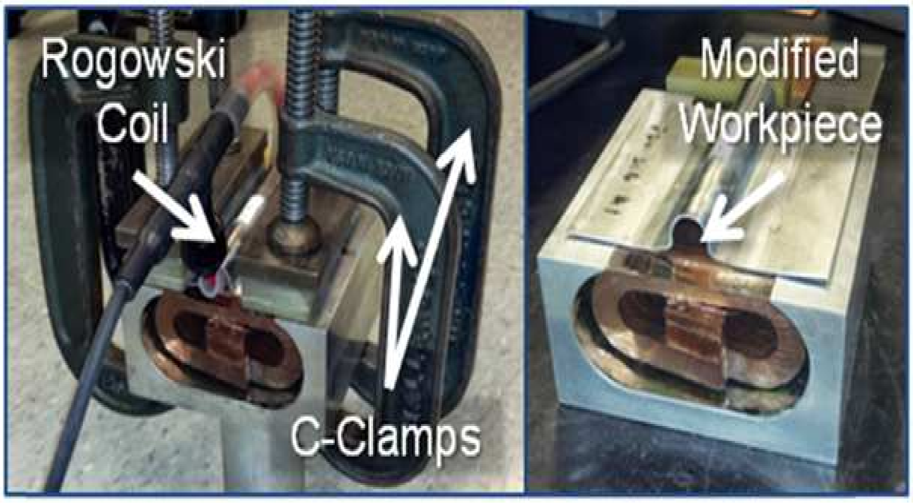

Figure 2.10: Experimental setup for measuring induced current in workpiece [35]

Different experimental methods to measure *K* adopted by [23] and [35] might have caused the discrepancy in *K* value. The experimental approach of *K* estimation using induced current [35] (figure 2.10) is not always feasible. To measure the induced current in the workpiece, enough space between the coil and the workpiece has to be maintained to place the Rogowski coil around the workpiece. Additionally, the testing energy should be low enough to avoid any forming of the workpiece during testing.

2.3 Numerical simulation

To investigate EMF process, numerical simulation is the best choice as it helps to get a realistic insight into the procedure, which is difficult in practice. Most of the times, experimental studies have limitations in the measurements of the parameters due to complex setup and transient operation. The numerical model allows the examination of a wide range of parameters in a short duration, and it also saves the experimental cost. In the past, the EMF process is investigated by various numerical modelling software, as shown in table 2.1.

Table 2.1: Software used in the literature for EMF coupled physics modelling

Sr. no.	Electromagnetic	Structural	Ref. no.
1	ANSYS	ANSYS	[36],[37],[38],[39]
2	ANSYS	ABAQUS	[40],[41],[42],[43]
3	ANSYS	ANSYS / LS DYNA	[32],[44],[45]
4	COMSOL	COMSOL	[46],[47]
5	Analytical/FDM	ABAQUS	[48]

The numerical modelling is developed in 2D axis-symmetric and 3D. The involved physics in EMF are coupled by two approaches, namely, loosely coupled approach and sequentially coupled approach.

Loosely coupled approach

In loosely coupled simulation approach, magnetic and structural physics are solved separately.

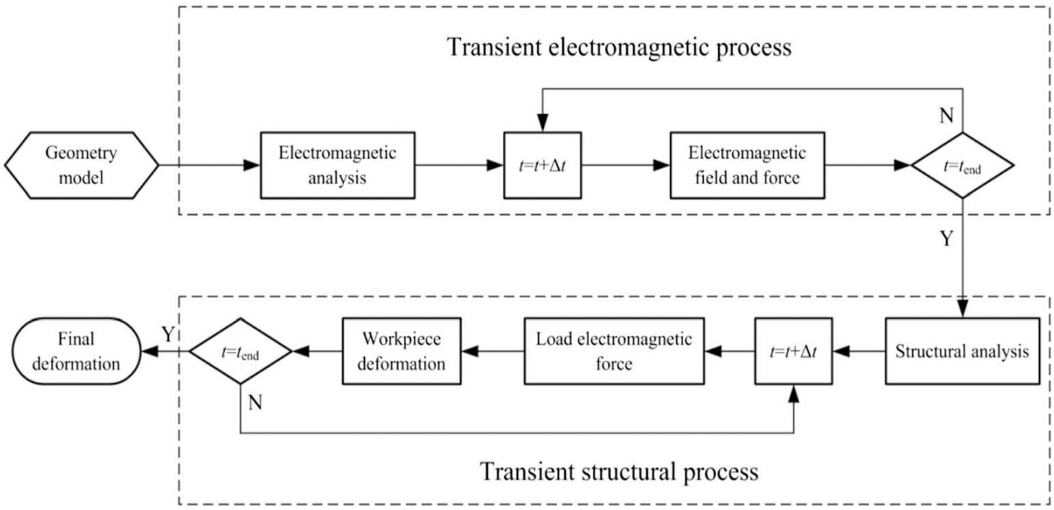

Figure 2.11: Flowchart of the loose coupling method [49]

First, the magnetic field and magnetic force is calculated considering workpiece is stationary and then this force is communicated to structural physics to calculate workpiece deformation. Figure 2.11 shows a typical loose coupled approach. The loose coupled approach is one way which does not consider the workpiece forming effect on the magnetic force or on the discharge circuit parameters.

Sequentially coupled approach

The sequentially coupled simulation approach is shown in figure 2.12. In this, both the magnetic and structural physics are solved at every time step, and the feedback of workpiece displacement is taken into account to calculate the magnetic pressure at the next time step. During the forming process, workpiece goes away from the coil and hence the acting magnetic force at next step is less than the case when the workpiece is stationary.

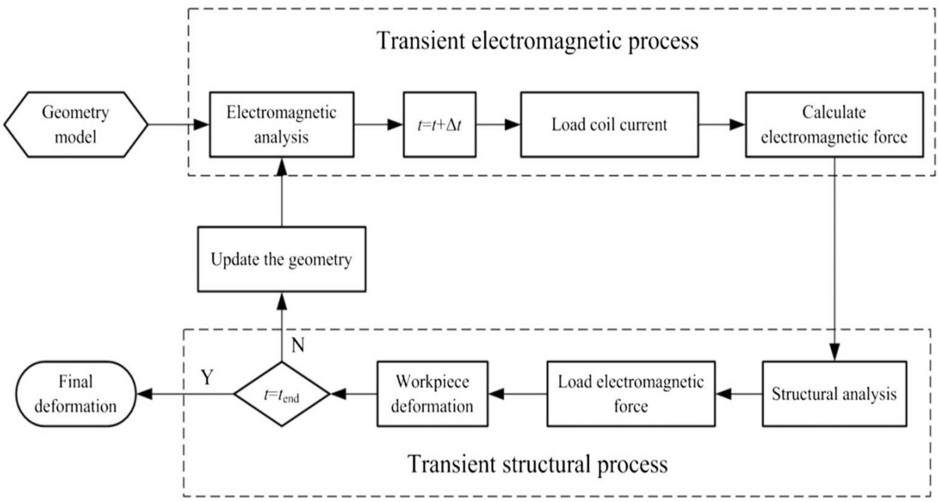

Figure 2.12: Flowchart of the sequential coupling method [49]

Comparison of both the approaches is made in [50] [43][37] literature papers. Author [50] found that a loosely coupled approach leads to an overestimation of workpiece final expansion which is as high as 30%. Therefore a loosely coupled approach is useful for smaller displacement and fast deformation process. This observation is in line with [43] findings. Authors observed a good match at a low voltage between experimental and loose coupled approach results. However, at high voltage sequential coupled simulation showed more accuracy than the loosely coupled approach.

In the EMF analysis, the discharge circuit is simplified as series RLC circuit having a constant value of *R* and *L*. In a practical case, due to workpiece forming, magnetic coupling between the coil and tube changes and because of that *R* and *L* becomes dynamic. The reason for the constant discharge circuit parameters assumption is that only first wave of magnetic pressure is used to deform the material as observed in some studies [44]. This means that the second and further magnetic pressure waves where the dynamics discharge circuit is high have no use in workpiece forming. Contrast to these, it is also observed that not only first pulse but subsequent pulses of current and pressure are also contributing to resultant forming [42].

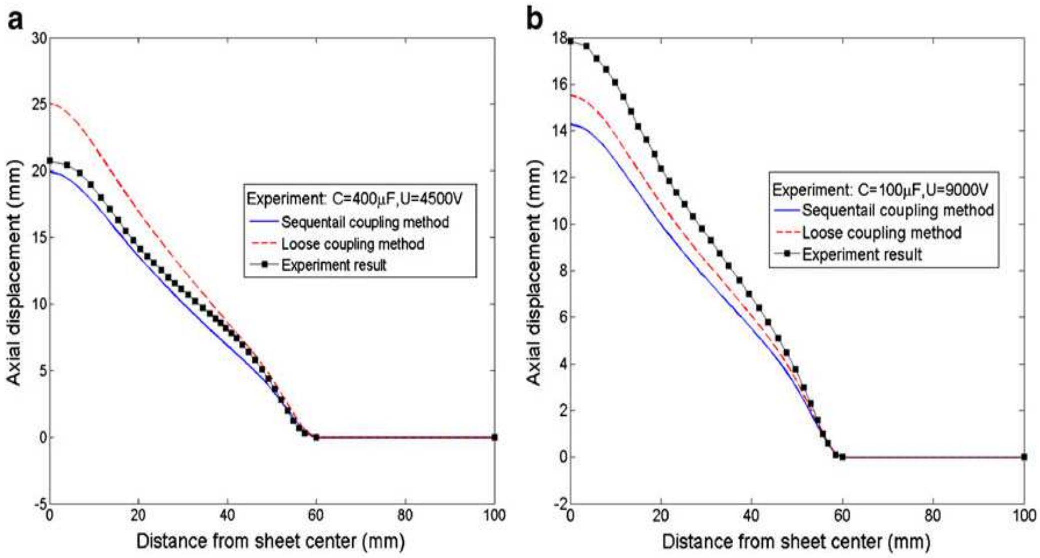

Figure 2.13: Displacement with one pulse and two pulses current 400 uF/4,500 V [42]

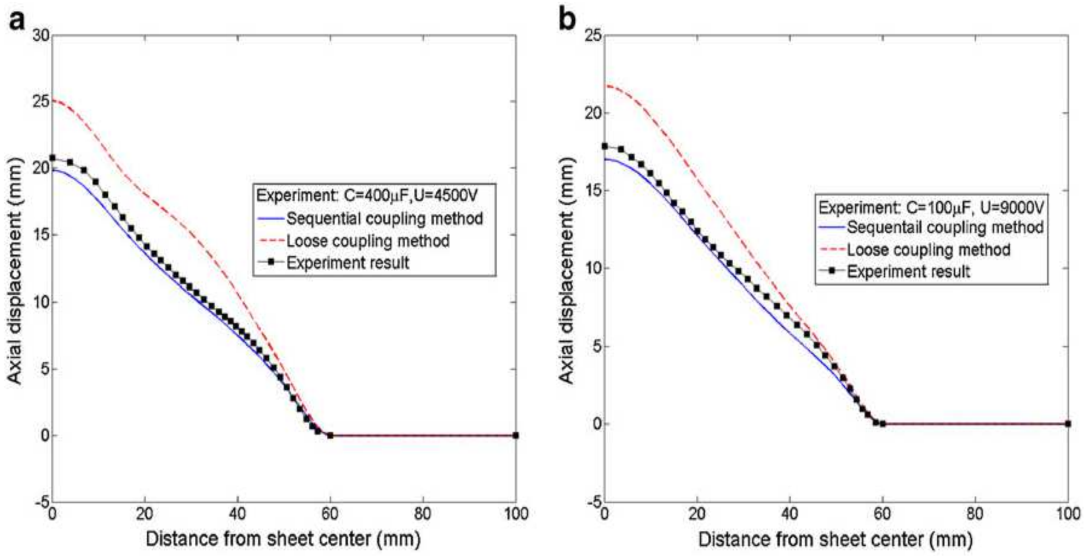

Figure 2.14: Displacement with one pulse and two pulses current 100 uF/9,000 V [42]

As shown in figure 2.13, at 400 μF, the final sheet deformation is the same when the first and second current pulse current excitation is considered. However, figure 2.14 shows that at 100 μF, the final deformation of the workpiece is high when considered second current pulse excitation. Here, the author found that the effect of the second current pulse on sheet deformation increases with the increasing of the discharge frequency. The importance of the dynamic nature of discharge circuit parameters is highlighted in [49]. In this, the author has modified a loosely coupled simulation by considering a current correction factor as seen in figure 2.15. The electromagnetic force obtained by loose coupled and fully coupled numerical model is compared and by that a current correction factor is calculated. With the modified loose coupled approach, the relative error is substantially reduced in sheet forming case.

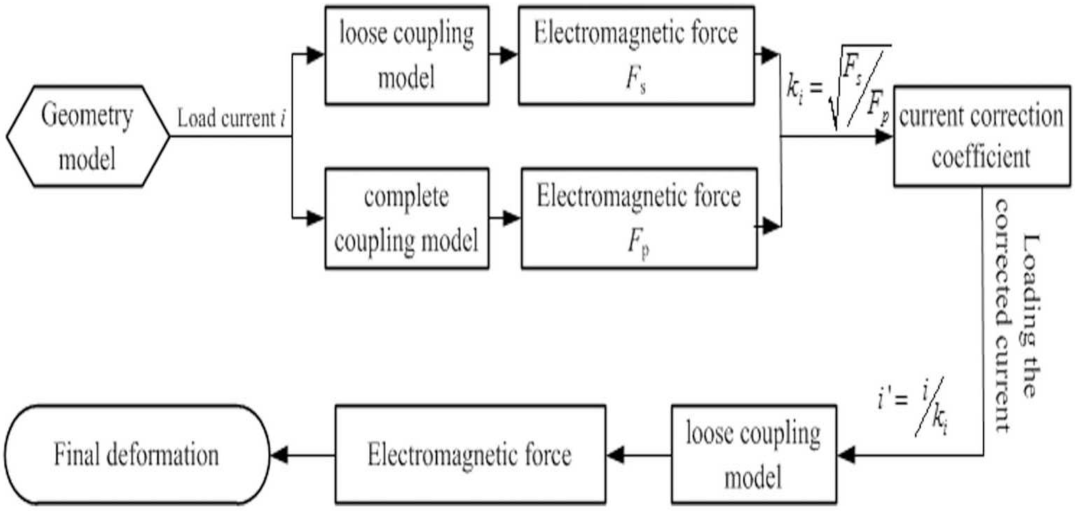

Figure 2.15: Modified loose coupled method with the current correction factor [49]

Being a complex and transient process, analytical estimation of workpiece deformation is not much preferred in the literature. Authors in [4][31][51] have used 1D calculations to estimate magnetic pressure and workpiece displacement. Newtons law of motion is used to estimate the workpiece acceleration against applied magnetic pressure. The analytical method is found handful for initial estimation of parameters.

2.4 Tool coil design aspects and failure modes

Design

The electromagnetic coil is the heart and core of the EMF process. Unpredictable life of the coil is a fundamental problem in EMF. Field strength limits, mechanical and thermal stress are critical parameters that decide the sustainability of electromagnetic coil (electromagnet). Thus, it necessitates a careful design and modelling of the electromagnetic coil. The design of the coil is decided by the geometry of the workpiece which is to be formed. For the sheet forming application, Authors [23] proposed a uniform pressure actuator (coil) as shown in figure 2.16 and 2.17. A conducting outer channel is provided around the coil acts as a return path for eddy current. The advantage of proving the return path is that the magnetic field generated around the entire coil is used for the forming process. This improves the Lorentz force on the workpiece and thereby improve the forming efficiency.

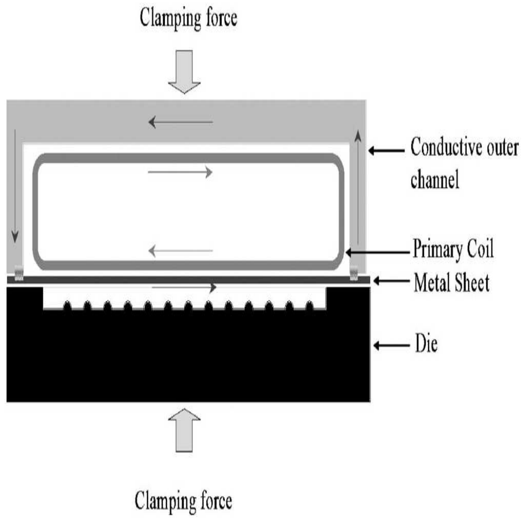

Figure 2.16: Copper channel with the coil [23] Figure 2.17: Uniform pressure coil [23]

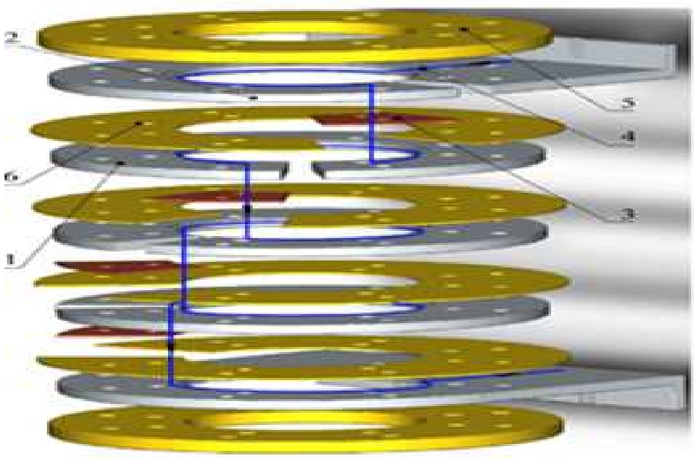

Figure 2.18: Bitter coil [52]

Authors [52], developed a bitter coil for electromagnetic compression forming and welding applications. As shown in figure 2.18, the coil turns are in the form of discs. Insulation discs are provided in between each coil discs and at the ends. The electrical continuity from one disc to other disc is obtained by small copper discs. Authors have considered an electrical, mechanical and thermal aspects in the coil design. Magnetic field measurement and short circuit test are performed to compare designed coil parameters with analytical ones. Apart from [23] and [52] no one discussed the coil design aspects in detail for the EMF applications.

Failure

Because of the stresses acting on the coil during EMF operation, failure of the coil is a common issue in all EMF applications. Despite this, very few literature papers have reported the coil failures cases. Golovashchenko [53] did the failure analysis of rectangular and spiral shaped coil for flat sheets application.

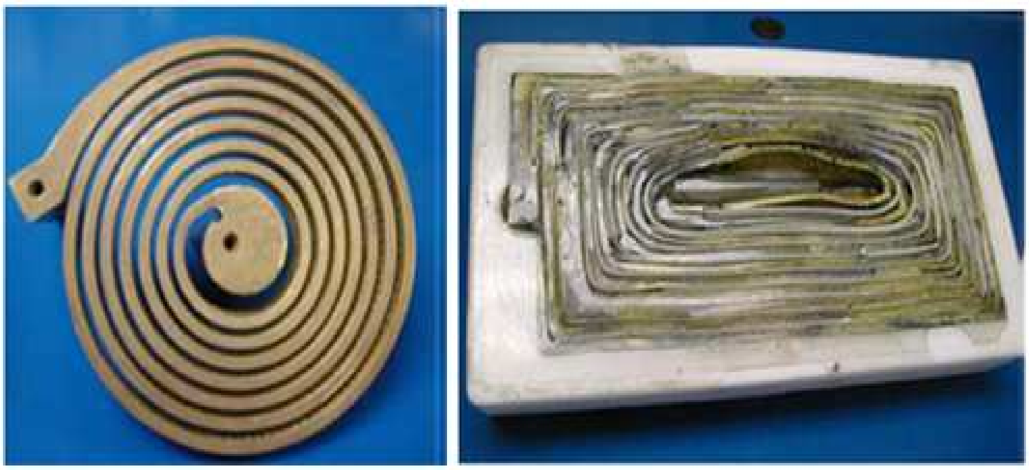

Figure 2.19: Circular and spiral flat coil with Central deformed turn [53]

Figure 2.20: Destruction of massive multi-turn coil made of steel [54]

As observed by the author, failure in both the coil of figure 2.19 is due to deformation of the central turn of the coil and expansion of clearance between first and the second turns. Recently authors [54] have observed the rectangular steel coil destruction. The coil adjacent coil turns are distorted, which leads to non-uniform clearance between coil and workpiece. This eventually changes the electromagnetic field magnitude and pattern compared to the initial coil. Mechanical strength analysis of the coil in the sheet forming case is demonstrated by [55][15]. Using numerical simulation, Von Mises stress acting on the coil is calculated and designed the coil such that it can withstand this stress with some factor of safety.

The thermal strength of the coil is also an important aspect. The efficiency of the EMF process is very less and a major part of the energy is converted into the joule heating of the tool coil. In a high production rate, accumulation of heat results in the reduction of the coil life. Despite this importance of the thermal loading, not enough information about the coil temperature and its impact on coil life is available. Increase in coil temperature increases the material resistivity that intern increases the Joule heating. [56] have measured the insulation surface temperature provided over the coil surface. Though the measurement is taken after the experiments, the author has found that the maximum temperature of the coil winding can easily overstress the insulation and reinforcement of the coil. Crowbar circuit is one of the option to reduce the thermal loading as suggested by [57]. It is observed that for the same output, the maximum temperature of coil winding is reduced from 1060^0C to 530^0C using the crowbar circuit. The analytical approach for joule heat losses in the electromagnetic coil is studied by [58]. Authors have found that at high energy, up to 20 $\%$ higher heat losses occurred when the temperature dependent conductivity is considered in the analytical approach. Recent time, the experimental measurements of pressure distribution [54] and coil surface temperature measurements [59] are attempted. Pressure-sensitive film technology is used in [54] to analyse the pressure distribution applied to sheet metal and in case of temperature measurement [59], a Fiber-based optical frequency domain refractometer (OFDR) is used. Still, diagnosis of the coil failure and improvement the coil life are the strong challenges in front of researchers.

2.5 Manufacturing complexities and industrial constraint of EMF technology

The EMF technique is capable to give strong contest to conventional forming and joining processes. However, in the past, the EMF technology is mainly adapted in academics and small -batch size productions. Applications of EMF technique on large metal forming still not fully developed. The major emf process applications are focused on delivering plastic deformation of small workpiece area. The obstacles that limit the application of EMF in the world of civil-industrial demands are discussed below.

The short lifetime of the forming coil

The electromagnetic coil is a vital component of the EMF process. Every EMF application has its own coil design requirements. The life of the coil is a major concern in almost all the EMF applications. Very few research works discussed the tool design with regard to the forming task, coil lifetime and coils durability. Because of the transient process and involvement of electrical, mechanical and thermal coupled physics, it is difficult to trace the exact coil failure reasons.

The EMF technique will only be adopted in mass production when technical and economic benefits are given. The initial cost of EMF setup is high because of costly components like the coil and the capacitors. The running cost increases due to frequent coil failure and due to the time that is required for replacing the coil. In a laboratory EMF system, coil replacement may be few minutes task. However, the situation changes if the system is integrated into a production line.

EMF complexity

EMF technique is highly dynamic and Multiphysics in nature that involves electrical, mechanical, thermal and metallurgical phenomenon. There are many parameters strongly influencing electromagnetic forming process. Hence, it is difficult to obtain a comprehensive and generalized methodology on controlling the high velocity plastic forming/welding behavior. A lot of research has been done in various applications of the process but most of the results are referred to special case studies. For e.g., there is no analytical formulation that can guarantee weld occurrence in EMW applications. Researchers that have presented the results of weld occurrence are of case specific. Lack of knowledge of precise correlations between manufacturing technique and strutting parameters have prevented the complete exploitation of the EMF potentials.

The complex coil-workpiece arrangement limits the experimental measurements and hence numerical modelling is suitable for analysis of the process. There was a lack of commercially available and user-friendly FE software which is suitable for the modelling of entire electromagnetic forming processes. They are typically incapable of solving complex industrially relevant applications. Recent progress in software and modelling are suitable for such tasks. Various simulation frameworks based on the Eulerian formulation [60] and smoothed particle hydrodynamics (SPH) [61] are developed recently. These models can able to predict the interface wavy morphology occurred during the impact welding. However, long calculation time, economic process design and optimization is still a concern.

Forming larger size parts requires a high magnetic field and energy. Increasing the input voltage and capacitance cause insulation problems, cost and safety issues. Also, it is a challenging task to design sustainable high magnetic field generating coil. Hence, present research directed over other possible methods to form large parts. Electromagnetic incremental forming (EMIF) is a way adopted by [62],[63] for large components forming. The important idea of EMIF is to use the form the material at a certain length and then use a series of discharge consecutively to produce large parts. Another method is to combined other forming method with EMF. Authors Cui et al.[64] have combined the stretch forming and electromagnetic forming to form a large diameter sheet. Combination of EMF with electromagnetic heating is tried by researchers. The idea in electromagnetic heating forming (EMHF) is to reduce the deformation resistance of work pieces by preheating treatment, and then deform workpiece with small discharge energy.

Despite the potential advantages of EMF, much more efforts still required to overcome the obstacles of the existing EMF technique and to adopt the technique in industries at large scale.

Chapter 3

Experimental setup and numerical simulation model

In this thesis, Parametric influence on the electromagnetic tube expansion is analysed using analytical, numerical and experimental study. This chapter discussed different parameter selection criteria for EMF applications. Along with this, the experimental setup used for the analysis and the procedure followed during the experiments is presented. Further, the information of the developed numerical model is given and the simulation model results are validated by comparing them against the literature and experimental results.

3.1 EMF design framework and experiential setup

In EMF technique, the required Lorentz force for the workpiece forming is generated by the conversion of electrostatic energy into the electromagnetic energy. This necessitates the experimental system should capable of required electrostatic energy storage capacity. A typical flow of EMF requirements for different applications is given below.

- Based on the material property and geometry, the pressure required to deform the workpiece plastically with a certain velocity is estimated. In the case of EMW, the pressure requirement is based on the required impact velocity.

- The magnetic field is estimated to achieve the required magnetic pressure.

- The coil discharge current is calculated to achieve the magnetic field.

- The capacitor charging voltage is determined from the discharge current.

Magnetic pressure requirement

Lorentz force is associated with magnetic pressure. This magnetic pressure exerted on the workpiece both deforms and accelerates the workpiece. The generated magnetic pressure must be sufficient to overcome workpiece materials yield stress. EMF is high speed forming process. The material flow stress is increased and the ductility is decreased because of high speed forming. Hence, the magnetic pressure must be sufficient to deform the material with a certain velocity. The velocity can be estimated from material acceleration. For electromagnetic welding applications, the material should deform and impact over other material with impact velocity sufficient to obtain the weld. The required magnetic pressure is calculated as the sum of two components,

$P = P_{def} + P_{acc}$

P_{def}: pressure required to deform the workpiece

P_{acc}=pressure required to accelerate the workpiece

The minimum magnetic pressure to begin circumferential deformation of the tube can be obtained using the equation of motion of the workpiece [65].

$$P_{def} = \frac{2w_t}{D}\sigma_y \tag{3.1}$$

Where w_t and D are tube thickness and diameter respectively and σ_y is the yield stress of aluminium material. Newton's second law of motion is used to predict the workpiece acceleration and thereby velocity.

$$P_{Acc} = \frac{F}{A_w} \tag{3.2}$$

$$F = mass \times Acc \tag{3.3}$$

$$Acc = \frac{P_{Acc}}{w_t \rho} \tag{3.4}$$

$$Acc = \frac{(Velo)^2}{2S} \tag{3.5}$$

From Equation 3.4 and 3.5,

$$P_{Acc} = \frac{w_t \rho (Velo)^2}{2S} \tag{3.6}$$

Where, F=force, w_t =workpiece material thickness, ρ= density of material, Acc= acceleration, Velo= velocity, s=displacement, A_w= area of workpiece

Magnetic Field

The Lorentz force is associated with magnetic pressure and hence the pressure exerted on the workpiece is a direct consequence of the magnetic field. The magnetic field originates from the discharge current that flows through the coil. The magnetic pressure calculated by Equation 3.7.

$$P_{mag} = \frac{B^2}{2\mu_0} \tag{3.7}$$

That gives

$$B = \sqrt{2\mu_0 P_{mag}} \tag{3.8}$$

Current and voltage requirement

The current magnitude required to generate the magnetizing field is can be deterimined from Equation 3.9

$$B = \frac{\mu_0 N i}{l_c} \tag{3.9}$$

Based on the required magnetic field, the current i can be estimated. Accuracy of B estimation can be improved by using coil geometry based B calculations. Once the necessary current is estimated, the required voltage can be found from following current Equation 3.10

$$i(t) = \frac{V}{\omega L_T} e^{-\beta t} sin\omega t \tag{3.10}$$

Where,

$$\omega = \sqrt{\frac{1}{L_T C} - \beta^2} \tag{3.11}$$

$$\beta = \frac{R_T}{2L_T} \tag{3.12}$$

Selection of Capacitor

As observed from the above equation, the current is dependent on discharge circuit parameters like R, L and C. Energy stored in the capacitor is given by Equation 2.1. Thus the energy required for workpiece deformation can be obtained from varying C and V. Capacitance affects the discharge current frequency as seen from Equation 3.11. The skin depth decides upper limit of capacitance.

$$\delta = \frac{1}{\sqrt{\pi f \sigma \mu}} \tag{3.13}$$

Where f is the coil damping current frequency, σ is workpiece electrical conductivity and μ is the permeability. The magnetic field diffusion in the workpiece depends on the workpiece skin depth. When the skin depth is small in comparison to the thickness of the workpiece, the penetrated magnetic field is usually neglected. The capacitance must be set such that it would make skin depth δ small in comparison to the thickness of the workpiece. As explained in chapter 5, selecting very less capacitance is also not suitable for forming process.

Power supply

Once the capacitance and system resistance and inductance are fixed, the power supply must be able to charge the capacitors to the required charging voltage. Increasing the voltage level increases the peak current and thereby magnetic field and pressure.

Tool coil

Coil selection is based on the EMF application. As shown in section 2.4, Different coil shapes are used according to requirements. The coil should be designed keeping its resistance and inductance to a minimum. As seen from Equation 3.9, the magnetic field generated by the coil is dependent on the number of turns of the coil and length of the coil. whereas, from Equation 3.14, the coil inductance is affected by the number of turns of the coil, its area and length.

$$L_c = \frac{\mu_0 N^2 A_c}{l_c} \tag{3.14}$$

The designed coil must be able to generate required magnetic field with minimum resistance and inductance. As shown in the chapter 4, coil failure is the major concern in EMF technique. Thus, the coil should be provided with suitable insulation. The tool coil is connected to capacitor banks via connecting cables. For our experiments, we have used a helical coil for the tube expansion experiments. The design methodology of the helical coil is explained in chapter 4.

Effect of workpiece material properties

Important workpiece parameters for EMF process are the geometry, the electrical conductivity, and mechanical properties. The coil shape is decided based on the workpiece geometry. A thicker workpiece eventually required more pressure to deform and accelerate. High electrically conductive material has less skin depth and high eddy current density. Hence, the energy required to generate the same magnetic pressure for high conductive material is less than low conductivity material. More energy is transferred in Joule losses in the smaller electrically conductive material. The work piece material should have good permeability to generate eddy currents. Usually electrically conductive material has better permeability. Materials yield strength is important parameter as it decides the required magnetic pressure and thereby energy requirement. High yield strength and dense material required more energy to obtain its plastic deformation. Materials stress-strain property is important to estimate materials travelling velocity and displacement. Thermal conductivity of the material has not significant influence due to transient nature process. In the case of EMW, during the impact, the temperature rise causes local melting of the least conductive material. As the process is short, the melting observed only on outer interface layer. Aluminium-magnesium (Al-Mg) alloys (5XXX series) have great attention in the automotive industry due to their high strength to weight ratio, corrosion resistance, weldability and recycling potential. Therefore, Al 5052-O tube has been chosen for forming experiment in this work. The Al 5052 material composition is given in table 3.1 whereas the mechanical and electrical parameters are given in table 3.2.

Table 3.1: Al 5052 chemical composition

Component	Wt %	Component	Wt %
Al	95.7-97.7	Fe	Max 0.4
Mg	2.2-2.8	Si	Max 0.25
Cr	0.15-0.35	Zn	Max 0.1
Mn	Max 0.1	Cu	max 0.1
Other, total	Max 0.15		

Table 3.2: workpiece properties [66]

Material	Aluminum 5052
Tensile strength	89.6 MPa
Ultimate Tensile Strength	193 MPa
Density	2680 kg/m^3
Modulus of Elasticity	70.3 GPa
Poisson's ratio	0.33
Electrical conductivity	20 MS/m

Experimental setup

We have used an electromagnetic manufacturing system having an energy capacity of 40 kJ. Figure 3.1 shows the experimental set up of 40 kJ system. The system has three compartments. First is the power supply, second is the capacitor bank with trigatron and third is the coil-workpiece bench. This system is rated for 20 kV charging voltage and 224 μF as maximum capacitance. There are total 4 capacitor banks of 56 μF capacitance each. Both the number of capacitor banks and charging voltage can be changed to control the discharge energy and voltage. The system operation is controlled through PLC (Programmable Logic Controller).

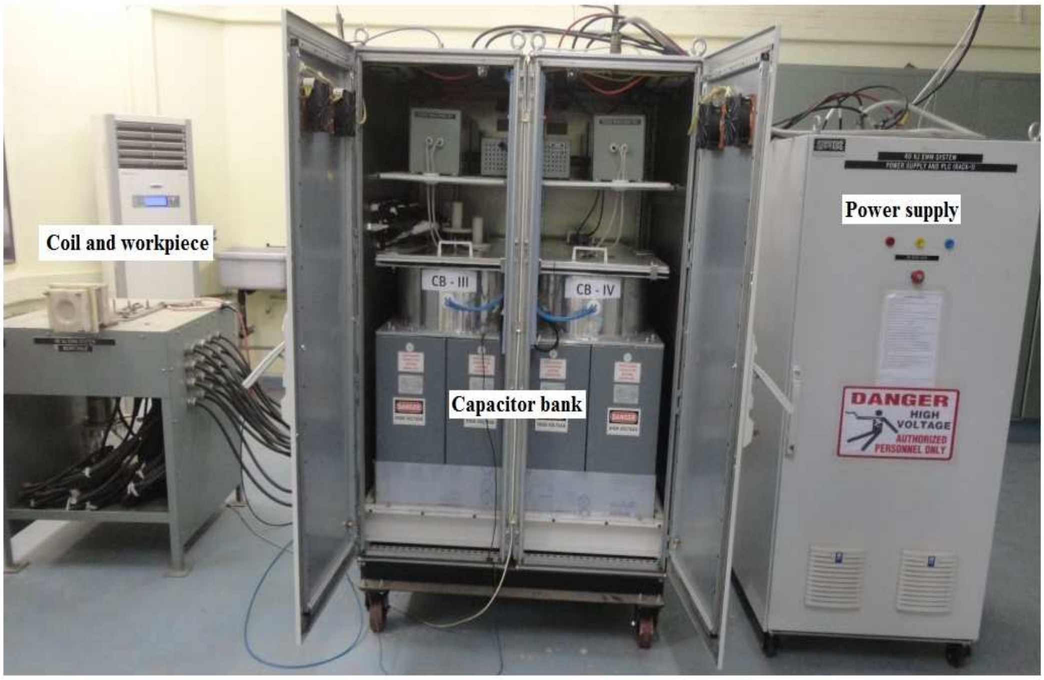

Figure 3.1: 40 kJ Machine used for the experiment

A constant current power supply is used to charge the capacitors. The capacitor usually takes a few seconds to get charge and the charging time of the capacitor is controlled by the charging current. The power supply has a facility for setting charging current. Resistors are also provided in the power supply rack and known as dump resistors. Whenever required, the capacitive energy can be dumped into these resistors. There is a provision provided to dump the capacitive energy that remains after the capacitors are discharged into the coil.

Trigger based spark gap is used as a switch to discharge the electrostatic energy stored in the capacitors into the coil. The gap between the spark gap is adjusted in such a way that the charging voltage of capacitance is less than the self-breakdown voltage of the spark gap. Trigger pin is connected to the spark gap and trigger control is used to discharge the stored energy of the capacitor in the coil at the required voltage which is below the self-breakdown voltage of spark cap.

Measurement tools

Coil current measurement

The current passing through the coil is measured by the Rogowski coil. The Rogowski has sensitivity factor 1V/100 kA. It is capable of measuring the current up to 1MA with MHz frequency.

Magnetic field and tube displacement measurement

The search coil is used to measure the magnetic flux density. It is a small flat coil of fine insulated wire with a large number of turns. It is in-house developed and calibrated with a standard instrument. Search coil has output in terms of voltage where 1 volt = 11.8 Tesla. In house developed a laser based device is used to measure the workpiece displacement with time.

System parameters

Increasing R causes more damping of the current waveform but on the other hand, it increases the heating issue. The R and L affects the discharge current magnitude and frequency. Capacitors are connected to the coil through cables. The cables have its own resistance and inductance. Again, coil has its resistance and inductance. The entire resistance and inductance of EMF system must be kept minimum to obtain the required workpiece forming with less energy. The system parameters are necessary for estimating discharge current analytically. We have performed the short circuit test [67] to determine the resistance and inductance of the system. These parameters are mainly of the path from the capacitor bank to the discharge terminals of the coil. Table 3.3 gives the 40 kJ system parameters R_{sc} and L_{sc}. Short circuit test is performed at 17 kV operating voltage and 112 μF capacitance.

Table 3.3: Short circuit test results

$System$	V	C	I_{peak}	f_{sc}	R_{sc}	L_{sc}
40 kJ	17 kV	112 μF	182 kA	16.1 kHz	10 mΩ	0.9 μH

3.2 Typical operating procedure

The following general procedure is used for the experiments

- The helical coil is connected to the high voltage terminals. These terminals have a connection to the capacitor bank via cables. The coil position is mentioned horizontally along its axial length.
- The tubular workpiece is placed over the coil, and after that Delrin insulator is used to fix the coil and tube. This helps to keep a uniform gap between coil and workpiece and also to avoid movement of the tube and coil during the forming operation.
- Rogowski coil is placed across the helical coil and its signal end is connected to the oscilloscope.
- Capacitor banks are selected depending on the required capacitance.
- The capacitors are charged to specified voltage using a constant current power supply.
- Using the trigger control, the stored energy in the capacitors is discharged in the coil.

High voltage and other safety

One of the drawbacks of EMF process is the significant requirement of safety aspects due to the involvement of high current and high voltage. Following are the safety measures provided for the system and the precautions that are taken at the time of experiment testings.

- All the switching operations are controlled through PLC based controlling system.
- Grounding is provided to the cabins carrying the manufacturing instruments.
- After every experiment, the dump resistors are used to discharge the remaining energy of the capacitor (if any).
- The ground rod is used at the capacitor terminals after the experiments to make sure the complete discharge of energy stored in the capacitors.
- Earmuffs are used during the experiments to protect the ear from high noise that usually occurs at the time of tool coil failure.

3.3 Numerical simulation model

An accurate and precise numerical model can avoid the number of experimental testings. It also saves time and cost. In the complicated system and in transient operations, the numerical model helps to get an insight of the process, which is difficult in practical. In this work, we have developed an axisymmetric, 2D sequentially coupled simulation model using COMSOL Multiphysics software. It is a finite element based software and can able to couple different physics. We have used AC/DC, structural mechanics and thermal modules of the software. Following are the assumptions made during the model development.

Assumptions

- The targeted geometry of the coil and tube is considered as axis-symmetric. The cylindrical coordinate system is used for the developed 2D model that consists of axial and radial components. The circumferential component effect is less and is neglected here.

- Being the conductive materials, the effect of magnetic flux density on material permeability is less and hence permeability of coil and workpiece is assumed constant.

- The effect of temperature on material properties is not considered. The EMF is a transient process so the change in material properties due to the temperature has less effect on the process parameters [40].

- The discharge circuit parameters are assumed constant during the forming process.

- Displacement current and free charge density is neglected.

Magnetic field model

In the electromagnetic field model, magnetic vector potential method [68] is used as given below to solve the Maxwell equations.

$$\nabla \cdot \vec{B} = 0 \tag{3.15}$$

$$\nabla \times \vec{E} = \frac{-\partial \vec{B}}{\partial t} \tag{3.16}$$

$$\nabla \times \vec{B} = \mu \vec{J} + \mu \epsilon \frac{\partial \vec{E}}{\partial t} \tag{3.17}$$

Where *E* is the electrical intensity (V/m), *J* is the current density in the coil (A/m^2), *B* represents magnetic flux density (T), μ is the magnetic permeability of medium (H/m), ϵ is permittivity of the medium (F/m). Representing magnetic and electric field using magnetic vector potential *A* such that

$$\vec{B} = \nabla \times \vec{A} \tag{3.18}$$

$$\vec{E} = -\frac{\partial \vec{A}}{\partial t} \tag{3.19}$$

Substitution of equations 3.18 and 3.19 in equations 3.15-3.17 can give

$$\nabla \times (\frac{1}{\mu}\nabla \times \vec{A}) = \vec{J} - \sigma\frac{\partial \vec{A}}{\partial t} \tag{3.20}$$

Where σ is conductance of medium (S/m) and $\sigma\frac{\partial A}{\partial t}$ is the induced current density in the tube (A/m^2). According to Lorentz formula, EM force acting on Workpiece is given as

$$\vec{F} = \vec{J} \times \vec{B} = \frac{1}{\mu}(\nabla \times \vec{B}) \times \vec{B} \tag{3.21}$$

In the axisymmetric case, *F* can be further divided into the axial and radial components

$$\vec{F_r} = \vec{J_{ephi}} \cdot \vec{B_z} \tag{3.22}$$

$$\vec{F_z} = \vec{J_{ephi}} \cdot \vec{B_r} \tag{3.23}$$

Structural model

The obtained force in the electromagnetic model is used as an input in the mechanical model. In the structural mechanics physics, tube displacement is calculated using the following equation.

$$\rho\frac{\partial^2 \vec{u}}{\partial t^2} - \nabla \cdot \sigma_s = \vec{f_m} \tag{3.24}$$

Here, ρ is the mass density of workpiece, *u* is displacement vector, σ_s is stress tensor and f_m is magnetic force density. The underdamped coil current is given as input to the magnetic field model. At each time step, tube geometry is updated based on Lorentz force. Both the electromagnetic and structural models are solved till tube settles to its final displacement value.

Strain rate dependent Johnson-cook plasticity model is used to define the workpiece stress as given in equation 3.25

$$\sigma_s = [A_w + B_w(\epsilon_p)^n][1 + C_w ln(\dot{\epsilon}_p)][1 - [\frac{T - T_0}{T_m - T_0}]^m] \tag{3.25}$$

$T_0 \leq \mathrm{T} \leq T_m$

Table 3.4: Johnson cook parameters [69]

Material	A_w	B_w	C_w	n	m
Al 5052	167 MPa	596 MPa	0.001	0.551	1.34

In equation 3.25, ϵ^p is an effective plastic strain, $\dot{\epsilon}^p$ is strain rate and A_w, B_w,C_w and *n* are material constants [69] . The first bracket represents stress as a function of strain. Second and third bracket represents stress as function of strain rate and temperature respectively. The The temperature influence is ignored here.

Thermal model

The heat equation is used in thermal physics to estimate the temperature rise in numerical simulation. The heat transfer in the material is given by equation 3.26.

$$\rho C_p \frac{\partial T}{\partial t} + \nabla \cdot (-K_T \nabla T) = Q \tag{3.26}$$

Where C_p is the heat capacity, ρ is the density of materials, k_T is the thermal conductivity, T is the temperature and *Q* is the heat source. In the developed model, *Q* refers to the Joule heating of the conductors. The room temperature is taken as 25^0C.

Flowchart of the coupled simulation model

Figure 3.2 shows the flowchart of the sequential coupled model used for simulation. First the 2D geometry is formed in COMSOL that consist of coil, workpiece, insulator and air domain as shown schematically in figure 3.3. Next, the materials are assigned to the different domains of geometry. Among the physics module, magnetic field submodule of the AC/DC module is selected and assigned to the entire geometry. Under the solid mechanics module, plasticity submodule is considered and it is applied to the workpiece only. In Heat transfer module, joule heating submodule is considered and assigned to the coil, workpiece and insulator.

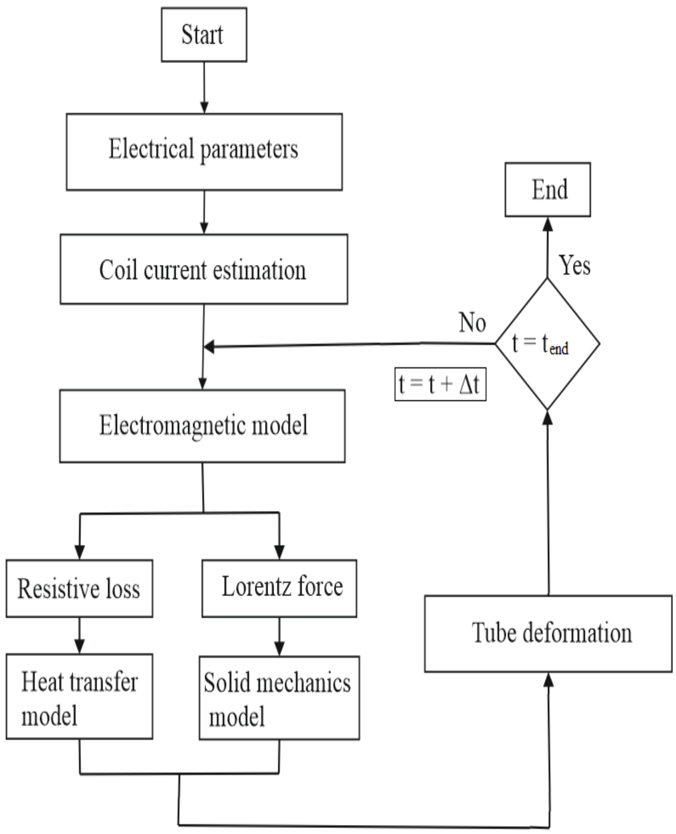

Figure 3.2: Flowchart of sequential coupled Simulation

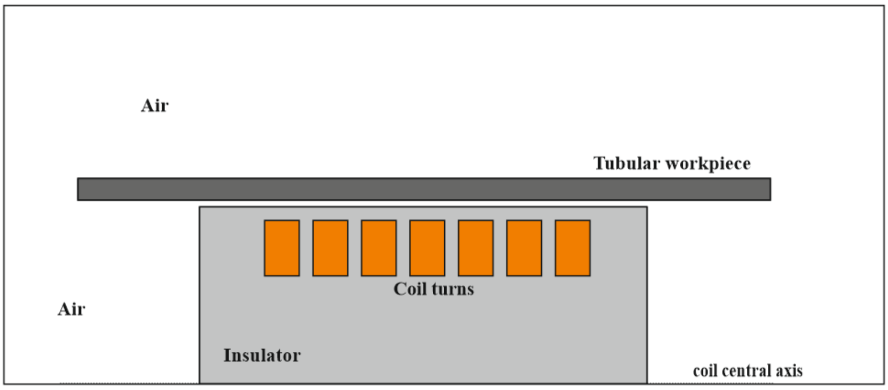

Figure 3.3: Schematic of different domain arrangement in COMSOL

Based on the selected physics, the material parameters are updated. In study, time dependent study type is selected in and the time step is kept as 0.5 μs. Based on the system and coil-workpiece parameters, At each time step, the discharge current of the coil is estimated and is given as input to the magnetic field model. The magnetic field model calculates the Lorentz force and is given as input to the structural model. Before the next step, the updated magnetic field because of tube deformation is taken into account to calculate the force. The process continues till current reaches zero.

Meshing

The 2D symmetric model with mesh division is shown in figure 3.4 and mesh parameters are given in table 3.5. Triangular meshing is used for air and insulator domain, whereas the rectangular type of mesh is used for the coil and tube.

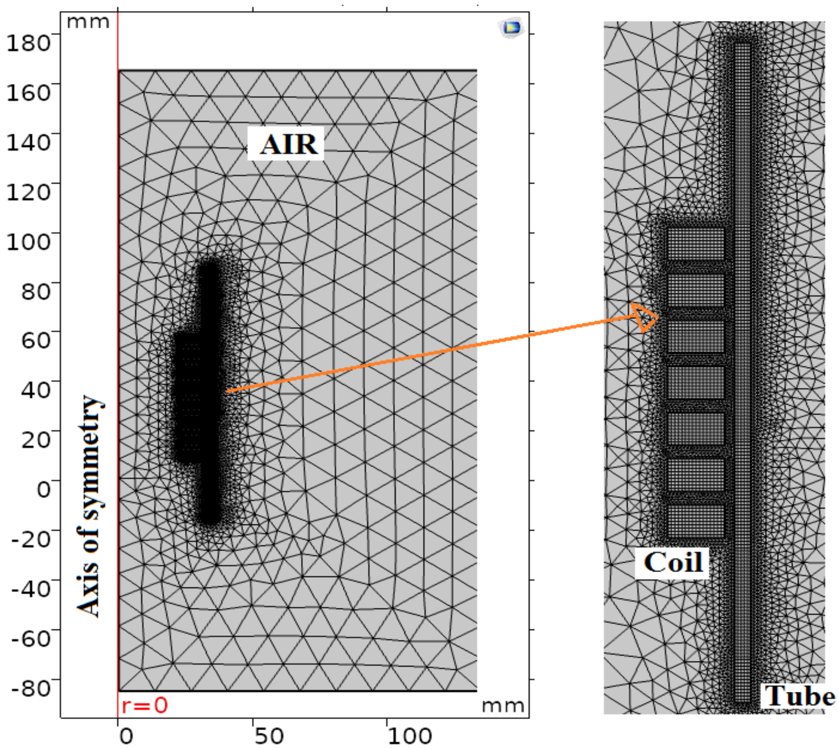

Figure 3.4: meshing used in the numerical model

Table 3.5: Mesh parameters

Number of elements	10159
Triangular elements	8039
Quad elements	2120
Average element quality	0.847
Minimum element quality	0.5078

To account the skin depth effect in numerical simulation, meshing in the tube is kept very fine (6 elements in the thickness direction).

3.4 Numerical model results comparison

To validate the numerical model results, we have compared the numerical model results with experimentally measured magnetic flux density and tube displacement results as well as with reported literature results of the magnetic field measurements.

Magnetic flux density- Experimental and numerical

In this, we have compared the magnetic flux density (B) produced by the maraging steel coil at the different operating voltage and different locations of the central axis. In this thesis, a copper helical coil is used for the experiments, but due to complications in measuring B for this helical coil, for numerical model validation purpose only, we have used maraging steel coil as shown in figure 3.5. The dimensions of the coil are shown in figure 3.6.

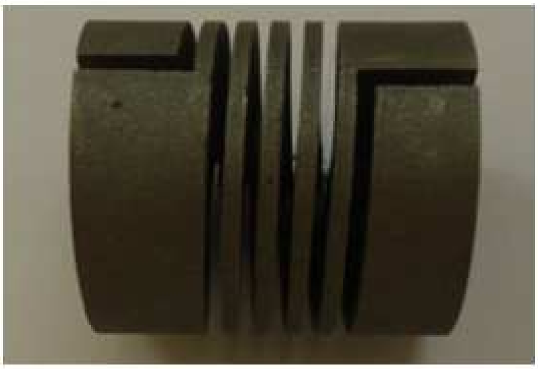

Figure 3.5: Maraging Steel coil

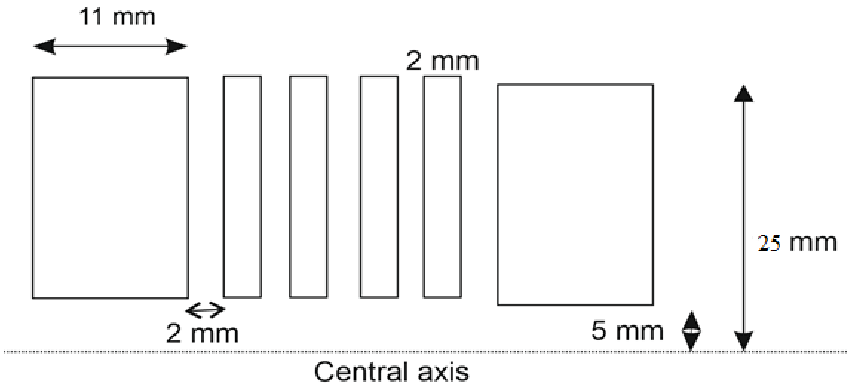

Figure 3.6: Coil 2D arrangement and dimensions

The search coil is used to measure the B. The Oscilloscope recorded waveform of the current measured by the Rogowski coil and B measured by a search coil are shown in figure 3.7.

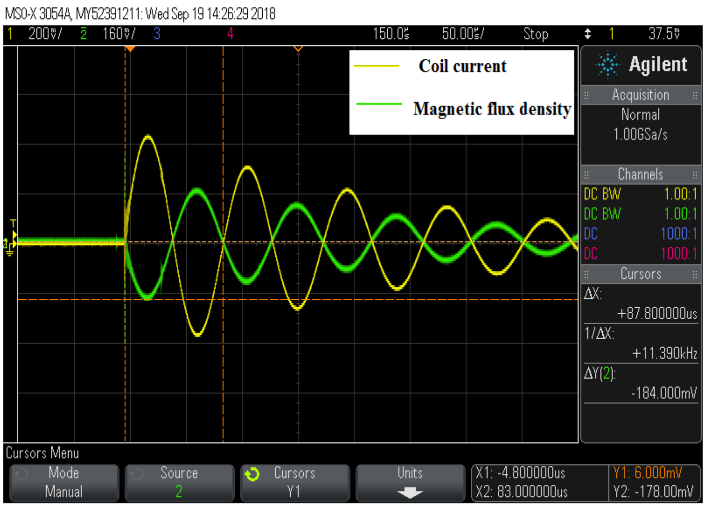

Figure 3.7: Magnetic flux density and coil current recorded waveform

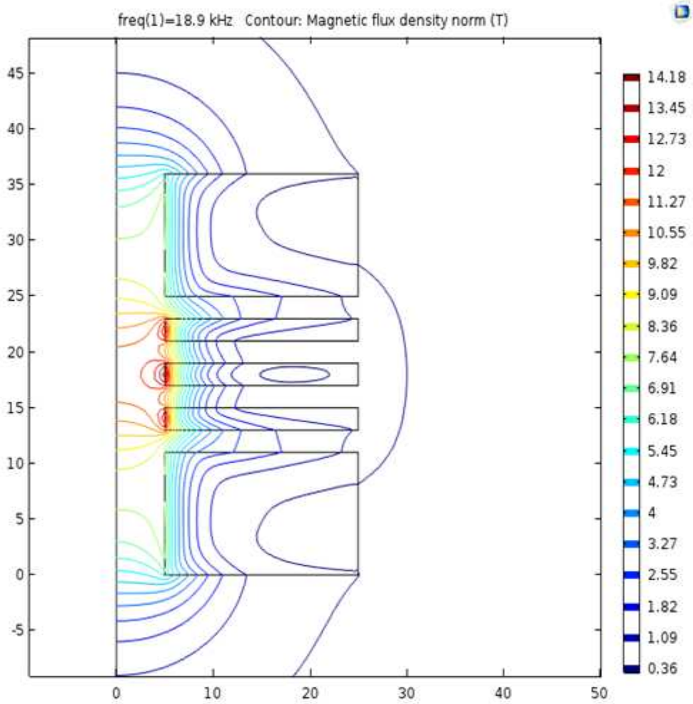

Figure 3.8: Magnetic flux density contour plot by simulation

For the maraging steel coil, A 2D numerical model is developed in COMSOL. Figure 3.8 shows the contour plot of magnetic flux density along with B magnitude colour column. The comparison of experimental and numerical B field is given further.

Magnetic flux density at the different operating voltage

In this, the magnetic flux density is measured at the centre of the central axis. Keeping the same capacitance, the charging voltage varied to observe the effect of increasing energy on the magnetic field. Table 3.6 gives the operating conditions and measured values of peak current and damping frequency whereas figure 3.9 shows the B field comparison.

Table 3.6: Experimental results

V (kV)	C(μ F)	I_{peak} (kA)	f (kHz)
3	112	34.22	11.8
4.25	112	50.22	11.8
5.28	112	61.5	11.8

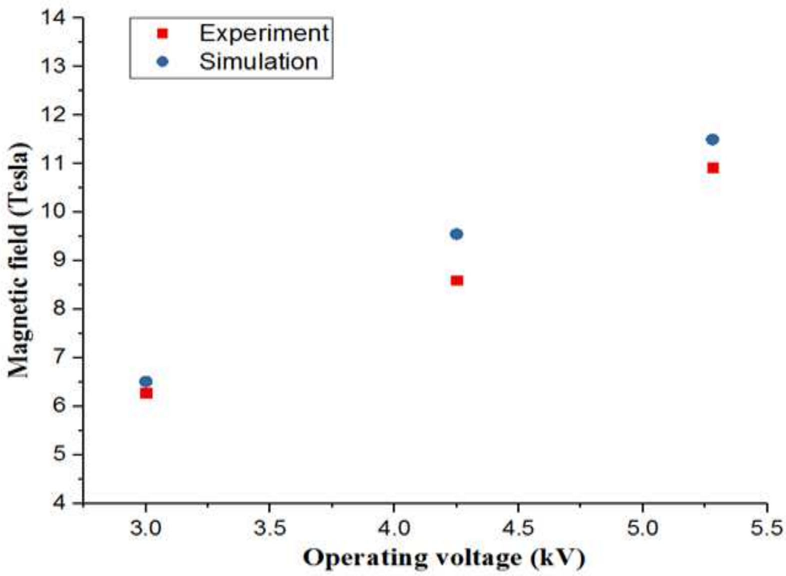

Figure 3.9: Magnetic flux density different operating voltage

As depicted by figure 3.9, the flux density magnetite is increased with the charging voltage.

Magnetic flux density at a different position

The magnetic field is also measured at different locations of the central axis as shown in figure 3.10.

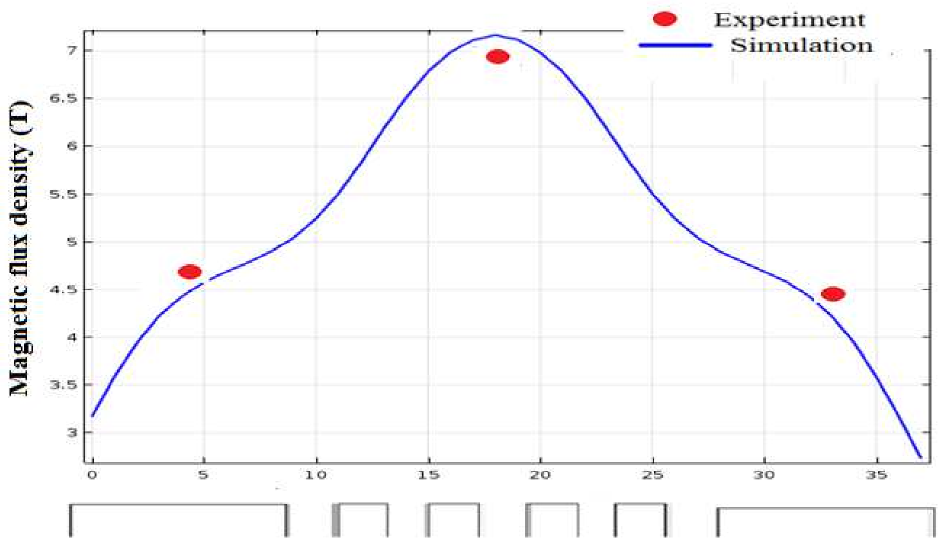

Figure 3.10: Magnetic flux density along the axial direction(V=3.2 kV,C= 112μF)

The field concentration at the centre is maximum and decreases towards both end turns of the coil. It can be seen that the magnetic flux density estimated by numerical model is well matched with the experimental values.

Magnetic flux density in case of a coil-sheet arrangement

The magnetic field calculated by the numerical model is also validated with the literature [70] results. Figure 3.11 shows the electromagnetic sheet forming model and figure 3.12 shows dimensions. Authors,Takatsu et al [70] have measured the magnetic flux density produced by flat spiral coil experimentally.

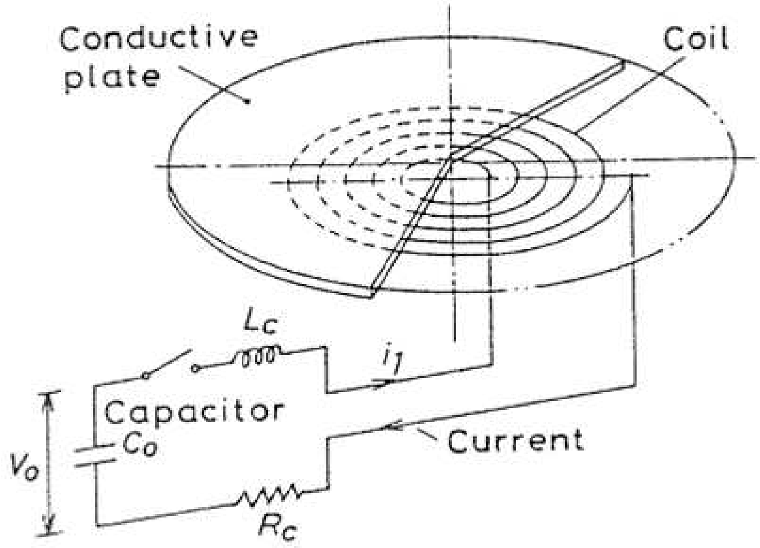

Figure 3.11: Model of electromagnetic sheet metal forming [70]

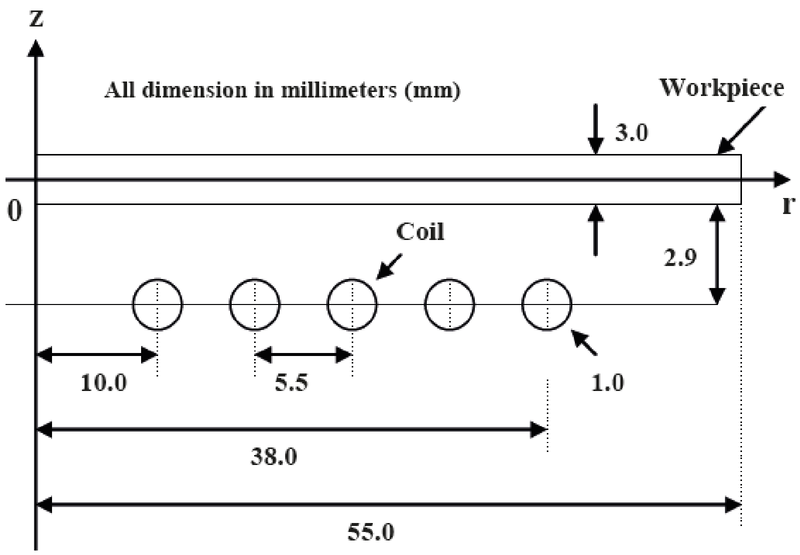

Figure 3.12: sheet forming model dimensions [48]

Table 3.7 gives the parameter details of the system used by Takatsu et al.[70]. Based on the parameters mentions in [70], COMSOL 2D model is developed and the magnetic field is measured. Figure 3.13 shows the arrangement and 3.14 shows the obtained flux density plot obtained at peak current.

Table 3.7: System parameters and working conditions

Coil (Copper)	No. of windings	5
	maximum radius of ring of coil	1 mm
	maximum radius of spiral coil	39 mm
	Pitch	5.5 mm
Circuit conditions	Capacitance	40 μ F
	Charging voltage	2 kV
Workpiece (Al 1050)	Thickness	3 mm
	Diameter	110 mm
	Gap distance	2.9 mm

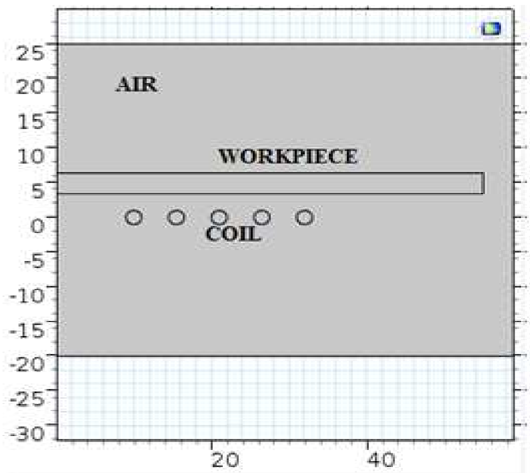

Figure 3.13: Arrangement in COMSOL

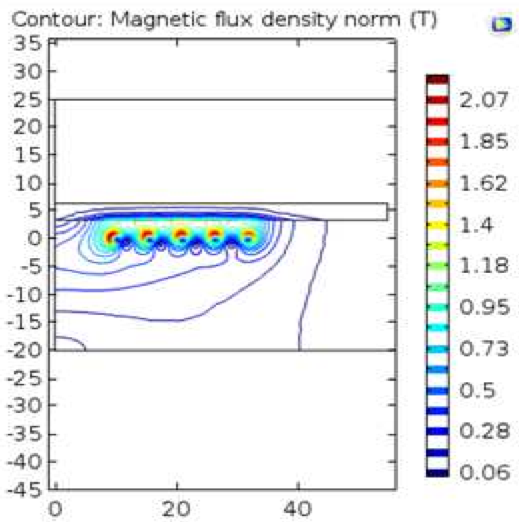

Figure 3.14: contour plot of magnetic flux density with workpiece

The magnetic flux density is measured along the radial direction and 1.6 mm above the flat spiral coil surface. The operating voltage was 2 kV and peak current amplitude was 7.48 kA. Further, the axial and radial components of magnetic flux density are measured and compared with experimental results obtained in Takatsu et al. [70] paper.

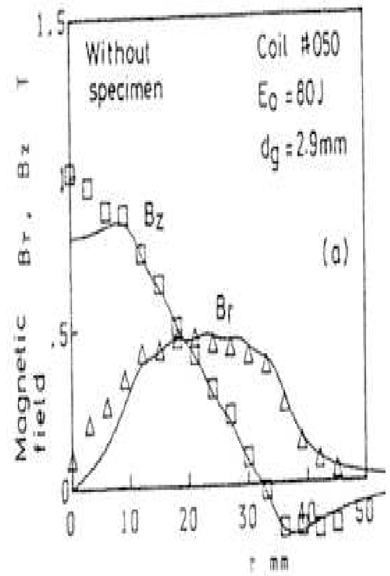

Figure 3.15: Flux density by [70]

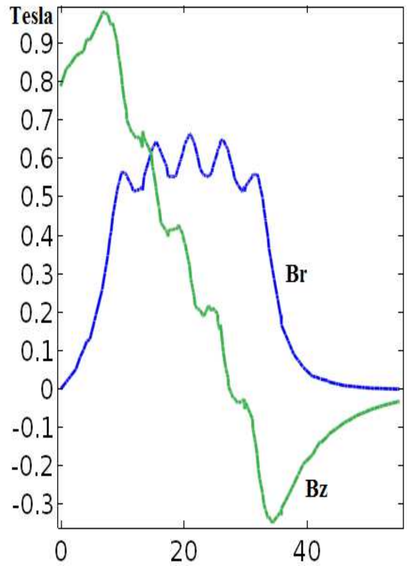

Figure 3.16: Flux density without workpiece - COMSOL

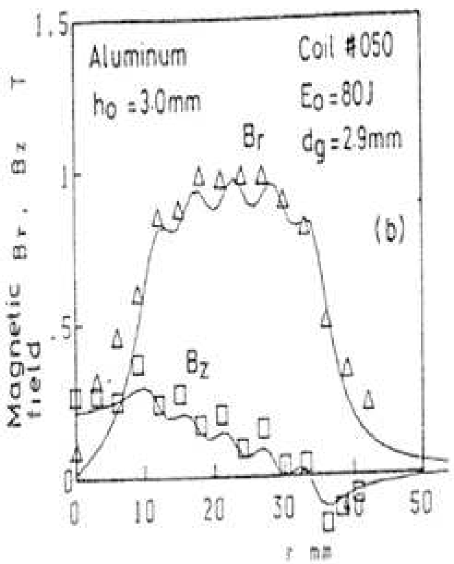

Figure 3.17: Flux density by [70]

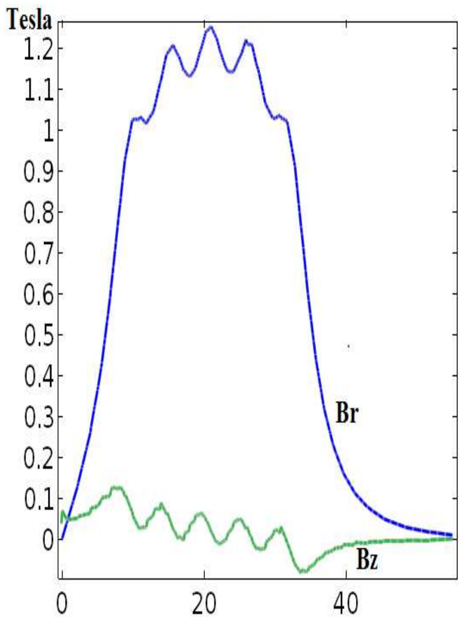

Figure 3.18: Flux density with the workpiece COMSOL

Figure 3.15 and 3.16 show the magnetic field above the flat coil surface without placing the workpiece. Similar way figure 3.17 and 3.18 show the magnetic field as the same place after placing the workpiece. As can be seen from figure 3.17 and 3.18, the radial component of the magnetic field is higher than the axial component. That is why the axial movement of the sheet is high. Nature and magnitude of the magnetic flux density obtained by the developed numerical model showed sufficiently good agreement with the Takatsu et al. [70] results with a maximum error between them is 14 %.

Tube displacement - Experimental and numerical

To compare tube displacement obtained in experiment and numerical model, We have measured the tube displacement at the centre point with the help of laser based device. Along with the magnetic field, the tube displacement obtained by experimental and numerical method is compared here. A laser based device is used to obtain the tube displacement plot. Maximum forming point of the tube is at the centre. Parameters of coil and tube used are given in the table 3.8.The details of the coil, tube and experimental arrangement are discussed in chapter 4.

Table 3.8: System parameters and working conditions

Coil (Copper)	No. of turns	7
	active length	47 mm
	Pitch	2 mm
Circuit conditions	Capacitance	112 μ F
	Charging voltage	16.8 kV
Workpiece (Al 5052)	Thickness	2.4 mm
	Diameter	70 mm
	Length	100 mm

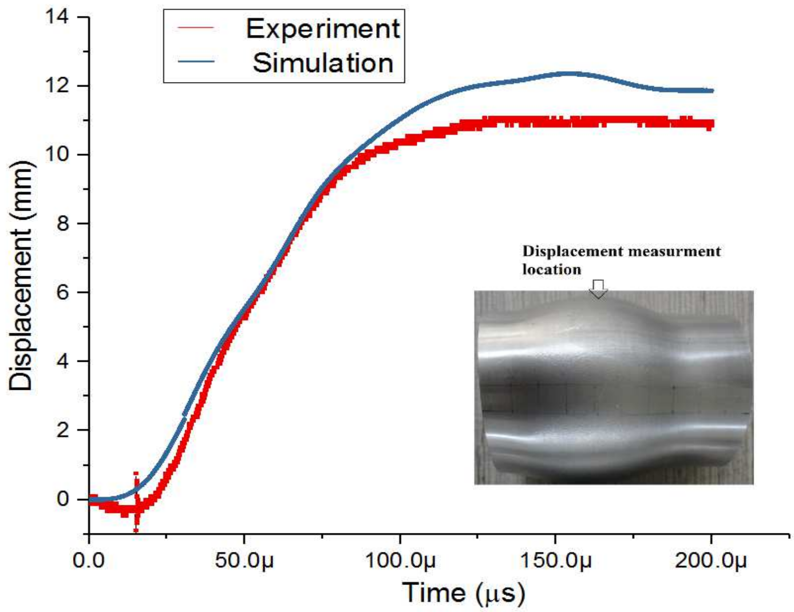

Figure 3.19: Tube displacement- experimental and numerical

Figure 3.19 shows that tube displacement with time predicted by developed numerical model is well agreed with the experimental results having a 10% error in tube final displacement. The higher estimation of displacement by the numerical model may be due to the fact that the time varying discharge circuit parameters during the forming process are not considered in the numerical model.

Summary

In this chapter, the details of the experimental system and measuring instruments used for the electromagnetic forming study are explained. Along with this, the information about the developed 2D numerical model is presented. Further, the numerical model results are validated. Experimentally observed magnetic field and the tube displacement results showed a good match with the results of the numerical model. In further chapters, the developed numerical model is used in the analysis of the electromagnetic forming process.

Chapter 4

Helical coil design methodology for electromagnetic tube forming

An electromagnetic coil is an important part of the EMF system. As seen in chapter 2, design of electromagnetic coil is depended on the nature of the workpiece to be formed. To study the electromagnetic expansion process of tubular workpiece, we have first designed a driving coil. The analytical model is developed to calculate the magnetic field, magnetic pressure and tube velocity. FEA based numerical model is also developed in COMSOL and it is used to validate the analytical and experimental results. Further, the numerical model is used to study the mechanical and thermal aspects of the designed coil.

4.1 Analytical approach

Current, magnetic field and magnetic pressure estimation

Electromagnetic tube expansion schematic diagram is shown in figure 4.1. Its electrical equivalent circuit is as shown in figure 4.2. Coil has its own resistance and inductance defined by

R_c and the by L_c respectively. The tube is magnetically coupled with the coil and has resistance R_w and inductance is L_w. As observed in figure 3.1, The capacitor terminals are connected to the coil terminals by cables. Thus the capacitor to the coil path has its own resistance and inductance defined by R_s L_s respectively. Magnetic coupling between the coil and tube is

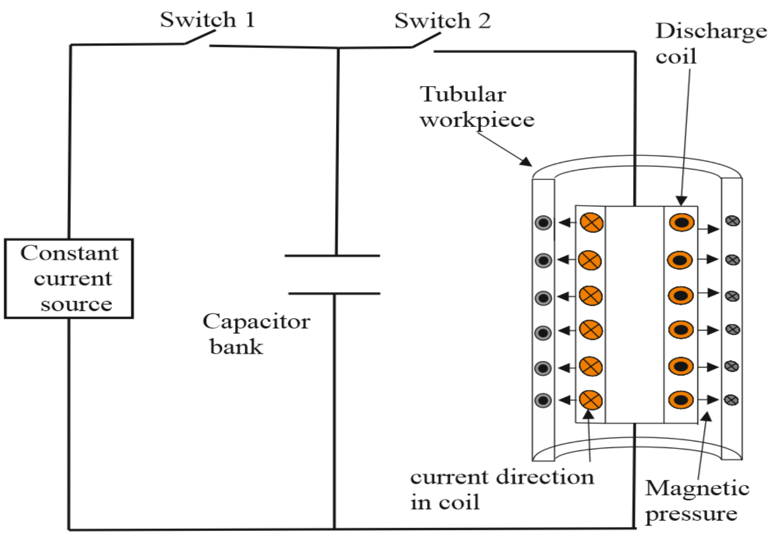

Figure 4.1: Schematic of the electromagnetic tube expansion process

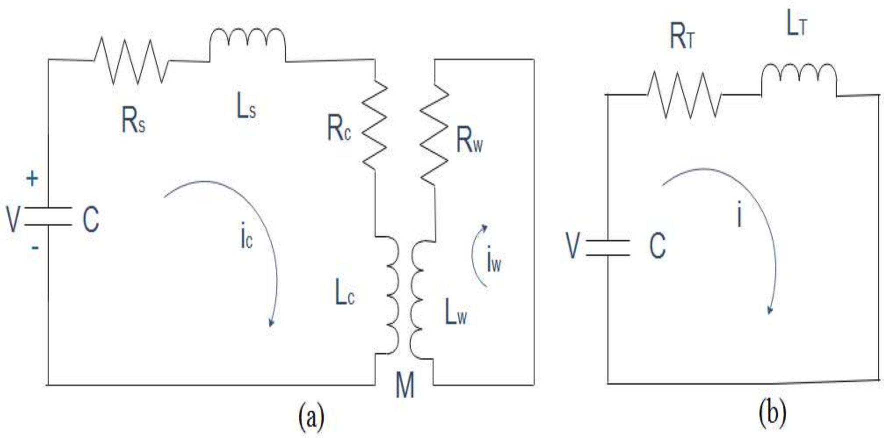

Figure 4.2: Electrical equivalent circuit of EMF (a) complete form, (b) reduced form

represented by M. The equivalent circuit referred to primary is shown in figure 4.2(b). The tube is considered as a single turn secondary of the transformer. Applying the Kirchhoff's voltage law to the two current loops of figure 4.2 (a), the following equations can be arrive in the frequency domain.

$$V = i_c(R_s + R_c + j\omega L_s + j\omega L_c) - i_w(j\omega M) \tag{4.1}$$

$$0 = -i_c(j\omega M)) + i_w(R_w + j\omega L_w) \tag{4.2}$$

After simplifying the above equations and separating real and imaginary parts, we get

$$L_T = L_s + L_c - \frac{M^2}{L_w} \tag{4.3}$$

$$R_T = R_s + R_c + \frac{M^2 R_w}{L_w^2} \tag{4.4}$$

Equivalent inductance and resistance of figure 4.2(b) are defined by equations 4.3 and 4.4 respectively [71]. From the reduced equivalent circuit of figure 4.2(b), following differential equation can be written

$$L_T \frac{\partial i(t)}{\partial t} + R_T i(t) + \frac{1}{C}\int i(t) = 0 \tag{4.5}$$

Initially, the capacitor is in discharge condition. The operator set the initial voltage across the capacitor. There is no current in the coil at the start. Equation 4.5 can be solved for current $i(t)$ using the two initial conditions. First is the zero coil current and capacitor charging voltage *V*. The resulting current *i(t)* flowing through the coil is obtained from the above differential equation and initial conditions.

$$i(t) = \frac{V}{\omega L_T} e^{-\beta t} sin\omega t \tag{4.6}$$

$$\omega = \sqrt{\frac{1}{L_T C} - \beta^2} \tag{4.7}$$

$$\beta = \frac{R_T}{2L_T} \tag{4.8}$$

Where ω represents the damped angular frequency of the discharge current and β is the damping coefficient. The nature of coil current is damped sinusoidal. We have designed a solenoidal coil for the tube expansion experiments. Solenoid coil having N number of turns generates a magnetic field when current i flow through it. The magnetic field strength responsible for magnetic force is given by equation 4.9[72].

$$H = \frac{Ni}{2\beta r_1}\tau(\alpha, \beta) \tag{4.9}$$

$$\tau(\alpha, \beta) = \frac{\beta}{\alpha - 1}\ln[\frac{\alpha + \sqrt{\alpha^2 + \beta^2}}{1 + \sqrt{1 + \beta^2}}] \tag{4.10}$$

where factor $\tau(\alpha, \beta)$ is depends on the coil geometry [73], [74] Figure 4.3 shows the dimensions

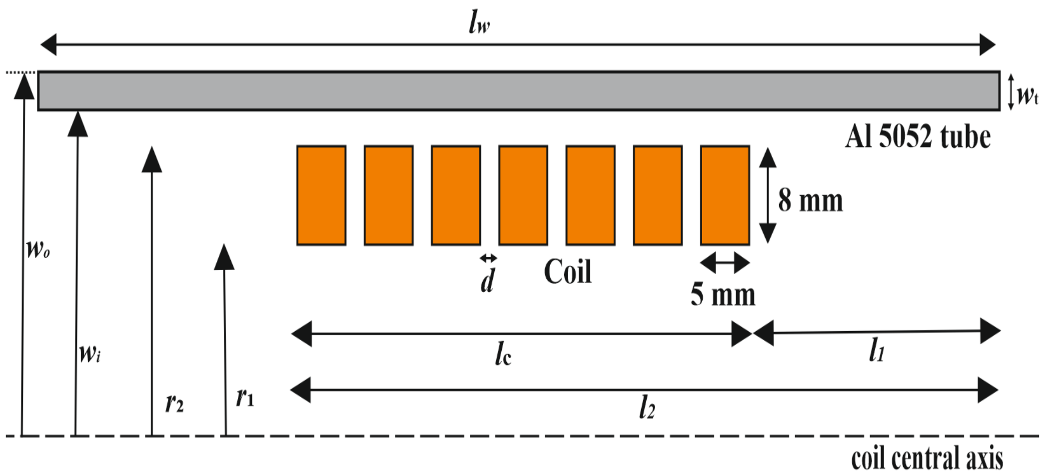

Figure 4.3: Dimensions of the driving coil and Al 5052 tube

of the coil and tube. The coil has active length l_c and inner and outer radius r_1 and r_2 respectively. For a fixed number of turns and coil geometry, the magnetic field is proportional to coil current and this current can be varied through charging voltage of the capacitor. The Lorentz force responsible for workpiece forming is given by equation 4.11. J_ϕ is the induced current density, and B is the magnetic field. figure 4.4 shows the coil, workpiece current direction and acting force direction.

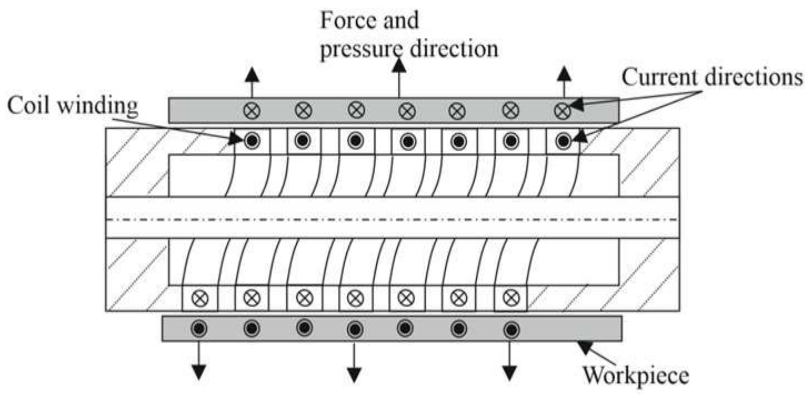

Figure 4.4: Schematic of the coil and conducting tube

$$\overline{F} = \overline{J_\phi} \times \overline{B} \tag{4.11}$$

$$P_{mag} = \int_{W_i}^{W_0} F dr = \frac{1}{2\mu}(B_{gap}^2 - B_{pen}^2) \tag{4.12}$$

$$P_{mag} = \frac{1}{2\mu} B_{gap}^2 \tag{4.13}$$

Magnetic pressure relation with the Lorentz force is shown by equation 4.12. Where P_{mag} is the magnetic pressure generated by the coil [8], μ_0 is the magnetic permeability of free space, B_{gap} is the magnetic flux density present in the gap between the coil and tubular workpiece whereas B_{pen} is the penetrated magnetic flux density inside the workpiece. The magnetic field diffusion in the workpiece depends on the workpiece skin depth. When the skin depth is small in comparison to the thickness of the workpiece, the penetrated magnetic field is usually neglected. The coil current rise time must be set such that, it would make skin depth δ small in comparison to the thickness of the workpiece.

$$\delta = \frac{1}{\sqrt{\pi f \sigma \mu \mu_0}} \tag{4.14}$$

Where f is the coil damping current frequency, σ is workpiece electrical conductivity and μ_r is the relative permeability. The magnetic pressure acting on the tube is given by equation 4.13

where B_{gap} can be obtained using equation 4.15. K_H is the distribution coefficient depends on the effective gap between the coil and tube [8]. δ_{wp} and δ_{coil} are the skin depth of workpiece and coil respectively.

$$B_{gap} = K_H \mu_0 H_z \tag{4.15}$$

$$K_H = \frac{1}{\pi}(\arctan \frac{2z + l_c}{g_{eff}} - \arctan \frac{2z - l_c}{g_{eff}}) \tag{4.16}$$

$$g_{eff} = g_{air} + \frac{1}{2}(\delta_{wp} + \delta_{coil}) \tag{4.17}$$

Conducting workpiece description

Aluminium 5052 material tube is used for the experiment. The material properties can be found in table 3.2. The length of tube l_w is 100 mm and thickness w_t is 2.4 mm. Diameter of the tubular workpiece is given by D and chosen 70 mm.

Coil geometry and material selection

Coil radius is selected in such a way that the coil outer surface should be close to the tube inner surface to have a strong coil and tube coupling. As it provides more utilization of electromagnetic energy to deform the tubular workpiece. The length of the coil is determined by the work length of tubular workpiece [26]. In this work, the coil diameter is 60 mm, and the active length of the coil is kept 47 mm. According to [75], for the same current, a coil of circular, rectangular and square cross section of the equal area gives almost the same induced current density. We have chosen a rectangular cross section of conductor for the coil. Electrical conductivity, compressive strength, allowable working temperature and specific heat capacity are the factors that are to be taken into account while selecting the material for the coil. Based on these factors, the copper conductor has been selected because of its good electrical conductivity and high working temperature. Once the coil geometry is fixed, the next parameter that decides the magnetic field is coil's Ampere turns Ni. The required magnetic field can be obtained by various combinations of current and coil turns. Numbers of turns of the coil are determined based on maximum limiting current, the dielectric and mechanical strength of insulation between turns. The advantages of more turns are the uniformity of the magnetic field as well as the less current requirement. On the other hand, more turns increase inductance and resistance of the coil and thereby reduce the frequency of the coil current. Figure 4.5 shows

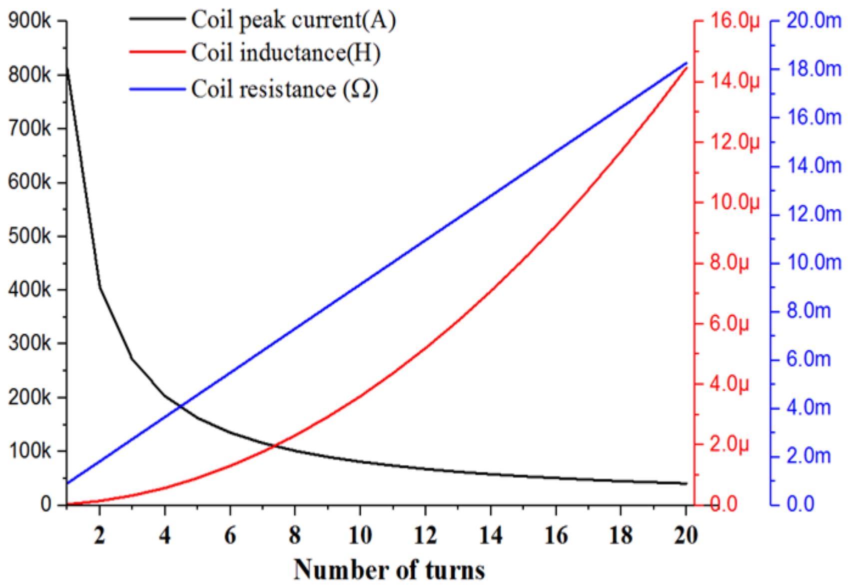

Figure 4.5: Variation in peak coil current, coil resistance and coil inductance with the number of turns

the variation of coil peak current, resistance and inductance with the number of turns. Here the peak current is calculated considering charging voltage of 16 kV, capacitance of 112 μF. N and i are varied such as to get constant ampere turns and thereby constant magnetic field as given by equation 4.9. Based on the observations, a 7 turn coil with inter turn gap of 2 mm is designed. The inductance and resistance of the coil and tube are calculated based on formulas given by [76].

$$L = \frac{\mu_0 \pi}{8} r_1 \frac{(\alpha_1 + 1)^2}{\beta_1} N^2 g(\alpha_1, \beta_1) \tag{4.18}$$

$$R = \frac{\rho}{f_f}\frac{N^2}{r_1}\frac{\pi}{2}\frac{\alpha_1 + 1}{\beta_1(\alpha_1 - 1)} \tag{4.19}$$

The g (α_1, β_1) factor is dependent on coil geometry. f_f is the filling factor (fraction of conducting material in the volume of the coil [77] and ρ is the resistivity of the material. To calculate the coil-tube mutual inductance M, Roiti's formula [78] is used as shown in equation 4.20. The formula is approximated by neglecting the higher order terms of x contributing decimal corrections.

$$M = 4\pi^2 r_2^2 n_1 n_2 [x_2 - x_1 + \frac{r_2 w_0^2}{8}(\frac{1}{x_1^3} - \frac{1}{x_2^3}) - \frac{r_2 w_0^2}{16}(\frac{1}{x_1^5} - \frac{1}{x_2^5})] \tag{4.20}$$

where $x_1 = \sqrt{l_1^2 + w_0^2}$ and $x_2 = \sqrt{l_2^2 + w_0^2}$, $n_1 = \frac{1}{l_w}$, $n_2 = \frac{N}{l_c}$

Temperature effect on material properties ignored here as any small rise in temperature has little influence on electrical and mechanical properties of the workpiece material [40][46].

Electrical insulation and mechanical strength

The strength of the coil is defined by the strength of its reinforcement as concluded by [53]. In EMF, dielectric strength and ultimate compressive strength of insulating material used for the coil is important. Adequate electrical insulation between the turns is required for sustained operation as high voltage appears across each turn of the coil. This can be estimated from the thickness and dielectric strength of insulating material.

$$b_s = \frac{e}{d} \tag{4.21}$$

Where b_s is the dielectric strength of insulation, *e* is the voltage potential to be insulated and *d* is the spacing between the turns. During workpiece forming the repulsive stress acts on the coil turns and thereby on the supporting insulation of the coil.

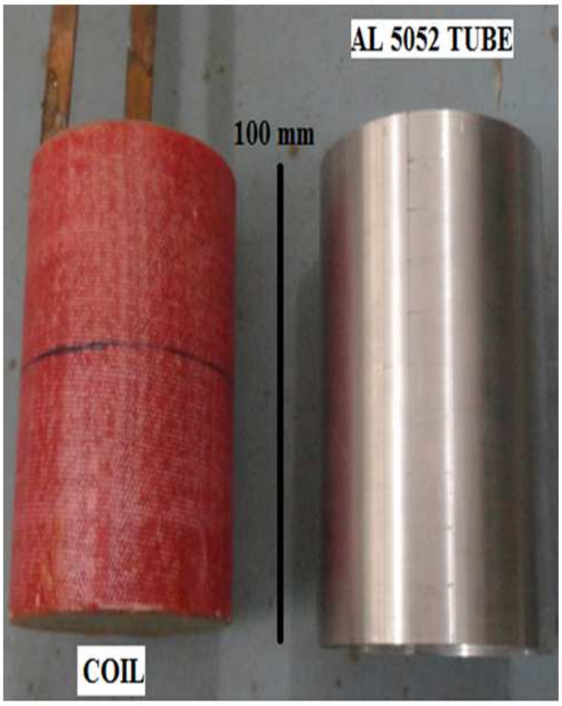

Figure 4.6: The coil with reinforcement and used Al 5052 tube

In addition to repulsive stress, there is a force exists on inter turn insulator because the coil turns carrying current in the same direction. In the design, coil turns are supported by fibreglass insulation. The copper conductor used has 5 mm $\times$ 8 mm cross section and over its length, it is coated with high voltage insulation paint. Further, insulation is provided by applying a layer of Kapton Polyimide tape over the coil surface. Figure 4.6 shows the designed coil and the Al5052 tube used in the experiment.

System description

Available pulse power generator ratings like maximum storable energy, maximum allowable current, inherent resistance and inductance of the system are needed to be known before designing the coil. Details of the pulse generator supply used for the experiments is given in chapter 3. The system has 20 kV maximum charging voltage and 224 μF maximum capacitance.

The capacitor to the coil connecting path has its own resistance that will add in the discharge current path. The system parameters R_s and L_s are determined from the peak current, damping frequency of short circuit current and known capacitance. Table 4.1 gives the parameters used for EMF experiments.

Table 4.1: Discharge circuit parameters

Component	Parameter	Value
system	Resistance (R_s)	10 m Ω
	Inductance (L_s)	0.9 μH
Coil	Length (l_c)	47 mm
	Inner radius (r_1)	22 mm
	Outer radius (r_2)	30 mm
	Inner turn distance (d)	2 mm
Workpiece	Length (l_w)	100 mm
	Thickness (w_t)	2.4 mm
	Inner radius (W_i)	32.6 mm
	Outer radius (w_o)	35 mm

Workpiece velocity estimation

To deform the tubular workpiece plastically, generated magnetic pressure by the coil must overcome the tube yield stress. The minimum magnetic pressure to begin circumferential deformation of the tube can be obtained using the equation of motion of the workpiece [65].

$$P_{mag} = \frac{2w_t}{D}\sigma_y \tag{4.22}$$

Where w_t and D are tube thickness and diameter respectively and is the yield stress of aluminium material. Using equations 4.13 and 4.22, the resultant pressure P that is responsible for the tube forming is given as

$$P = \frac{B_{gap}^2}{2\mu_0} - \frac{2w_t}{D}\sigma_y \tag{4.23}$$

The stress strain relation for the material in the plastic state is defined by Johnson Cook model. For simplicity, the effect of strain rate and temperature on material stress is not considered in the analytical model.

$$\sigma_y = A_w + B_w \epsilon^n \tag{4.24}$$

Where σ_y is the stress acting on the workpiece, ϵ is the plastic strain and A_w, B_w and n are material constants as defined in chapter 3. Under the action of magnetic force, Newton's second law of motion is used to predict the workpiece acceleration and thereby velocity and displacement.

$$Acc = \frac{P}{w_t \rho} \tag{4.25}$$

$$Velo = \int_0^t \frac{P}{w_t \rho} \tag{4.26}$$

In the analytical model, at each time, the acceleration, velocity and displacement changes are calculated. The parameters like M, L_T and R_T are assumed constant during the forming.

Details of the experimental setup and developed numerical simulation model are given in the previous chapter.

4.2 Results

For the 16 kV charging voltage and 112 μF capacitance, the experimentally obtained coil current has a peak current of 116 kA with the damping frequency f of 11.7 kHz. Figure 4.7 shows the experimentally obtained tube expansion whereas figure 4.8 shows the surface plot of tube expansion obtained by COMSOL simulation.

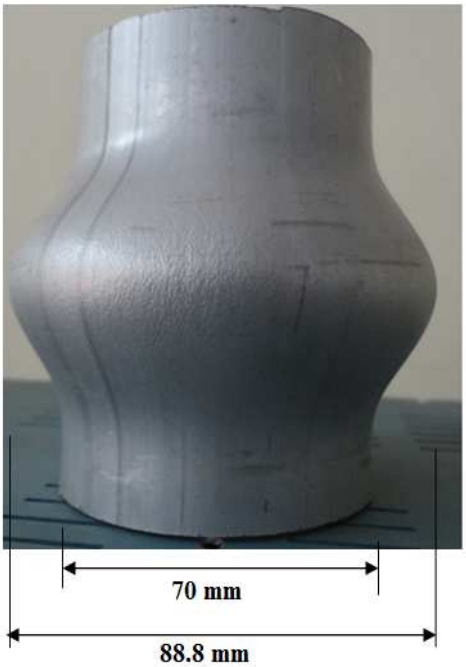

Figure 4.7: Tube expansion at 16kV,112μF

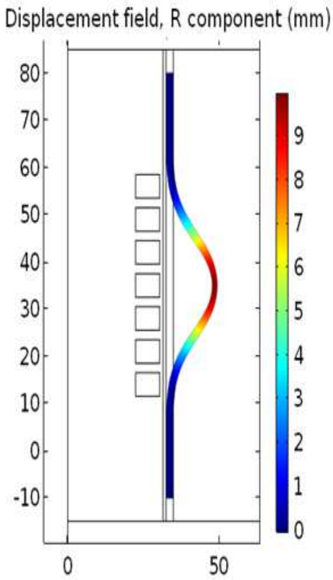

Figure 4.8: Tube displacement surface plot-Simulation

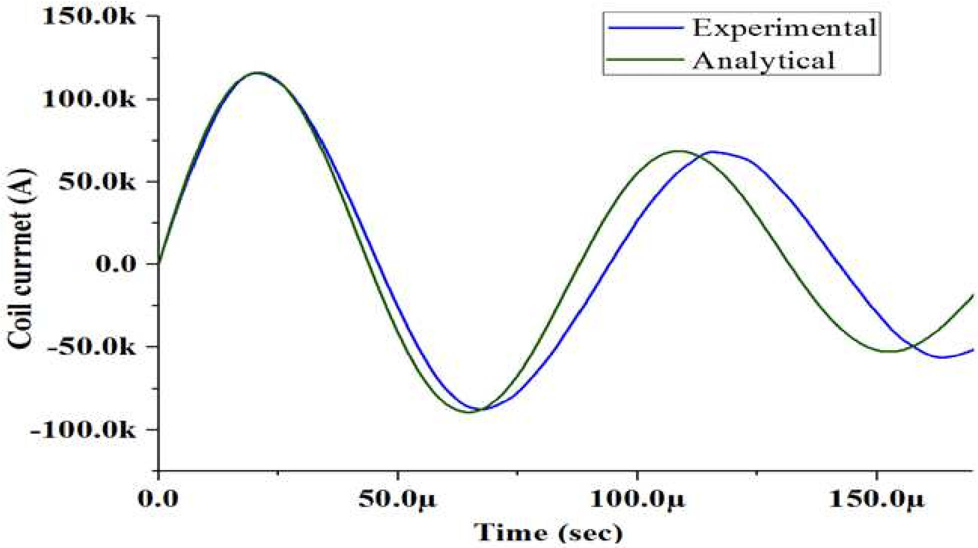

Figure 4.9: Discharge current of the coil - analytical and experimental

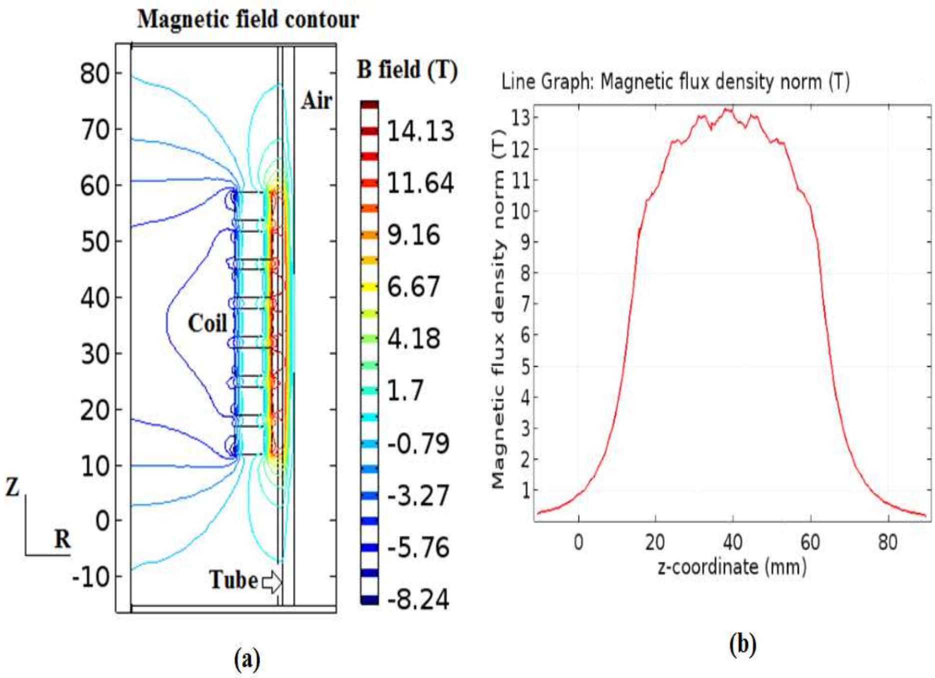

Figure 4.10: Magnetic flux density (a) contour plot at peak current and (b) along the surface of the tube

Coil current estimated by analytical model is in good agreement with the experimentally measured current as observed in figure 4.9. The difference in the waveforms can be seen after the first current pulse. As the tube moves away from the coil, change in coil-tube coupling causes change in L_T and R_T during the forming process. This has caused the difference in both the current waveforms. More details about this aspect is studied in chapter 6.

Being paramagnetic material, the permeability of aluminium tube is assumed constant in the simulation. Figure 4.10 shows the coil-tube flux linkage. The estimated analytical magnetic flux density at peak current is 13.8 T and is in line with simulation results. Eddy current induced in the tube because of coil's magnetic field and this current is flowing from the tube surface due to a skin depth phenomenon. This skin depth also affects the electromagnetic flux propagating through an aluminium conductor. In figure 4.10, flux density around 14 T can be observed near the coil surface as indicated by red colour. Flux density along the tube surface facing coil is also shown in figure 4.10. The inductance and resistance of the developed coil are measured by an LCR meter at 10 KHz frequency. Comparison of measured and analytical parameters is given in table 4.2.

Table 4.2: Inductance and resistance of the coil

Sr. No.	Parameter	Analytical	Measured
1.	Resistance of the coil (R_c)	6.4 mΩ	6.1 mΩ
2.	Inductance of the coil (L_c)	1.5 μH	1.6 μH

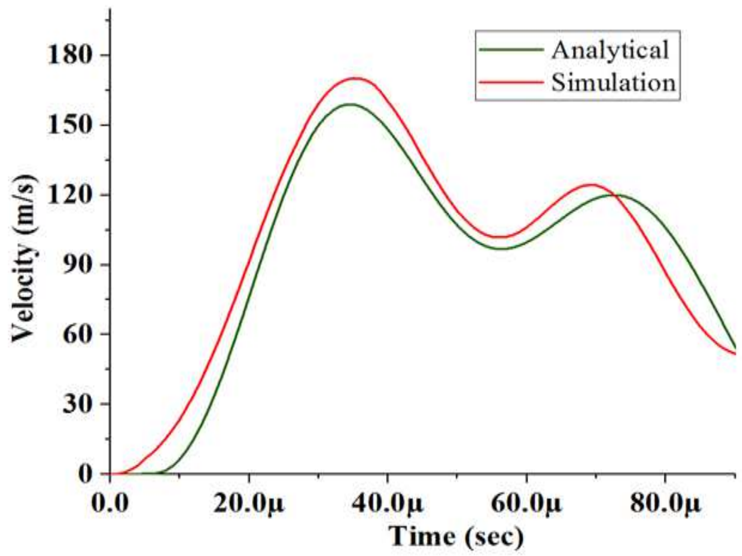

Figure 4.11: Velocity of tube centre by simulation and analytical model

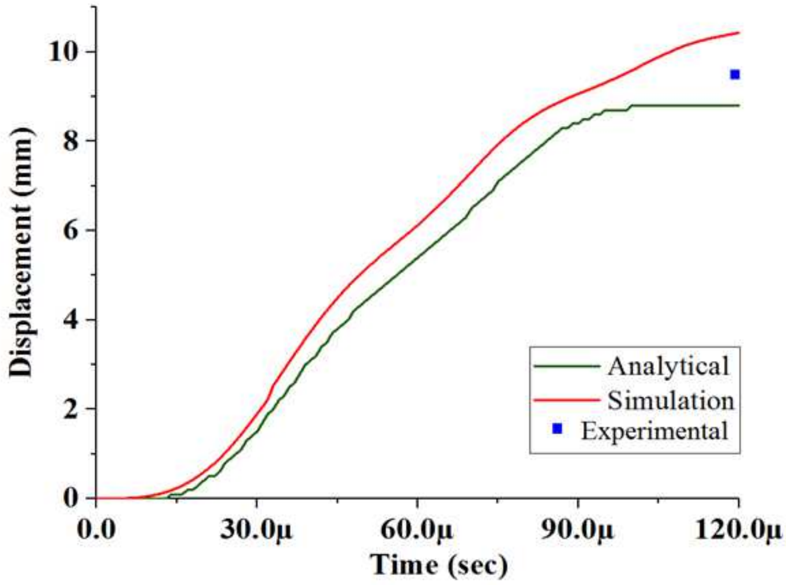

Figure 4.12: Displacement of the tube at centre

Maximum forming point of the tube is at its centre. Figure 4.11 shows the velocity and figure 4.12 shows the displacement of the tube at the centre. It can be seen that the analytically predicted velocity and tube displacement are in good agreement with simulation results. Experimentally observed tube displacement at the centre is 9.4 mm and is close to the predicted results. Since the analytical model is one dimensional and simplified, it might have caused the discrepancy in the results.

4.3 Mechanical and thermal aspects

Along with electrical aspects, mechanical and thermal aspects are also important in designing the coil for EMF applications. In the performed electromagnetic tube expansion experiments, it is observed that the designed solenoid coil can withstand for more number of shots when operated below 150 kA. However, the coil has failed when operated at higher current. In order to diagnose the cause of coil failure, developed 2D numerical model is used. A sequential coupled approached is introduced in the numerical model to solve magnetic, mechanical and thermal physics. Table 4.3 gives mechanical and thermal properties of copper and fibreglass which are the coil and its insulation material respectively.

Table 4.3: Mechanical and thermal properties of materials

Properties	Copper	Fibre Glass (E)
Heat capacity (J/Kg.K)	385	800
Thermal conductivity(W/m.K)	350	1.3
Density (Kg/m^3)	8700	2550
Youngs modulus (GPa)	120	72
Tensile strength (MPa)	210	1700

To account the mechanical aspects, the effect of Lorentz force is considered on coil as well as on the coil reinforced material. For thermal aspects, heat transfer module is added and it is coupled with magnetic and mechanical physics. The governing equations can be found in chapter 3.

Results

As mentioned earlier, it has been observed that the coil fails when the peak current is above the 150 kA. Figure 4.13 and 4.14 show the failed coil images. The first observation is the black shades over the coil surface that denote the burning happened of insulating material. Next observation is the damage of inter-turn insulation along with burning. It is also noticed that there is no sign of the physical contact between the copper turns.

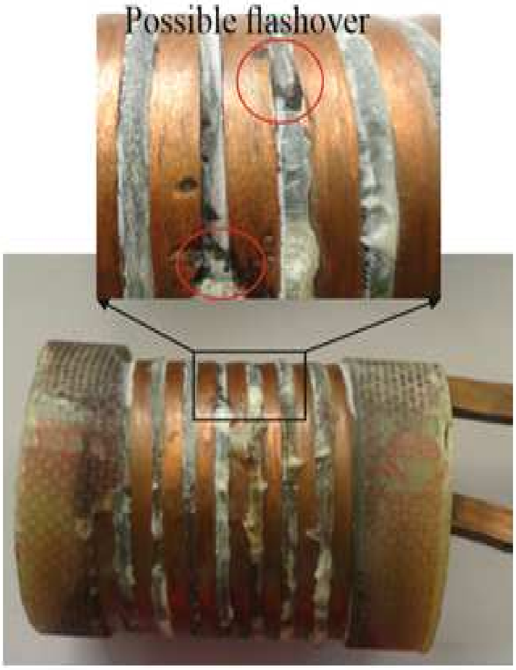

Figure 4.13: Failed coil 1

Figure 4.14: Failed coil 2

The possible causes of the coil failure are electrical, mechanical and thermal. Considering the dielectric strength of the insulating material of the coil and from experimental observations, it can be concluded that the dielectric breakdown is not the cause which initiates the coil failure. Hence, it must be either mechanical or thermal loading of the coil that initiated the coil failure. To analyse this, developed sequentially coupled numerical model is used. In the model, the discharge current recorded on the Oscilloscope is fed to coil turns. The time step is kept as 1 microsecond.

Rise in temperature

Heating of the coil is mainly due to Joule heating. Figure 4.15 shows the maximum and average temperature rise of the coil over time having peak current 152 kA and damping frequency of 9.5 kHz. Figure 4.16 shows the surface plot of temperature at the time of peak maximum temperature.

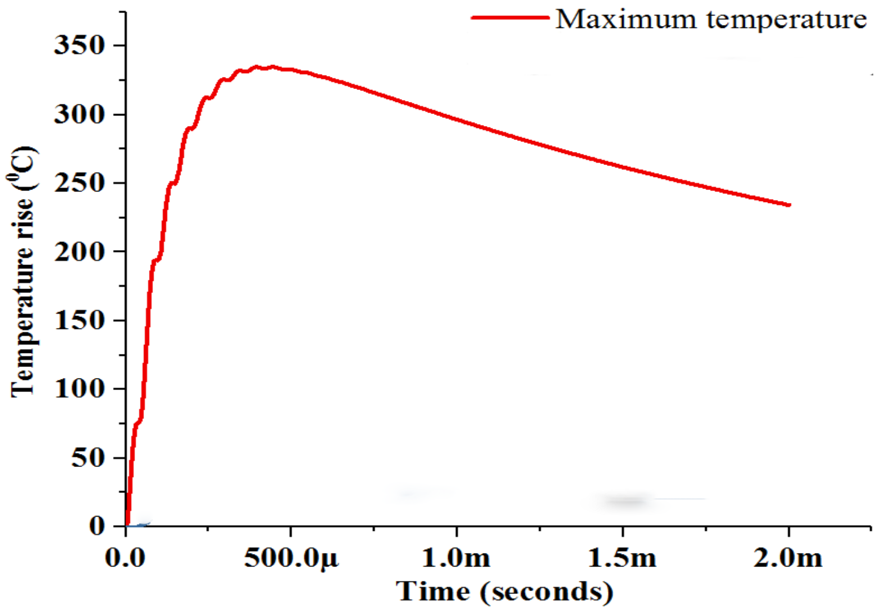

Figure 4.15: Maximum and average increase in coil temperature(152 kA,9.5 kHz)

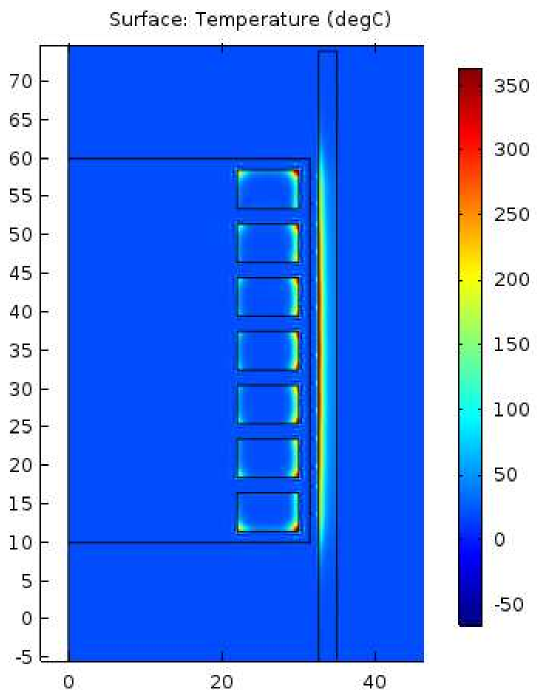

Figure 4.16: Surface plot of the temperature

Due to the skin depth phenomenon, the current density in the coil and the tube is non uniform. This causes the heating at the corners of the coil turns higher compared to the rest of the coil cross section area as observed from figure 4.16 . The average temperature of the coil is very less compared to the maximum temperature. This is due to the good thermal conductivity of the copper, causing fast heat dissipation. Numerical simulation carried out at other peak current and the maximum temperature of the coil is recorded. Table 4.4 shows the rise in the coil temperature at different peak currents.

Table 4.4: Maximum and average temperature rise of coil

I_{peak} (kA)	f (kHz)	Maximum temperature (^{0}C)
168	9.5	406
152	9.5	335
116	11.5	201

Due to high current density at corners of coil turns, the temperature of the insulation attached to the coil corners is high. Poor thermal conductivity is also one of the issues with the insulating material that results in local increase in the temperature at the coil corners. As referred by [79], exceeding the glass transition temperature of glass-reinforced epoxy laminate materials causes a gradual decrease of its strength as the material changes from a brittle to a plastic condition. This softening temperature is in the range of 135^0C to 260^0C. From table 4.4 it can be seen that the maximum temperature of the coil increased well above this limit when operating peak current is in range of 150 kA or above.

Mechanical stress

The mechanical stress acting on the coil is mainly because of the Lorentz force which is in radial as well as in axial direction. During the EMF process, as the coil imparts the radial force on the workpiece, the repulsive force act on the coil turns and thereby on the insulator supporting the coil. The radial force is maximum at coil central turns and minimum on end turns. In addition to this, coil turns carrying the current, imparts an attractive force on each other which is an axial force.

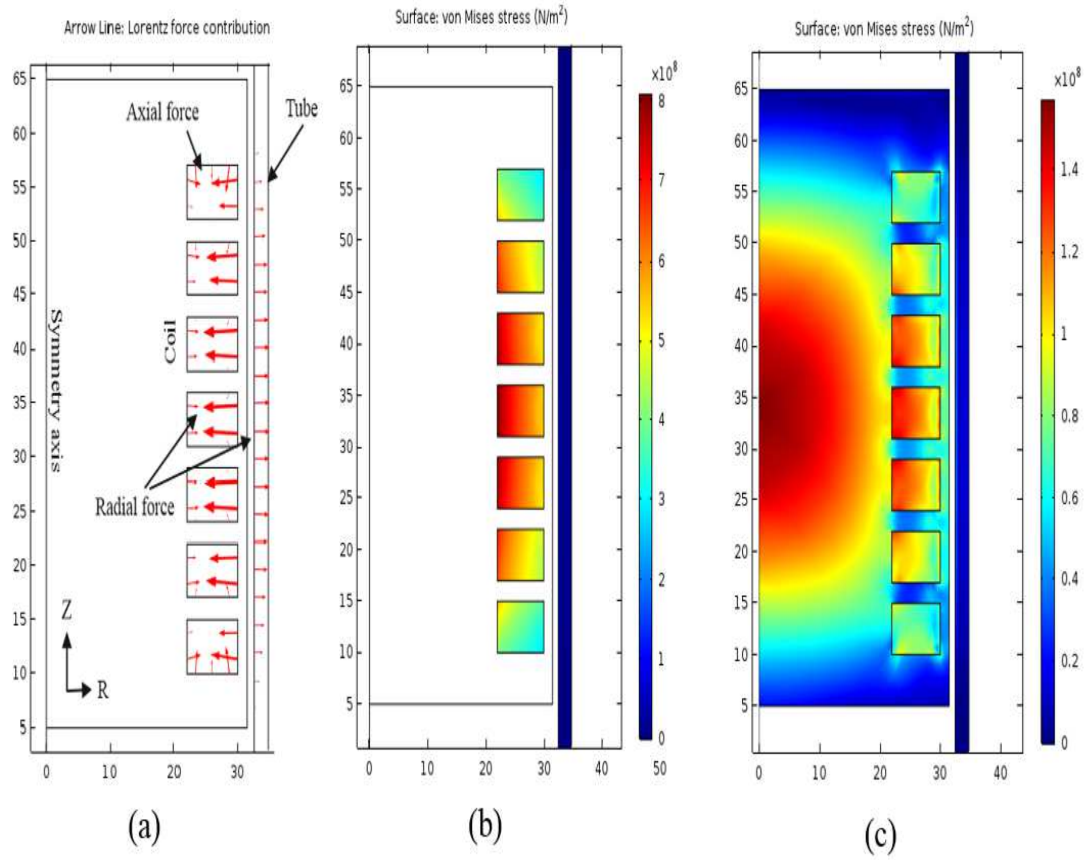

Figure 4.17: (a) Lorentz force directions (b) von Mises stress without insulation (c) von Mises stress with insulation at (168 kA, 9.5 kHz)

Arrows in figure 4.17(a) show the acting force directions at a peak coil current. Number and size of the arrows reflect the magnitude of the force. It can be seen that the axial force is maximum at the end turns of the coil and minimum on the central turns. This axial force tries to compress the coil turns and thereby increasing the stress on the inter-turn insulation. The radial force is maximum at the central turn compared to end turns. This force tries to push the coil turns away from the tube. The axial and radial components of force combine form the von Mises stress on the coil.

Table 4.5: von Mises stress acting on coil and insulator

I_{peak} (kA)	f (kHz)	Max.stress without insul.(GPa)	Max.stress with insul. (GPa)
168	9.5	0.8	0.14
152	9.5	0.68	0.12
116	11.5	0.51	0.08

Figure 4.17 (b) shows the von Mises stress acting on the coil when we do not consider insulation and 4.17 (c) shows the stress when we provide fibreglass insulation around the coil turns. Table 4.5 gives the peak values of the von Mises stress for each of this case. When the insulation is not provided to the coil, the mechanical stress acting on coil turns is higher in magnitude compared to the case when insulation is provided. This is because, when the insulation is provided, the stress has been transferred from coil turns to the attached insulation. The Maximum stress is high at the inner diameter side of the coil turns when the insulation is not provided and it is high at the coil centre axis when the insulation is provided. The von Mises stress at the coil central turns is higher than at end turns which clearly due to the significant contribution of radial force acting on the coil. The tensile strength of The coil insulating material is 1.7 GPa. From table 4.5, it is seen that the maximum stress on the coil insulation is very much less than the tensile strength of the insulating material. Thus it can be concluded that the mechanical loading is not an initial or alone cause for the observed coil failure.

Based on experimental observations and the numerical model results, the coil failure might be occurred as per the further mentioned sequence. At first, due to high temperature at the corners of coil turns, the coil insulator has got weaken mechanically. This might not be in the first test but during subsequent operation of the coil. During the test when the coil failed, the weak insulation of the coil got damaged that further leads to flash over between the coil turns. Thus, thermal loading on the coil seen to be the initial cause that leads to further electrical and mechanical failure of the coil.

We have assumed the coil and tube are of axisymmetric in nature. In practice, the coil has helical in nature and due to this a close observation of formed tube shows that the forming is not exactly axisymmetric. A 3D model is necessary to analyse the helical effect of the coil on the electromagnetic expansion of the tube. The future aim is to develop a 3D numerical model to improve numerical simulation accuracy.

4.4 summary

A helical coil with 7 turns is designed and tested for aluminium tube expansion. The coil has a generated peak magnetic field around 14 T and deformed the 2.4 mm aluminium tube with a peak velocity of 160 m/s. The developed analytical and simulation model results are in agreement with experimental observations. In the coil failure diagnosis, it is observed that the von Mises stress acting on the coil insulator is below the insulator tensile strength. The thermal effect must have weakened the mechanical and electrical strength of insulating material, and caused the coil failure. The heating of the coil plays a vital role in the coil failure compared to the mechanical loading.

Chapter 5

Study on Effect of Coil Current Frequency on EMF

The frequency of capacitor discharge current is an important parameter in the electromagnetic forming process. Study of this chapter aims to obtain an optimum frequency of discharge current. Optimum frequency refers to the frequency at which maximum deformation of tube occurs at constant discharge energy. Simulation and experimental study of electromagnetic expansion is carried out on aluminium tubes (Al 5052). First the numerical simulation results are validated with experimental results and then the simulation model is used to find the optimum frequency of discharge current and to study the effect of process parameters like the tube thickness, inductance and resistance of the system on optimum frequency.

5.1 Experimental testing

With the experimental setup described in chapter 3 and system parameters as given in table 4.1, EM tube expansion experiments are performed on the Al tube. Experiments are carried out at different operating voltage and capacitance value. Capacitance is varied by selecting different

Table 5.1: Experimental results

Exp.No.	Energy(kJ)	Capacitance(μF)	Voltage(kV)	Tube radial forming(mm)
1	10.108	56	19	4.5
2	14.336	112	16	9.4
3	16.184	112	17	10.5
4	18.144	112	18	13.3
5	20.216	112	19	14.7
6	21.504	168	16	11.5

capacitor banks. Figure 5.1 and 5.1 depicts some of the tube forming images and table 5.1 gives the obtained tube deformation for each experiments. Here the tube radial deformation is measured at the maximum forming point of a tube.

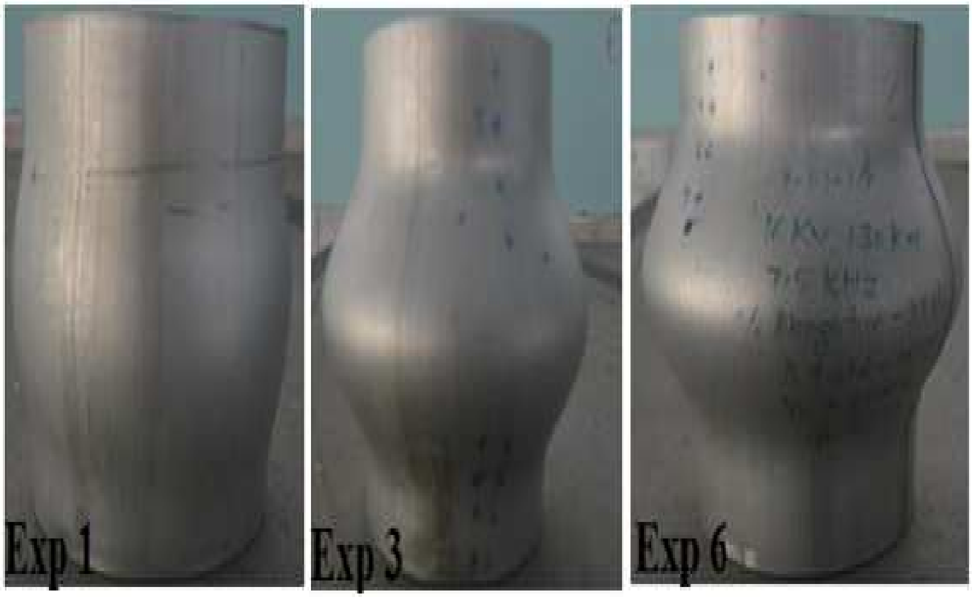

Figure 5.1: Forming images of the tube at different experiments numbers given by table 5.1

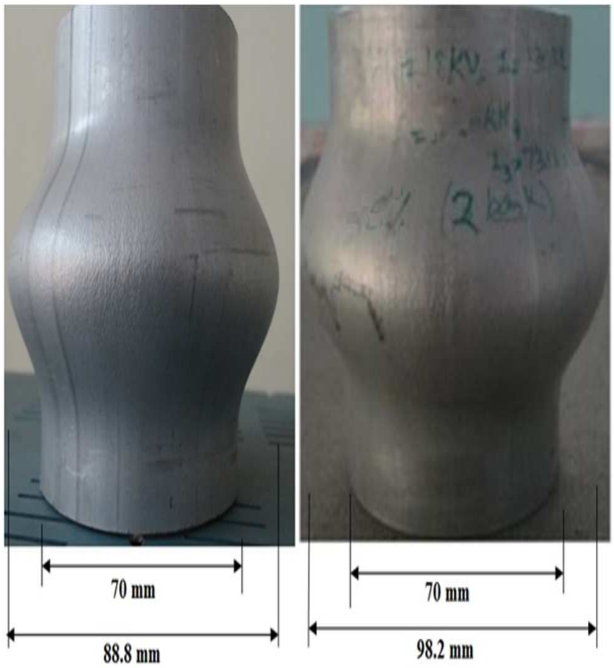

Figure 5.2: Expanded tubes (a) 26.8% (b) 40.2% change in diameter

Expansion of tubes goes increasing with an increase in discharge energy E_c. Maximum deformation of the tube occurred in the central region and less towards the tube ends. This happened because of tube length is higher than the coil length. Maximum magnetic flux concentration occurred at the tube surface facing the coil central turn, and that causes higher magnetic pressure at the middle part of the tube. For the operating voltage of 16 kV and capacitance of 112 μF, 26.8% increase in tube central diameter is obtained, whereas an increase in voltage to 18 kV showed a 40% increase in tube diameter. Comparison of experimental and simulation results are shown in figure 5.3.

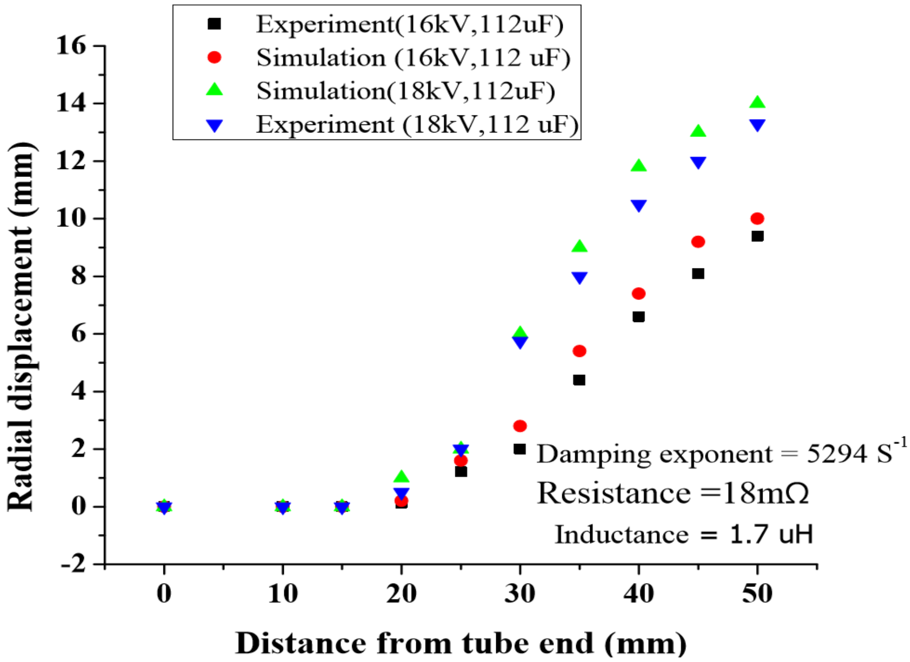

Figure 5.3: Radial displacement of the tube by experiment and by simulation

Numerical results of tube final displacement and experimental results have a maximum error of 8% thereby validating our simulation model. The reason for error can be attributed to the following reasons. (a) The difference in experimental and literature values of material properties and plasticity model constants.(b) Assumptions taken in the numerical model.

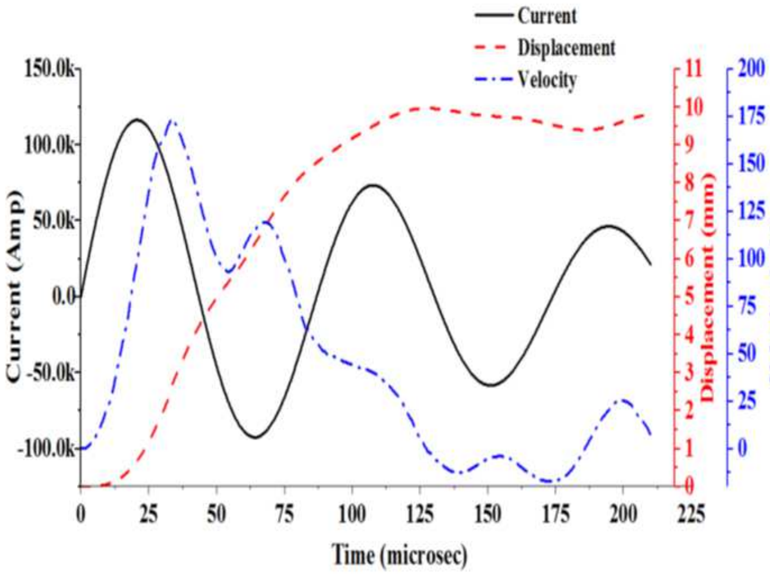

Figure 5.4: Coil current, tube velocity and displacement at 16 kV, 112 μF

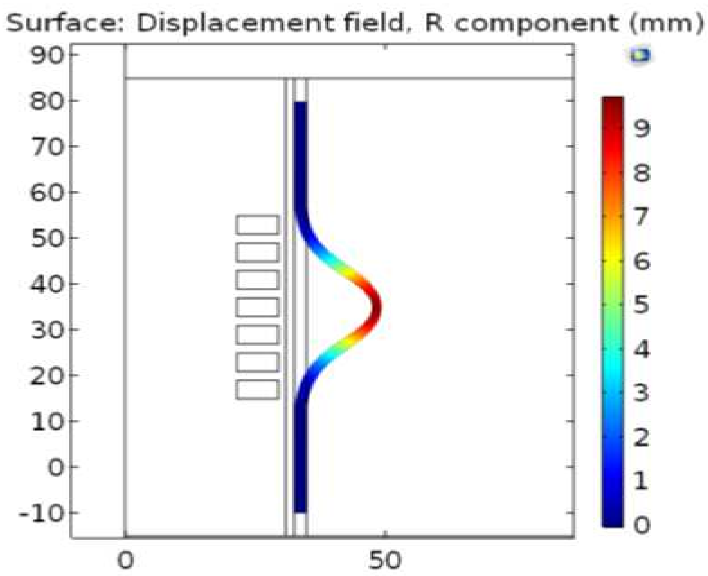

Figure 5.5: Radial displacement of tube obtained at 16 kV, 112 μF

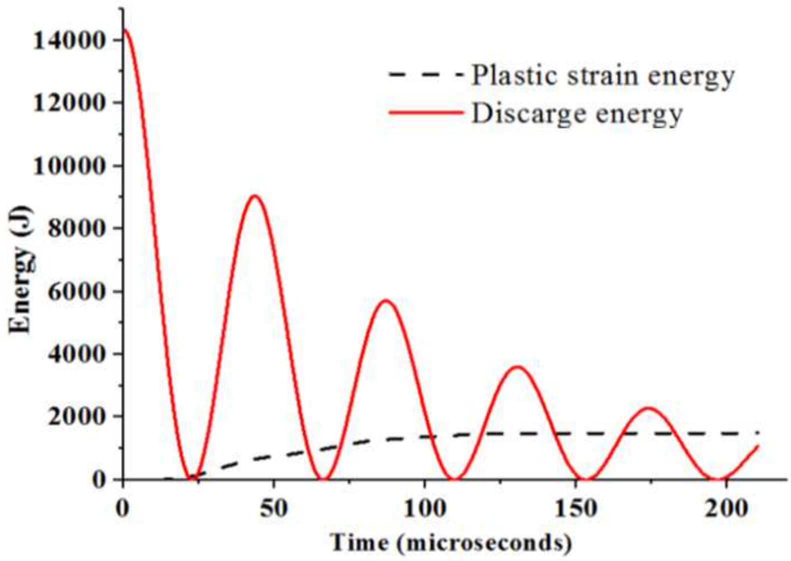

Figure 5.6: Energy plots at 16 kV, 112 μ F

Figure 5.4, 5.5 and 5.6 indicate the simulation results obtained at 16 kV, 112 μF condition. The displacement and velocity variation with time at the maximum displacement point of the tube is shown in figure 5.4. Peak velocity of the tube is found to be delayed by $\sim$15 microseconds from peak coil current which might be due to tube inertia. Figure 11 shows the surface plot of the tube deformation. Forming efficiency is obtained from the ratio of plastic strain energy of the tube to energy stored in the capacitor. Figure 12 shows this energy plots where 10.5% forming efficiency is obtained. This low efficiency can be understood in the following way: As observed in figure 10, tube deformation completes well before the total current dies out. Only first and second current pulses are utilized for workpiece deformation while the consequent pulses result in just heating. This affects the efficiency of the process.

5.2 Optimum frequency estimation

The simulation model is further used to observe the effect of frequency on forming of the tube at constant discharge energy condition. The energy stored in the capacitor is given by the equation 5.1. Here E_c is the energy stored in the capacitor bank, V is the charging voltage of the capacitor bank and C is the capacitance value.

$$E_c = \frac{1}{2}CV^2 \tag{5.1}$$

$$\delta_r = \frac{\delta}{h} \tag{5.2}$$

The operating voltage and capacitance can be varied in such a way to keep discharge energy E_c as a constant. Change in C causes change in the damping frequency of the coil as given by equation 4.1. The magnetic field diffusion in the workpiece depends on the skin depth. The skin depth δ is given by equation 4.14. δ_r is the relative skin depth as given by equation 5.2. It is the ratio of skin depth to workpiece thickness h.

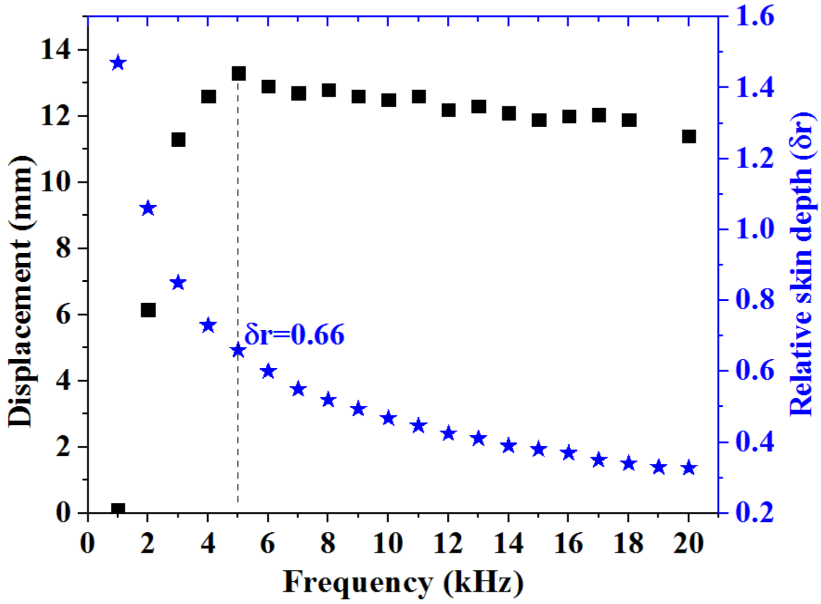

Figure 5.7: Radial displacement of the tube with a thickness 2.4 mm

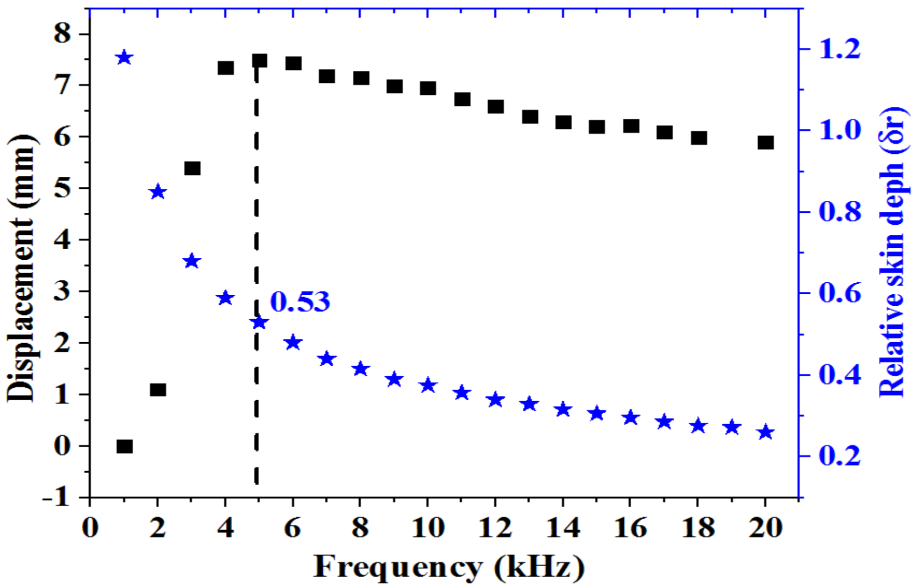

Figure 5.8: Radial displacement of the tube with a thickness 3 mm

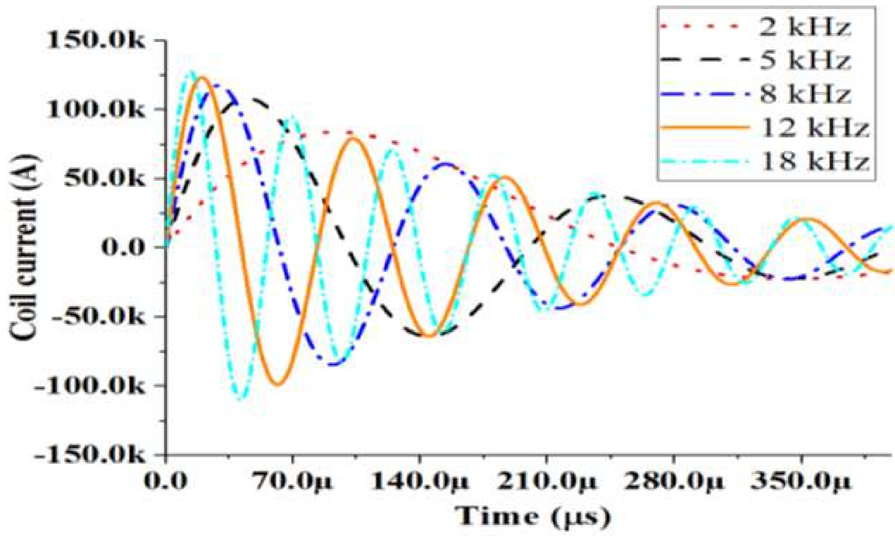

Figure 5.9: Coil current waveform at various frequencies

Figure 5.7 and 5.8 show displacement obtained at different frequencies for different tube thickness. The maximum displacement of the tube is found to occur at 5 kHz, and we called it optimum frequency. The relative skin depth δ_r at the optimum frequency in figure 5.7 and 5.8

is less than one. This observation is in contrast to the sheet forming case [29],[30] where δ_r is equal to and more than one when maximum forming occurs in the sheet.

The optimum frequency phenomenon can be explained with the magnetic pressure profile acting on tube and skin depth. Magnetic pressure is proportional to the square of magnetic flux density and the magnetic field is proportional to the coil current. Higher the current, higher the magnetic field. Skin depth δ increase with the decrease in frequency value[equation(4.14)]. When δ is more than the thickness of the tube, in other words, δ_r is more than one, the magnetic field penetrates through tube thickness. The effective magnetic pressure acting on the tube get reduced. That is why the tube forming reduces when the δ_r is more than one. Increase in frequency increases the current peak value with a decrease in current pulse duration as shown in figure 5.9. At high frequency, though the magnetic pressure is high because of higher peak current, the duration of this pressure pulse is very short due to rapid damping of the current pulse. As mentioned, [42] resultant workpiece forming is not only affected by peak current but also by the duration of the current waveform. That is why the tube forming slowly reduces when the frequency is increased beyond an optimum value. It means that not only the peak current but the optimum combination of peak current and the duration of the current pulse resulted in maximum tube forming. For the used experimental setup, the optimum combination occurred at 5 kHz. Further, the analysis is carried out to study the effect of different parameters on the optimum frequency and corresponding relative skin depth.

Effect of tube thickness

Figure 5.7 and 5.8 show the effect of tube thickness variation at constant discharge energy. It is observed that tube forming is reduced with an increase in tube thickness. With an increase in tube thickness, the optimum frequency is unaffected but the relative skin depth δ_r at the optimum frequency is decreased. This is because the optimum combination of the current peak and duration of the current pulse (current frequency) have resulted in a maximum push to the material. The tube thickness has no effect on the peak current or on the current frequency. The process efficiency of electromagnetic forming is shown in figure 5.10 for different thickness of tubes. Maximum efficiency occurred at same optimum frequency and it is more for thin tubes as these are more susceptible to deformation.

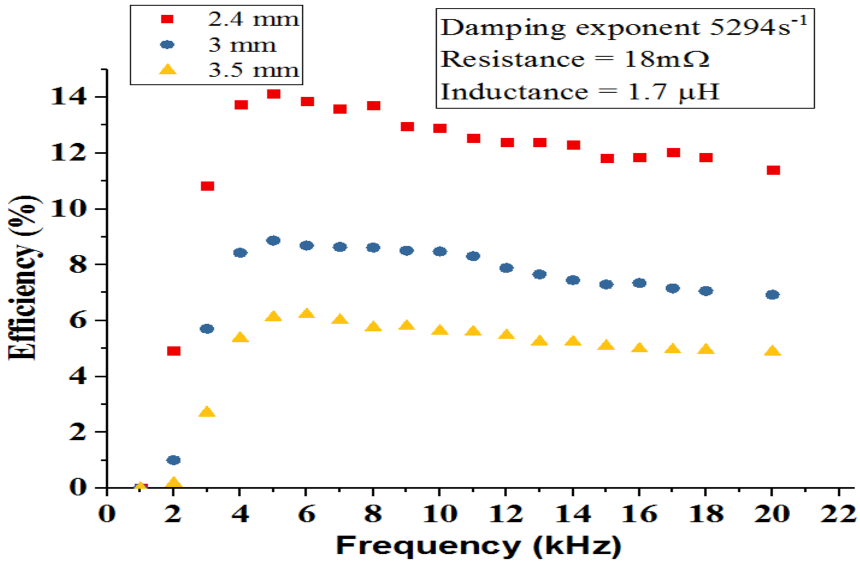

Figure 5.10: Process efficiency variation with frequency

5.3 Effect of system inductance and resistance

Variation in workpiece resistivity, Workpiece length, the coupling between the coil and the workpiece and coil material affect the magnetic pressure acting on the workpiece. From the electrical circuit point of view, all these variations affect the resultant inductance and resistance of the EMF system.

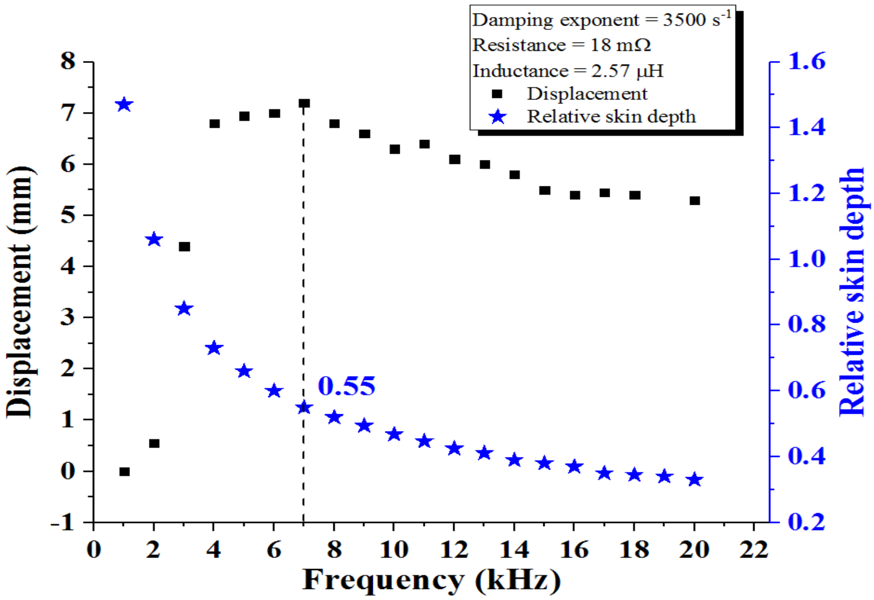

Figure 5.11: Effect of frequency variation with higher inductance on tube expansion

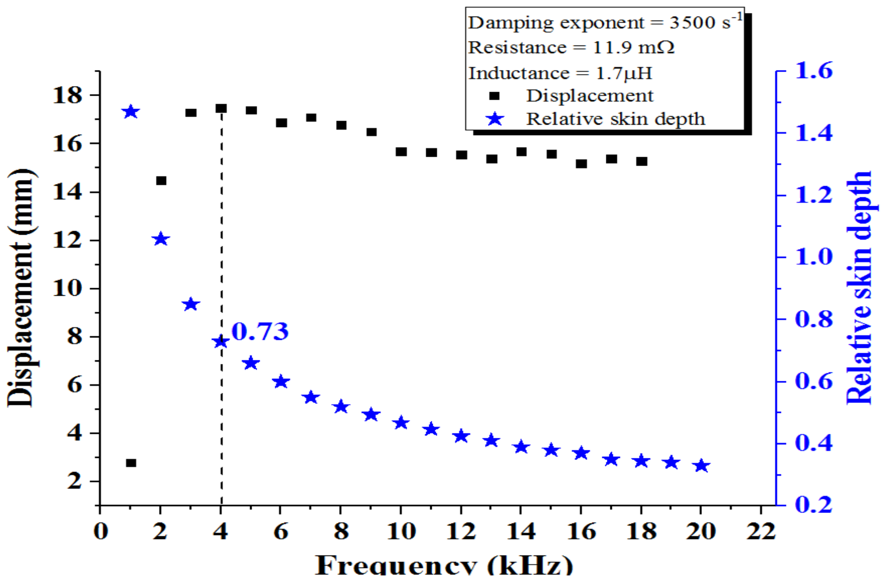

Figure 5.12: Effect of frequency variation with lower resistance on tube expansion

To take into account this parametric variation, the effect of resistance and inductance variation on optimum frequency is studied. The simulation model is used to study the effect of inductance and resistance value on optimum frequency. Figure 5.11 and 5.12 depict the tube expansion performed at reduced damping coefficient β value for 2.4 mm thickness tube. β depends on resistance and inductance of the system as given by equation 4.8). In the first case, β is reduced from 5294 S^{-1} to 3500 S^{-1} by increasing the inductance and in the second case β is reduced to 3500 S^{-1} by reducing the resistance value. Compared to previous results, it is observed that optimum frequency increased with an increase in inductance, whereas it decreased with a decrease in resistance. Thus, the optimum frequency does not remain constant. It depends on system parameters and this fact should be taken into consideration during the design of EMF system configuration. System parameters can be set in such a way that the coil current oscillates with optimum frequency. This gives higher process efficiency along with increase coil life.

5.4 Summary

Electromagnetic expansion of aluminium tubes is carried out experimentally and the tube displacement results are compared with results of the 2D numerical simulation model. Effects of system parameters on the optimum frequency and relative skin depth are further analyzed using a simulation model. From the observed results, the following conclusions are drawn

- The maximum expansion of tubular workpiece occurred at a frequency where the relative skin depth is less than one in contrast to sheet forming case observed in the literature.
- The frequency of current and the relative skin depth at which maximum forming occur are not constant. The optimum frequency changes with resistance and inductance of the system.

Chapter 6

Numerical and Experimental Study on the Variation of the Discharge Circuit Parameters

Discharge circuit parameters vary during the electromagnetic forming process. Initially, the workpiece and the coil are firmly mounted. The moment when workpiece starts going away from the coil due to the magnetic force, there is an increase in the coil-workpiece gap, which causes two interdependent effects. Firstly, the flux density between the coil and workpiece gets reduced, and this reduces magnetic pressure as the magnetic pressure is proportional to the square of the magnetic flux density (equation4.23). Secondly, the reduction in the coil-workpiece magnetic coupling affects the resultant discharge circuit parameters (equation 4.3 and 4.4. In EMF, the coil current is used as an excitation to predict workpiece forming in both analytical [31] and numerical models [32] [38]. The accuracy of analytical and numerical models depends on the exactness of the discharge circuit parameters because the current flow in the coil is a function of discharge circuit parameters. As seen earlier, the sequentially coupled simulation approach is preferred over the loosely coupled simulation approach for EMF simulation. However, the effect of workpiece forming on the discharge circuit parameters is also significant and it is not considered even in the sequentially coupled simulation models [37] [43] . Considering this fact, the importance of the discharge circuit parameter variation during a forming process is analysed in this chapter. A developed analytical model in chapter 4 is modified by considering the nature of the dynamics of discharge circuit parameters at each timestep. The estimated dynamics of discharge circuit parameters are compared with experimental measurements and its effect on discharge current is also studied. Further, the sequential coupled numerical simulation is carried out by two methods. One method that is followed in the literature where the coil current used as input to the sequential coupled numerical model assuming the constant discharge circuit parameters. The second method is a modified one where the discharge current which is fed to numerical model is calculated considering the dynamics of discharge circuit parameters. The obtained results in both the methods are compared with the experimental results.

6.1 Governing equations

The electrical equivalent circuit of EMF is presented in figure 4.10. The coil-tube magnetic coupling varies as tube deforms which affects the coil-tube coupled resistance and inductance. Taking this into account, the coil-tube coupled resistance and inductance are defined as a function of tube position [80]. The time *t* dependent inductance and resistance of the discharge circuit are defined by equation 6.1 and 6.2 respectively.

$$L_T(t) = L_s + L_c \frac{[w_i(t)]^2 - r_2^2}{[w_i(t)]^2 - r_2^2 + r_1^2} \tag{6.1}$$

$$R_T(t) = R_s + R_c + \frac{N r_1^2}{[w_i(t)]^2 + r_1^2 - r_2^2} R_w \tag{6.2}$$

Figure 6.1 shows the coil and tube arrangement with the dimensions. Here, the r_1 and r_2 are the coil inner and outer radius respectively. As the coil is stationary and only workpiece going to deform, the r_1 and r_2 values remain constant and only w_i, which is the tube inner radius is going to increase during forming. The discharge circuit parameters R_T,L_T, β, ω and *i(t)* given in equations 4.3- 4.8 will also change accordingly.

Analytical modelling performed here is similar to that mentioned in the chapter 4. The difference is only that, based on tube position at each timestep, the discharge circuit parameters are updated. The flowchart is shown in 6.2. At each timestep, increment in 'w_i' due to tube movement is communicated back to equation 6.1 and 6.2 to modify R_T and L_T accordingly. Further, the analytical results are compared to experimental and numerical results.

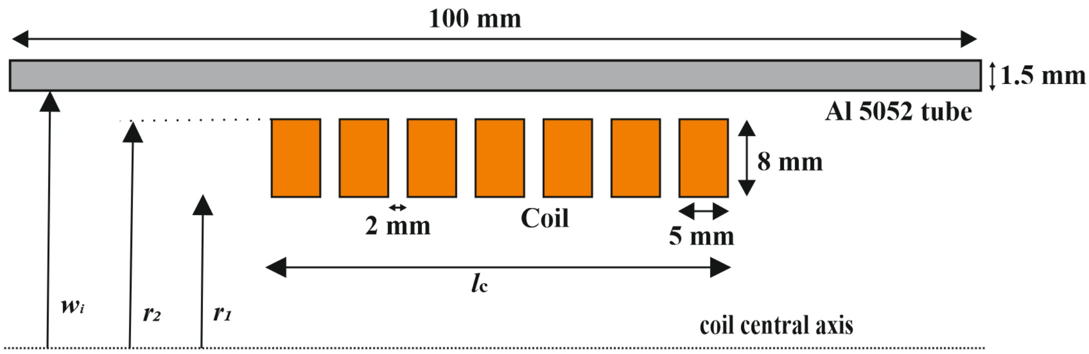

Figure 6.1: Arrangement of the coil and tube in 2D

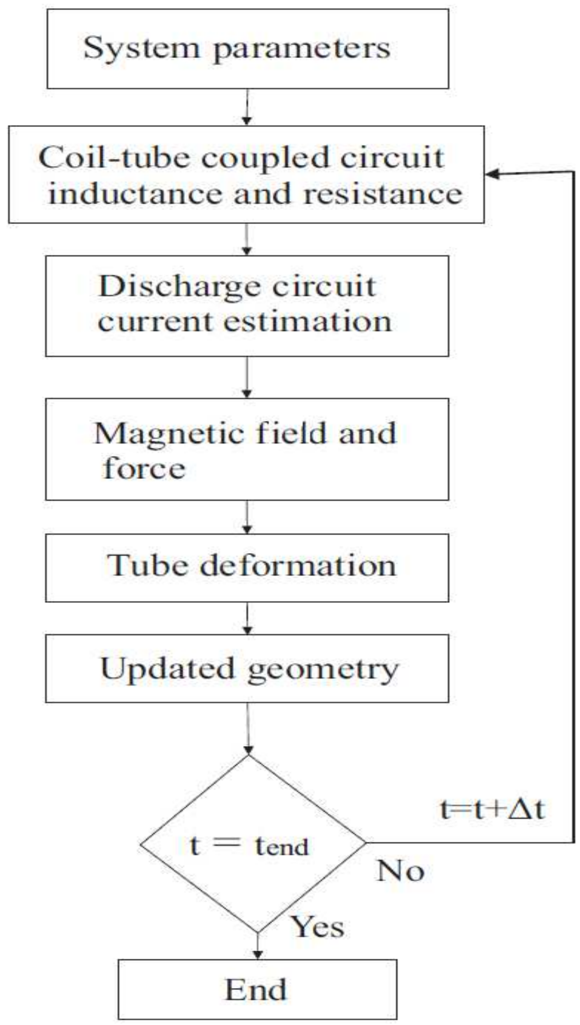

Figure 6.2: Flowchart of the analytical model

6.2 Experimental testing

EMF experiment is conducted on aluminium 5052 tubular workpiece. Table 6.1 gives the used parameter details whereas figure 6.3 shows the experimental arrangement of the coil and tube. The aluminium tube is placed over the coil, and the coil is connected to system high current discharge terminals. A supporting structure made up of Delrin is used to prevent the coil vibration and to maintain a uniform gap between the coil and the tube. A Rogowski coil is used to measure the discharge current.

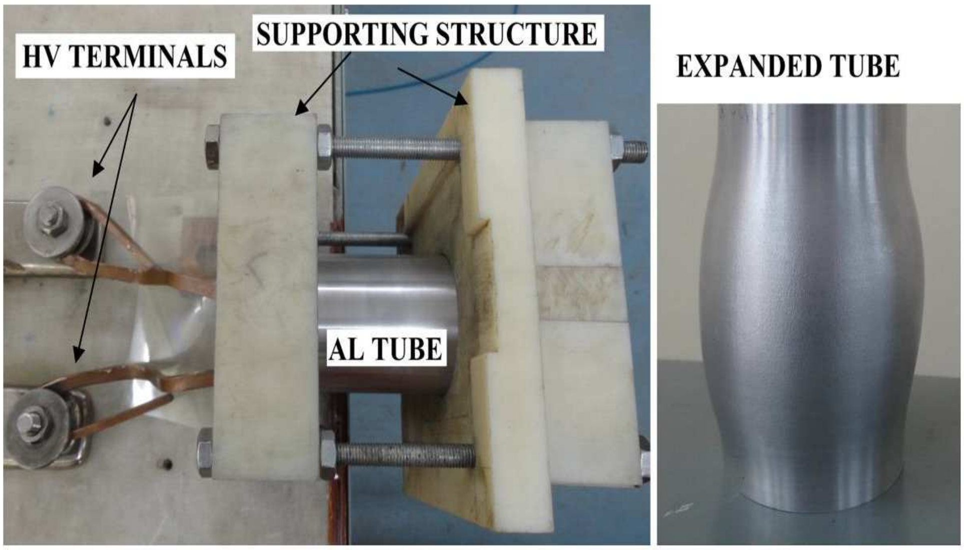

Figure 6.3: Experimental set up and expanded tube

Table 6.1: Discharge circuit parameters

Component	Parameter	Value
System	Capacitance (C)	112 μF
	Charging voltage (V)	13.6 kV
	Resistance (R_s)	8.8 m Ω
	Inductance (L_s)	0.7 μH
Coil	Length (l_c)	47 mm
	Inner radius (r_1)	21.4 mm
	Outer radius (r_2)	29.4 mm
	Inductance (L_c)	1.52 μH
	Resistance (R_c)	6 m Ω
Tube (Al 5052)	Length (l_w)	100 mm
	Thickness (w_t)	1.5 mm
	Inner radius (w_i)	33 mm

The coil-tube coupled system inductance and the resistance after the tube expansion are measured by an LCR meter and these parameters are used to compare with the analytical estimated results.

6.3 Results and discussion

Discharge circuit parameters variation

With the developed analytical model, the variation of discharge circuit parameters L_T, R_T and β during forming is estimated as shown in figure 6.4.

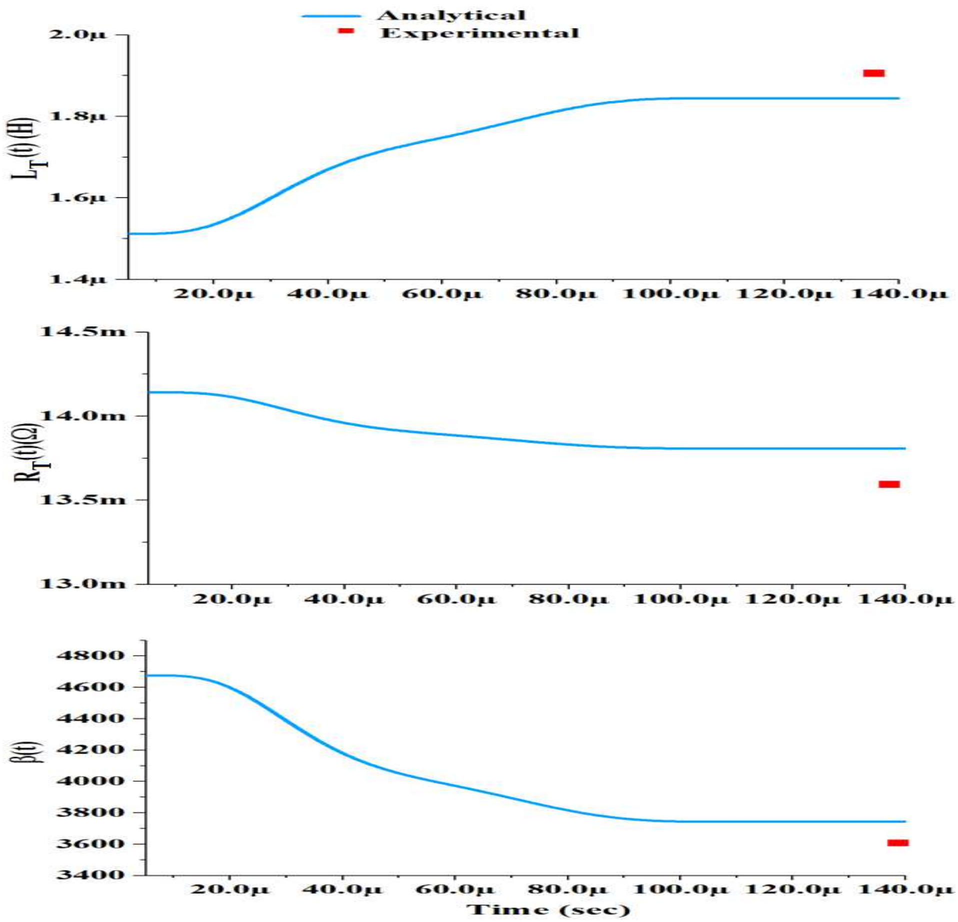

Figure 6.4: Variation of discharge circuit parameters with time

It can be observed that around 20 microseconds, the parameters start to vary as at this point, the acting magnetic pressure over the tube overcomes its yield pressure and the tube starts deforming. The coil-tube magnetic coupling *K* reduces as the tube is deformed which results in a decrease in the mutual inductance *M*. As per equation 6.1 and 6.2, this causes an increase in L_T and a slight decrease in R_T of the discharge circuit. The reason for the decrease in R_T can be understood by the skin depth phenomenon. The β coefficient is also decreased being dependent on R_T and L_T. The discharge circuit parametric variation remains constant after 100 microseconds which indicate the completion of the forming process. In the experiment, when the tube forming is completed, L_T and R_T parameters are measured and are found to be 1.88 μH and 13.6 mΩ respectively. At the end of the forming process, the estimated analytical parameters are found to be near to the experimental values as observed in figure 6.4. Further, the validity of estimated parametric variation during the forming process is done by comparing the estimated and experimental measured coil current waveform.

Coil current estimation

Here, the coil current is calculated for two cases. In the first case, the estimated dynamics of the discharge circuit parameters are taken into account and in the second case, the discharge circuit parameters are considered as constant. The estimated coil current in both the cases is compared with the experimental measurement as shown in figure 6.5. It can be observed that the experimentally recorded current waveform closely matches with the analytically estimated waveform that includes the discharge circuit dynamics. The other estimated coil current waveform, where circuit parameters R and L are assumed to be constant follows the experimental waveform until the first current peak (20 μs). This is because there is no movement of the tube till that time. However, after that, a clear difference in the current magnitude and the frequency can be seen.

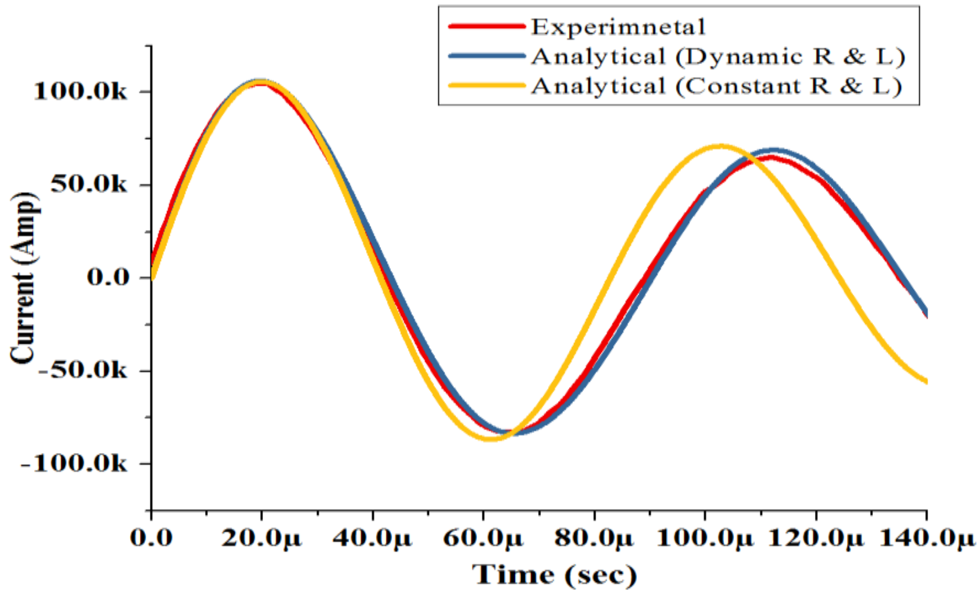

Figure 6.5: Discharge current waveform comparison

The tube movement away from the coil caused a significant increase in L_T and a minor decrease in R_T, which leads to a decrease in both current magnitude and current frequency.

Analytical and numerical results comparison

In this section, we checked the validity of the analytical model with the numerical model. In both the models, the dynamics of the discharge circuit is considered to obtain the coil current. The variation in the velocity and displacement of tube central point with time obtained by the analytical and numerical model is compared as shown in figure 6.6 and 6.7 respectively. A good agreement is demonstrated between predicted and simulation results. The final displacement of the tube central point observed in the experiment is 8.2 mm. An error of 4 $\%$ and 9 $\%$ have occurred when the experimental displacement is compared with analytical and simulation results respectively. After the first peak in velocity, a phase shift is observed between predicted and numerically obtained velocity as shown in figure 6.6, but this parameter is less critical in the final results.

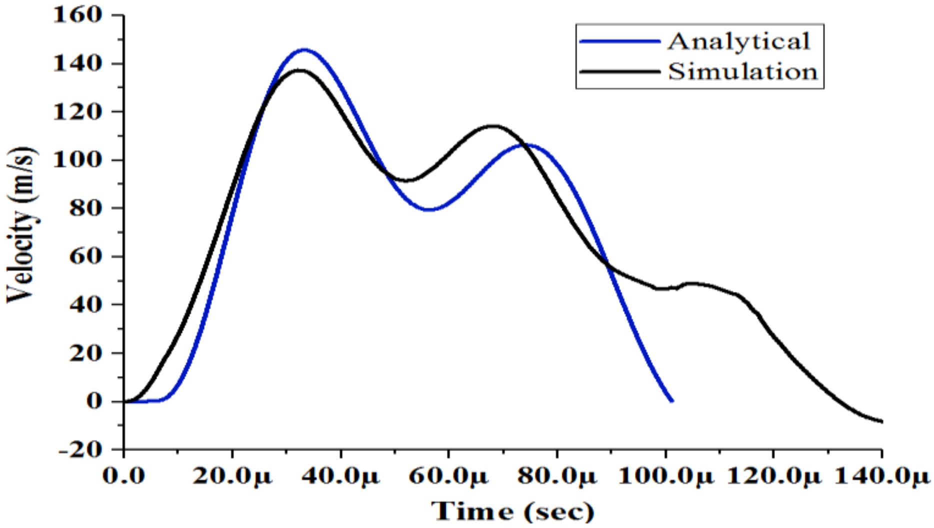

Figure 6.6: Tube velocity results predicted by analytical and simulation

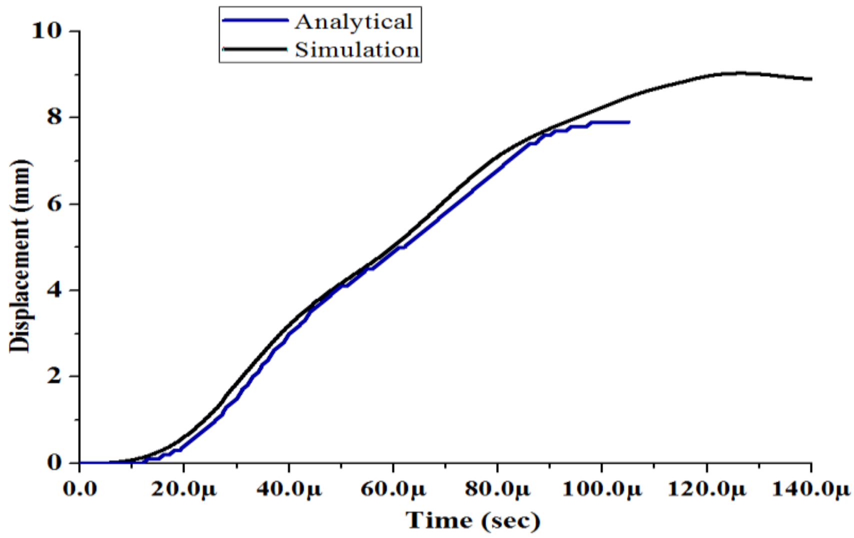

Figure 6.7: Tube displacement predicted by analytical and simulation

As observed in figure 6.7, the tube achieved its final displacement in the analytical model

($\sim$ 100 μs) prior to numerically predicted value ($\sim$ 120μs). The error between the numerical and analytical results can be due to the fact that the developed analytical model is a 1D. 1) The tube central displacement predicted by the model is only due to the force acting at the centre. Whereas in the actual case or in the numerical model, the tube central displacement is due to the cumulative effect of force at center as well as the force at nearby points of centre. 2) We estimated the dynamic nature of discharge circuit parameters based on the tube central point displacement, but in practice, the tube displacement is not the same along the length. It is highest at the centre and gradually decreases towards its end. In actual case and as interpreted by the numerical model, the tube achieved permanent displacement when it deforms plastically. The developed analytical model is a simplified one where the tube plasticity is not defined. In the analytical model, the tube displacement is estimated using Newton's law of motion where the acting magnetic force is one which is above the tube yield pressure. This condition meets till 100 microseconds and that is why the tube displacement and velocity in the analytical model are considered until 100 microseconds only.

Importance of discharge circuit dynamic parameters in numerical modelling

As stated earlier, the accuracy of the numerical simulation model depends on the accuracy of the coil current that is used as input to the numerical model. The impact of variable nature of discharge circuit parameter on the coil current is studied in the previous section. Using the estimated coil current waveforms of figure 6.5, the impact of the discharge circuit dynamics on the numerical model results is analysed in this section.

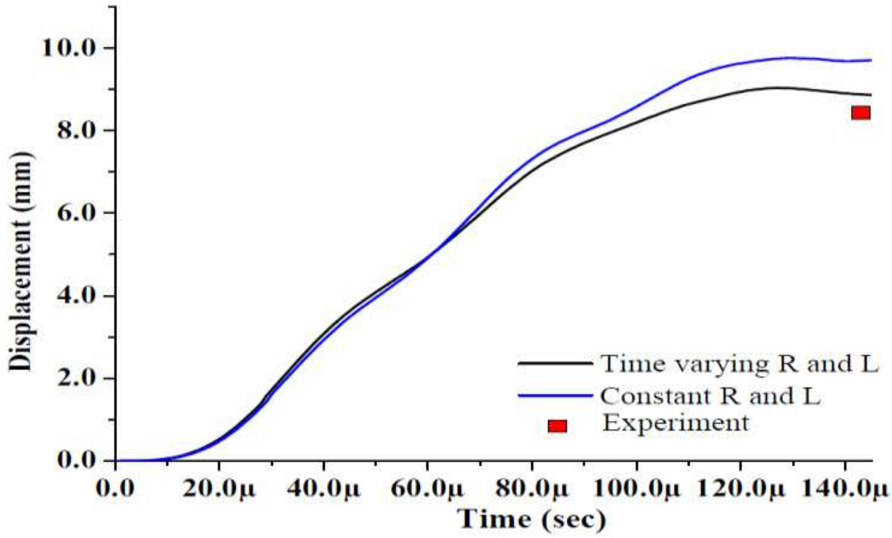

Figure 6.8: Tube displacement by simulation and experiment

Analytical estimated current shown in figure 6.5 gives the required coil current excitation in the numerical model for the following two cases.

- Coil current with constant R_T and L_T parameters
- Coil current with considering the dynamic nature of R_T and L_T

The simulation runtime is set, ensuring the complete tube displacement and current decaying. The final tube displacement at the tube central point is measured in both the simulation model and compared with experimental results as shown in figure 6.8. It is observed that negligence of discharge circuit parameter dynamics results in tube displacement estimation to the higher side. The error in final tube displacement between experimental and simulation result is reduced from 17 to 9 $\%$ under consideration of the dynamic R_T and L_T parameters to estimate the coil current. Thus the accuracy of the sequentially coupled numerical simulation is found to be improved by the considerations of discharge circuit parameters dynamics. Analytical and numerical results slightly differ from experimental results which may be due to the difference in the experimental and used literature values of material properties and plasticity model constants. The calibration error in the measuring instruments also might be one of the causes of the error. The developed analytical model that takes into account the varying nature of *R* and *L* parameters is found as a good choice to estimate the actual coil current and thereby can be used to improve the accuracy of the sequential coupled numerical model.

The analytical model developed in the present study is applicable to study the dynamics of discharge circuit parameters for axisymmetric EM tube expansion cases. However, the importance of dynamics of discharge circuit parameters is applicable in all EM forming cases where workpiece goes away from the coil by a large distance. The impact of the dynamics of parameters will be different for each type of forming cases. This impact more dominant in case of sheet forming cases as in the case of sheet forming, the influence of coil workpiece gap on acting magnetic pressure is high

6.4 Summary

In this chapter, the study of electromagnetic tube expansion is performed with an aim to investigate the importance of discharge circuit parameters variation during a forming process. An analytical model is developed that is able to predict the dynamics of discharge circuit parameters as well as tube displacement and velocity. Electromagnetic tube expansion study is carried out experimentally along with the numerical model. In the sequentially coupled simulation study, the error in the estimated tube displacement is reduced from 17 to 9 % when the dynamic nature of discharge circuit parameters is considered in the input current waveform. The results show that incorporating the dynamics of discharge circuit parameters is a key role in the analytical and numerical study of the electromagnetic forming process.

Chapter 7

Numerical and experimental study on Effect of Coil to Tubular Workpiece Magnetic Coupling

In EMF, electrical efficiency denotes the amount of transfer of electrostatic energy stored in capacitor banks to the electromagnetic energy in the tool coil, whereas mechanical efficiency is the ratio of electromagnetic energy to forming energy. The overall process efficiency in electromagnetic forming applications is very less [8] [29]. One of the factors for less efficiency is the leakage flux, and that is related to the coil and workpiece magnetic coupling. In the present chapter the importance of coil-workpiece magnetic coupling in electromagnetic forming (EMF) process and in the electrical representation of the process has been dealt. The analysis is carried out with the help of experiments, and the finite element based numerical simulation. Aluminium tube of 100 mm length and 1.5 mm thick is electromagnetically expanded using a 7 turn helical coil. Trials are taken for the different gaps between the coil and tube keeping the discharge energy constant. The coupling factor (K) variation with the coil-tube gap (h) is related with curve fitting and this *k-h* relation is used to estimate the discharge circuit parameters of EMF process.

7.1 Coupling factor *K* in EMF

A typical EMF system and its electrical equivalent circuit representation are seen earlier(Figure 4.1 and Figure 4.2). Equation 7.1 and 7.2 show the resultant R_T and L_T of the current discharge circuit. The coil-tube mutual coupling forms the mutual coupled inductance *M*. The relation between mutual inductance M and coupling factor *K* is given by Equation 7.3

$$L_T = L_s + L_c - \frac{M^2}{L_w} \tag{7.1}$$

$$R_T = R_s + R_c + \frac{M^2 R_w}{L_w^2} \tag{7.2}$$

$$M = K\sqrt{L_c L_w} \tag{7.3}$$

$$L_{cw} = L_c - \frac{M^2}{L_w} \tag{7.4}$$

$$K = \sqrt{1 - \frac{L_{cw}}{L_c}} \tag{7.5}$$

Lcw defines the coil-tube coupled inductance. Using equation 7.3 and 7.4, *K* can be obtained. By measuring the coil-tube inductance L_{cw} and coil inductance L_c, it is possible to calculate *K* without performing the forming experiment and without measuring tube induced current. K varies between 0 for uncoupled to 1 for the fully coupled system. As coil-tube gap (*h*) varies, the discharge circuit parameters R_T and L_T also change.

7.2 Experimental details

Electromagnetic tube expansion experiments are performed using a 7 turn helical coil. Coil-tube arrangement is shown in figure 6.1 and dimensions are given in table 6.1.

All the experiments are carried out at constant discharge energy condition where charging voltage is set to 13.6 kV and capacitance is 112 μF. h is the gap between the coil's outer surface to the tube inner surface and this is varied to analyse the magnetic coupling effect on tube expansion. Different diameter tubes are used to vary h. A 40 kJ rated capacity pulse generator is used for the experiments. A short circuit test is done to estimate L_s and R_s values of the system 3.3. Before connecting the coil to the high voltage terminals, the coil-tube coupled inductance L_{cw} and resistance R_{cw} are measured separately for each h value. A tube is placed over the coil, and the LCR meter is connected to coil terminals to get L_{cw} and R_{cw}. Coil parameters, R_c and L_c are also measured using an LCR meter. Based on these values, the coupling factor *K* is obtained using Equation 7.5 Different tube expansion experiments are performed with increasing the coil-tube gap by 1 mm and keeping the same discharge energy.

7.3 Numerical simulation

A finite element model in the COMSOL Multiphysics is also developed with certain assumptions. The details of the same is given in the chapter 3. When the helical coil is excited by the current, by the law of electromagnetic induction, an eddy current is induced in the tube having the direction of current opposite to that of the coil current. Similar to the transformer, for ideal coupling factor (*K*=1), the magnitude of current in the tube is *N* times the coil current where *N* is the number of turns of the tool coil. In the numerical simulation, the peak current of the coil is compared with the peak value of eddy current induced in the tube to calculate *K* as shown in equation 7.6.

$$K = \frac{I_w}{NI_c} \tag{7.6}$$

Where I_w is the eddy current flowing through the tube, and I_c is the current through the coil. Once the *K* is determined for each coil-tube gap, the electromagnetic and structural physics are solved numerically to observe the effect of this *K* on tube expansion at constant discharge energy.

7.4 Results

Effect of *h* on coupled circuit parameters

Table 7.1 shows the measured experimental parameters. With the increase in *h*, coil-tube inductance L_{cw} increased, whereas resistance R_{cw} decreased. Overall, the coil-tube coupled impedance increases with *h* causing a decrease in the damping coefficient β and peak coil current I_{peak}. The Observed results can be explained by coil-tube magnetic flux linkage phenomenon.

Table 7.1: Coil- tube flux linkage for different *h*

h(mm)	L_{cw} (μH)	$R_{cw}(m\Omega)$	β (1/sec)	I_{peak}(kA)
3	0.831	5.97	4823	105.8
4	0.953	5.61	4358	103.6
5	1.046	5.43	4075	101.9
6	1.120	5.12	3824	101.1
12	1.412	4.96	3257	94.8

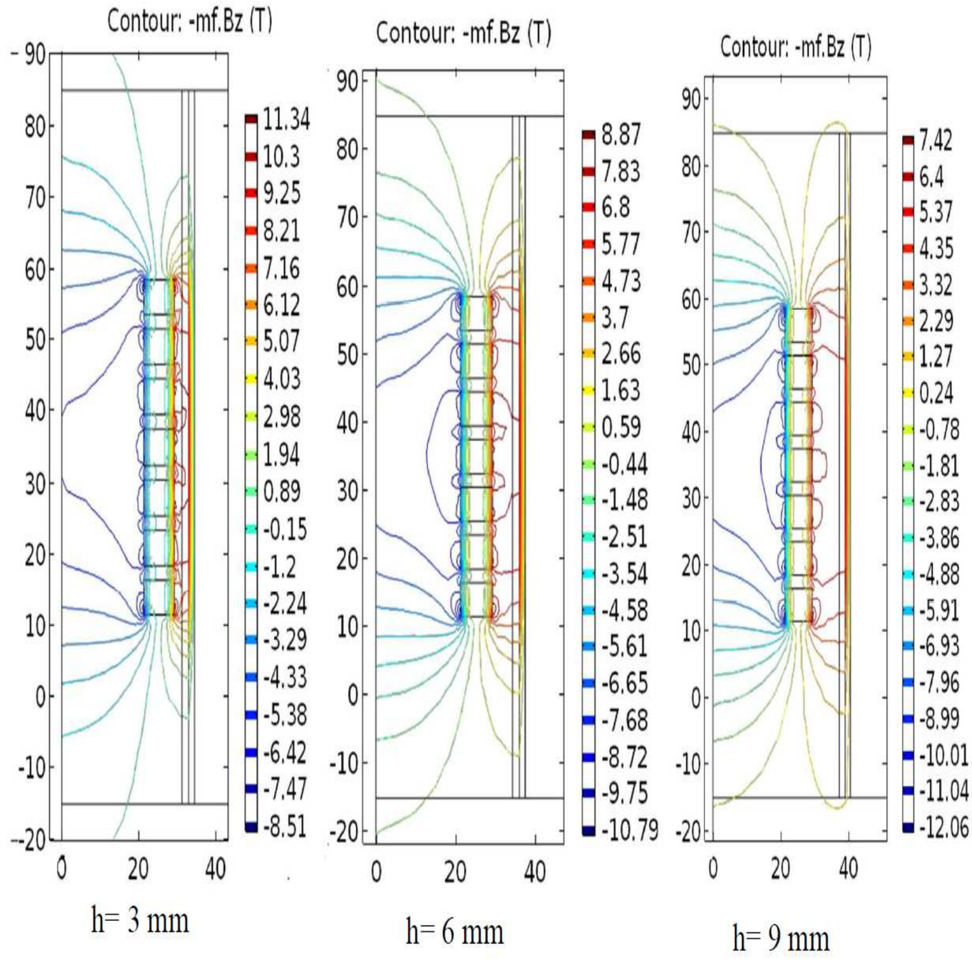

Figure 7.1: Coil- tube flux linkage for different *h*

Figure 7.1 shows the contour plot of axial magnetic flux density responsible for the radial magnetic force. Out of the total magnetic flux produced by the coil, some flux is not linked with the workpiece which is referred to as leakage flux. It can be observed from Figure 7.1 that smaller the gap between the coil and the tube, more the coil-tube flux linkage and hence better the coupling factor *K*. As per equation 7.4, the L_{cw} is reduced with *K* improvement. The reason for the decrease in R_{cw} with *h* can be explained by the skin depth phenomenon. Skin depth δ is the depth below the surface of the conductor at which the current density has fallen to 1/e of its maximum value. As *h* increases, L_{cw} increases and this reduces the damping frequency f (ω=2πf). δ increases with a decrease in *f* and thus increase in area for current flow causing a decrease in R_{cw}.

K variation with *h*

Figure 7.2 shows the variation of K with h. Obtained K value with experimental measurement (equation 7.5 is compared with the numerical one (7.6). A decrease in K is observed to increase in h.

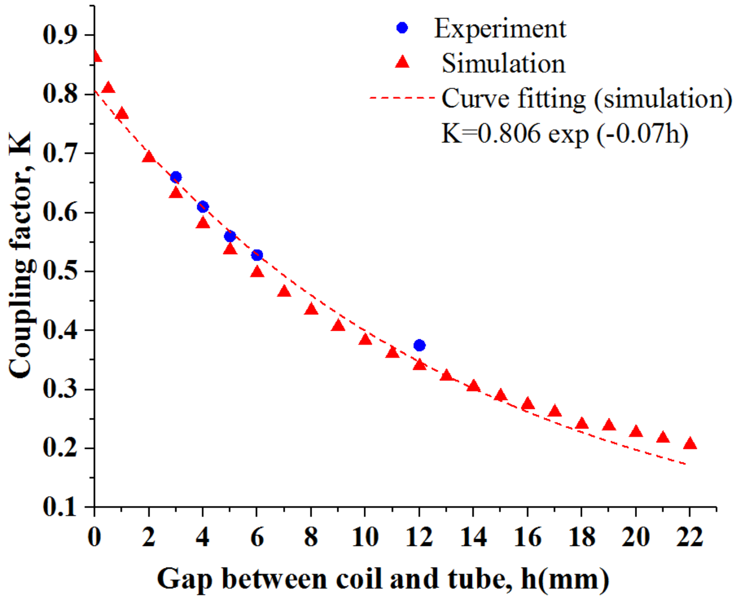

Figure 7.2: coupling factor K variation with h

The variation of K with h is fit by an exponential curve with the equation, $K = A_0 e^{-B_0 h}$ where A_0 and B_0 are the constants with values 0.806 and 0.07 respectively. A_0 represents the maximum value of K when there is no gap between the coil and the tube. The obtained relation of K is purely a function of the coil-workpiece gap h. In addition to coil-tube gap, K is also affected by coil mate-rial conductivity, coil and workpiece geometries. But these effects are not much dominant as compare to h over K. This is because, in most of the EMF applications, excitation coil is made up of copper and the workpiece is usually of electrically conductive material which does not undergo a significant change permeability or skin depth. Once K is known, equations 7.1- 7.3 can be used to simplify the discharge circuit in RLC series form.

Effect of *K* on tube displacement and process efficiency

In order to study the effect of K on tube radial displacement and the EMF process efficiency, Electromagnetic forming experiments and simulations are performed for different K values at constant discharge energy. Tube displacement is measured at the maximum forming point of the tube whereas process efficiency is obtained from simulation which is the ratio of plastic deformation energy of the tube to the stored energy in the capacitor.

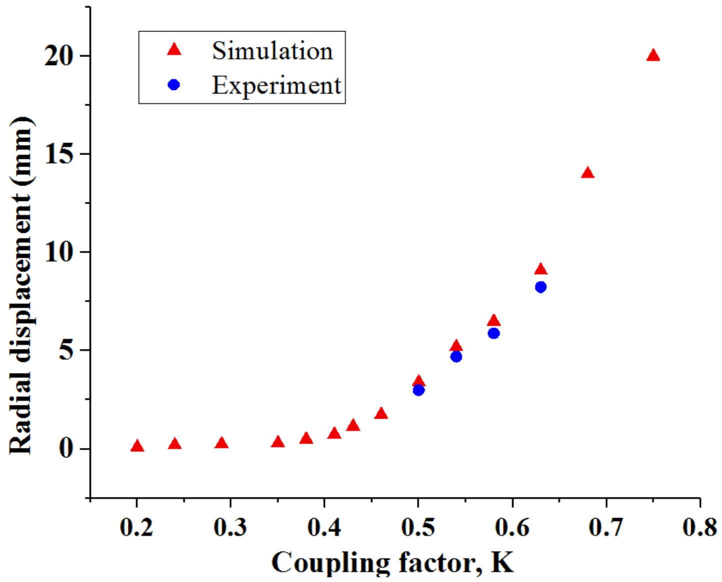

Figure 7.3: Variation of tube displacement with K

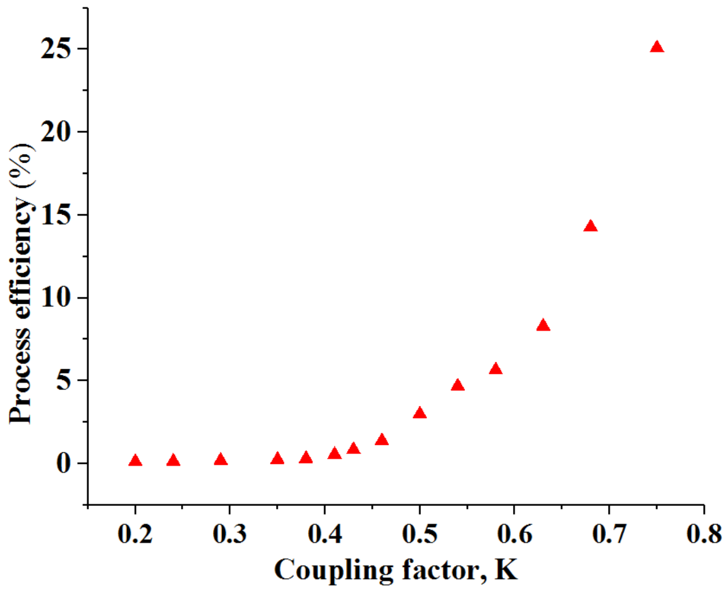

Figure 7.4: forming efficiency with K

As can be seen from figure 7.3, experimentally obtained results show good agreement with simulation results. It can be seen that the radial displacement of the tube and the process efficiency(shown in figure 7.4) follows a smooth exponential curve that increases as K increases. When the skin depth is small compared to workpiece thickness, the magnetic pressure acting on the workpiece is proportional to the square of magnetic flux density present in the coil-workpiece gap [8]. As depicted by figure 7.1, lesser the value of h, higher is the flux density and higher the magnetic pressure acting on the tube. The high pressure causes large displacement and thereby more process efficiency. Thus, the coil-tube magnetic coupling K has a significant effect on tube displacement and forming efficiency and this effect must be considered in designing EMF set up. Theoretically, the tubular workpiece should be kept close to the coil to get maximum process efficiency; but there are some constraints which are needed to be taken into account while selecting h. During discharging of capacitive energy into the coil, a high voltage appears across each turn of the coil and across the coil and workpiece. While placing the workpiece closer to the coil, short circuit and arcing between coupled materials must be avoided. Though the heating in EMF is considered as adiabatic, at higher temperatures in the coil, the insulation may provide the path for an electric short between the coil and the workpiece. These can be avoided by providing insulation over the coil which has sufficient electric and thermal properties.

Variation of discharge circuit parameters with *K*

The derived *K*-*h* relation and equations 7.1- 7.3 are used here to analytically calculate the nature of R_T and L_T variation with *h*. The analytical results are further compared with experimentally measured values. The inductance of the coil and tube can be calculated using equation 7.7 whereas the resistance of the coil and tube can be estimated using equation 7.8 [76].

$$L = \frac{\mu_0 \pi}{8} r_1 \frac{(\alpha_1 + 1)^2}{\beta_1} N^2 g(\alpha_1, \beta_1) \tag{7.7}$$

$$R = \frac{\rho}{f_f} \frac{N^2}{r_1} \frac{\pi}{2} \frac{\alpha_1 + 1}{\beta_1(\alpha_1 - 1)} \tag{7.8}$$

Where, g (α_1, β_1), α_1, β_1 are coil geometry dependent parameters. f_f is the filling factor (the fraction of conducting material in the volume of the coil) and ρ is the resistivity of the material. μ_0 is the permeability of free space and r_1 is coil inner radius. Equation 7.1 and 7.2 are modified by the inclusion of derived *K*-*h* relation as shown below.

$$L_T = L_s + L_c - [A_0 e^{-B_0 h}]^2 L_c \tag{7.9}$$

$$R_T = R_s + R_c + [A_0 e^{-B_0 h}]^2 \frac{R_w}{L_w^2} \tag{7.10}$$

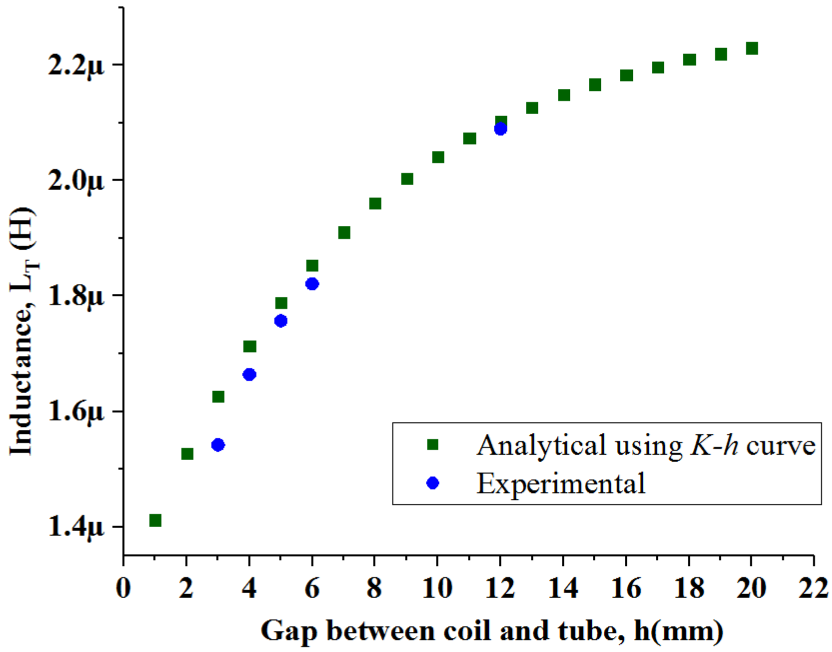
Inductance, L_T (H)
2.2μ
2.0μ
1.8μ
1.6μ
1.4μ
0
2
4
6
8
10
12
14
16
18
20
22
Gap between coil and tube, h(mm)
Analytical using *K-h* curve
Experimental

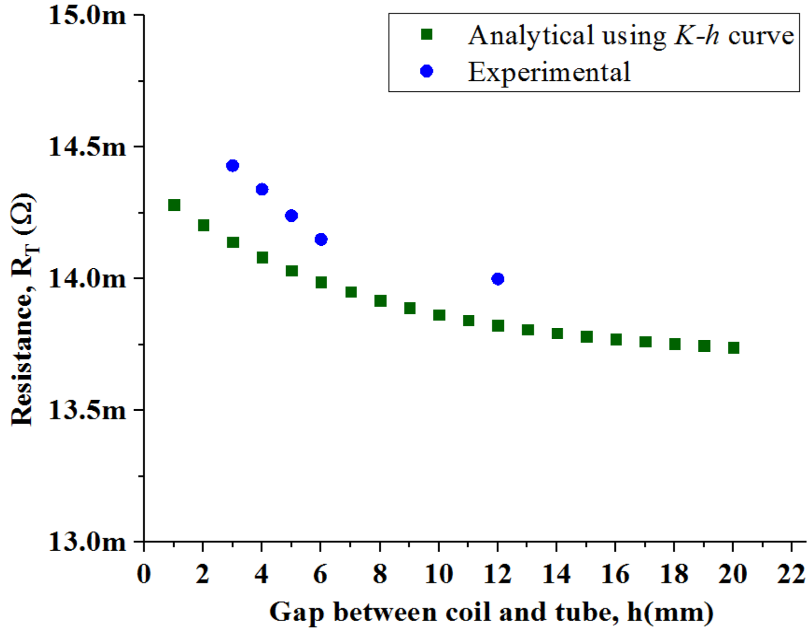
Resistance, R_T (Ω)
15.0m
14.5m
14.0m
13.5m
13.0m
0
2
4
6
8
10
12
14
16
18
20
22
Gap between coil and tube, h(mm)
Analytical using *K-h* curve
Experimental

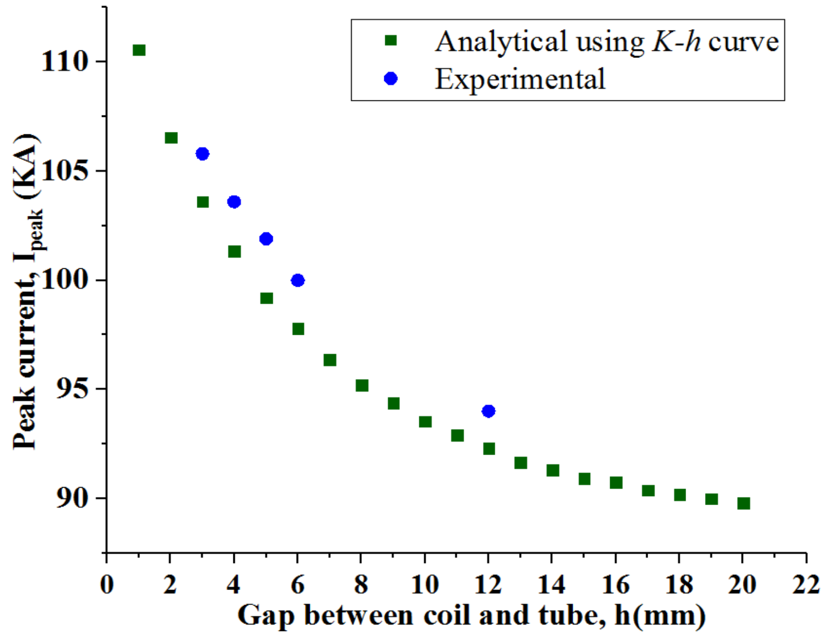

Figure 7.5: Discharge circuit parameters variation with h

Analytical estimated parameters using the derived K-h curve shows good match with experimentally measured values as can be seen in figure 7.5. With the increase in h, inductance increases exponentially whereas the resistance decreases slightly. Peak current of the discharge circuit also decreases exponentially with h.

K variation during the tube forming operation and stationary case

As shown in Figure 7.6, there are two different situations in EMF where K varies with h.

- Stationary (case A), where the h is the same along the axial direction
- Transient (case B), where the workpiece moves away from the coil during the tube forming operation. Here the gap between coil surface to tube maximum forming point is considered as h.

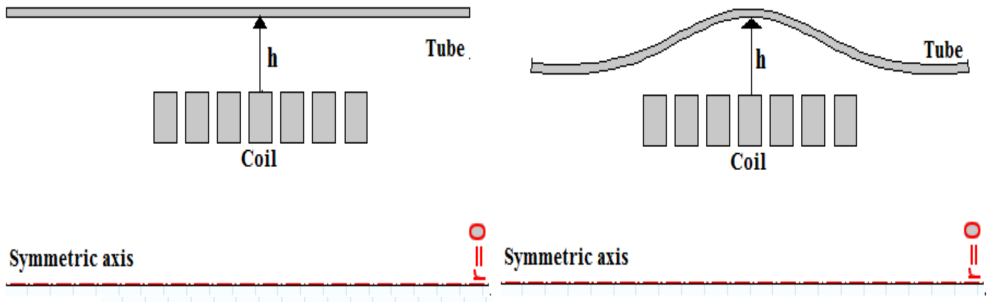

Figure 7.6: Schematic of (a) case A and (b) case B

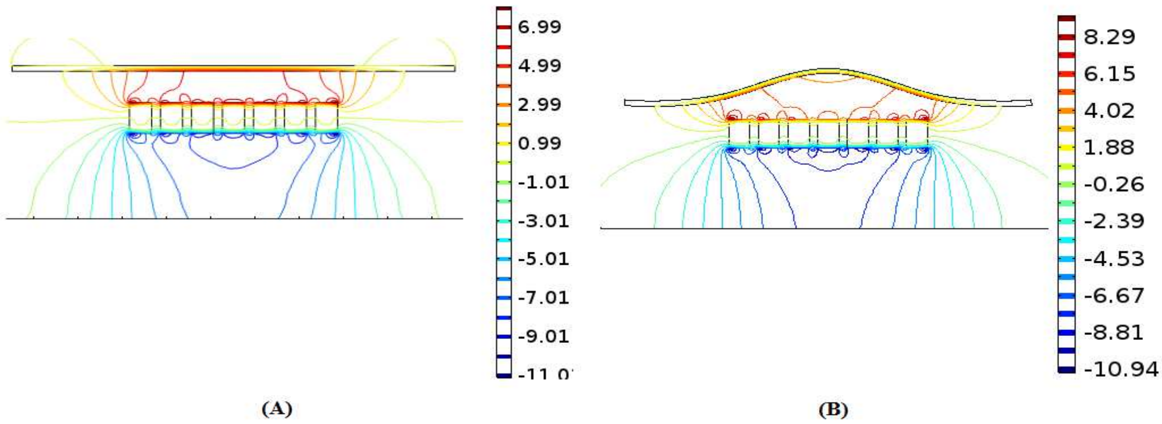

Figure 7.7: Magnetic flux linkage at peak current and h=8 mm, (a) case A and (b) case B

In both cases, though K varies with h, the nature of K-h curve is different. During the tube forming (case B), tube deformation is non uniform along the tube's length with higher deformation at the tube centre. As observed from Figure 7.7, though the h is the same in both the cases, the coil-tube flux linkage for the tube forming case is high compared to the stationary case. These results in higher coupling factor K for a tube forming case for the same h.

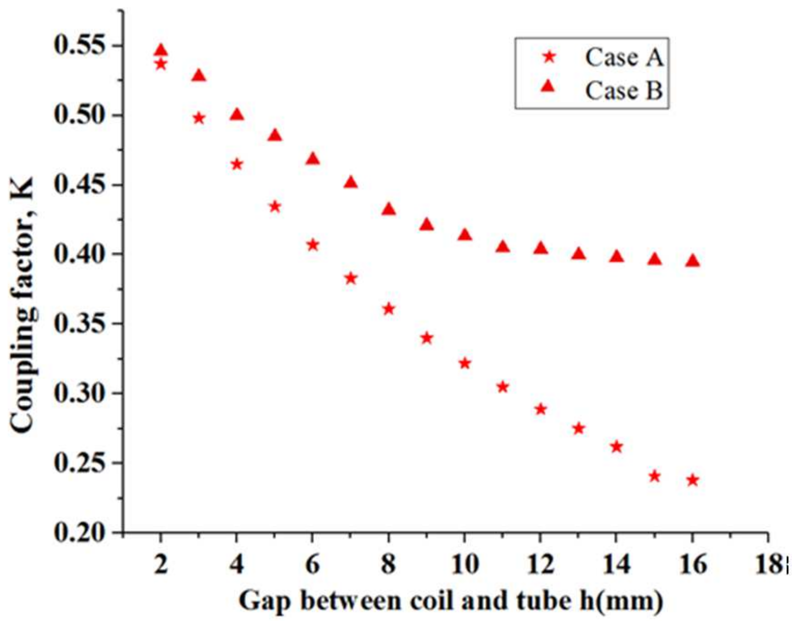

Figure 7.8: Coupling factor K variation with *h* for case A and case B

To compare the nature of *K*-*h* curve nature in both cases, numerical simulation method has been used. Figure 7.8 shows the *K*-*h* curve for each case. The results show that the derived *K*-*h* relation in this chapter is useful in the analytical estimation of discharge circuit parameters in the stationary case when there is no deformation in the tube. The discharge circuit parameters do vary during the forming, but the coupling factor variation is different in both cases and hence the derived *K*-*h* relation cannot be used to determine the discharge circuit parameter variation during the tube forming.

7.5 Summary

Electromagnetic tube expansion study is carried out on tubular workpiece made up of aluminium. The tool coil to tubular workpiece magnetic coupling is varied by varying the gap between them and coupling factor relation with coil-tube gap is obtained. Further, the effect of the coupling on different parameters is analysed.

- The coil-tube coupling factor (*K*) variation is an exponential decay: $K = A_0 e^{-B_0 h}$, where A_0 and B_0 are the constants with values 0.806 and 0.07 respectively and h is the coil workpiece gap in mm. This relation is useful for more accurate analytical simplification of the EMF discharge circuit as RLC circuit.

- Numerically simulated results which are in good agreement with experimental observation showed that the process efficiency and the tube displacement increase exponentially with the increment in coil-tube magnetic coupling factor *K*. Thus, positioning of the coil and the workpiece is an important aspect in designing the electromagnetic forming set up.

- With the increase in *h*, there is an exponential rise in inductance and exponential decay in peak current of discharge circuit. Resistance decreases slightly with *h*.

- The *K*-*h* curve during the tube forming process is also exponentially decreasing, but the nature of decay is different from the studied stationary case where the coil and tube are equidistance from each other along the axial length.

Annexure I

CERTIFICATION ON ACADEMIC INTEGRITY

1. I Mr. Shantaram Kisan Dond (name of the student) HBNI Enrolment No. ENGG01201404024 hereby undertake that, the Thesis titled " Parametric Influence on Electromagnetic Forming Processes " ***(bold & italics)*** is prepared by me and is the original work undertaken by me and free of any plagiarism. That the document has been duly checked through a plagiarism detection tool and the document is plagiarism free.

2. I am aware and undertake that if plagiarism is detected in my thesis at any stage in future, suitable penalty will be imposed as per the applicable guidelines of the Institute / UGC.

20/07/2020
Signature of the Student
(with date)

Endorsed by the Thesis Supervisor:
(I certify that the work done by the Researcher is plagiarism free)

Signature (with date)

20/07/2020.

Name: डॉ. (श्रीमती) अर्चना शर्मा/Archana Sharma
Designation: सह निदेशक/Associate Director
Department/ Centre:
Name of the CI/ OCC

Thesis Highlight

Name of the Student: Mr. Shantaram K. Dond

Name of the CI/OCC: Bhabha Atomic Research Centre **Enrolment No.:** ENGG01201404024

Thesis Title: Parametric Influence on Electromagnetic forming processes

Discipline: Engineering Science **Sub-Area of Discipline:** Electrical engineering

Date of viva voce: 16th July 2020

Electromagnetic forming (EMF) is a high-velocity forming method that uses a strong electromagnetic field to deform metallic workpieces. The Objectives of the thesis are to develop a numerical model to simulate the electromagnetic tube forming process and to study the effect of process parameters on electromagnetic forming results, process efficiency and coil life.

A 40 kJ EM manufacturing machine is used for the electromagnetic expansion experiments. EMF tests are performed on different dimension aluminium 5052 tubes. A 2D numerical model is developed using COMSOL Multiphysics software. In this, electromagnetic, structural and thermal physics are coupled sequentially, and time-dependent study is performed. A 1D analytical model is also developed to estimate required magnetic field, magnetic, resultant tube velocity and displacement. The developed analytical and simulation model results are in agreement with experimental observations. Firstly, a robust electromagnetic coil is designed and tested for aluminium tube expansion. Impact of thermal and mechanical loading on coil failure is further studied. For the used experimental setup, optimum frequency is found out and its dependency on various parameter is studied.

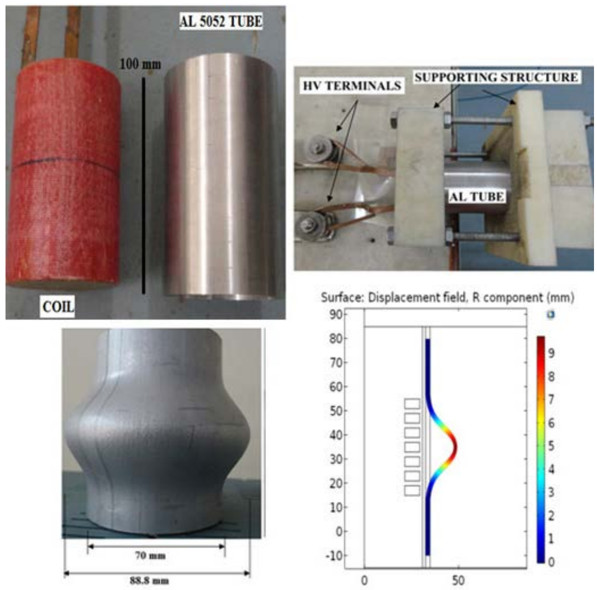

Figure 1. Designed coil for EMF, experiment arrangement of coil and tube, expanded tube and COMSOL results

In the study of effect of dynamics of discharge circuit parameters, significant improvements in estimated results are observed with consideration of discharge circuit parameters dynamics in the analysis. In next study, the coupling coefficient (K) variation with the coil-tube gap (h) is related with curve fitting, and this K-h relation is then used to analyse the discharge circuit parameter dependency on h. The EMF process efficiency and tube displacement are found to be improved exponentially with the increase in K. The studied aspects in this thesis will be helpful to design strong electromagnet and to improve the EMF process efficiency.